M 2022

U.PORTO
FEUP FACULDADE DE ENGENHARIA
UNIVERSIDADE DO PORTO

RECYCLING OF INDUSTRIAL AND URBAN WASTEWATER FOR GREEN HYDROGEN PRODUCTION USING PEM AND AEM WATER ELECTROLYSIS

MARIA INÊS DE OLIVEIRA ROMÃO
MASTER THESIS IN CHEMICAL ENGINEERING
PRESENTED TO THE FACULTY OF ENGINEERING
OF THE UNIVERSITY OF PORTO

Master in Chemical Engineering

Recycling of industrial and urban wastewater for green hydrogen production using PEM and AEM water electrolysis

Master Dissertation

of

Maria Inês de Oliveira Romão

Developed within the course of dissertation

held in

SEA+TECH

Supervisor at FEUP: **Prof. Adélio Mendes**

Coordinator at SEA+TECH: **Cristina Sousa**

July 2022

Acknowledgments

I would like to express my enormous gratitude to my coordinators at Sea+Tech, for giving me the opportunity of working on this field. For all the dedication and guidance during the work, for the support during the harder times, and for allowing and encouraging me to follow my own path during this dissertation.

I want to thank all the people in the LEPABE-AM group with whom I spent time during these 4 months: thank you for making me feel welcomed, and for all the valuable ideas and thoughts that you presented me with during that time. Thank you for showing me what research in engineering really is.

I would like to express my gratitude to Professor Adélio Mendes, my supervisor at FEUP, which, supported by his researchers Sofia Delgado and Eva Sousa, provided me the inspiration, guidance, encouragement, and support needed for developing this exciting dissertation.

A big, big thank you to my friends: the ones that FEUP gifted me, and the ones from far back in my life. Thank you for listening to my rants about life and for sticking with me during the best and worst moments of this journey. An even bigger thank you to my boyfriend, just for being himself, and never failing at making me smile.

To my family: my grandparents, my uncles and cousins, and my father, for the support and interest in my work. To my little sister, and her endless curiosity and enthusiasm: thank you for always encouraging me to be the best role-model I can be.

To my mom: thank you.

My thanks to Tintas CIN for allowing the use of their wastewaters in this work.

This work was financially supported by LA/P/0045/2020 (ALiCE), UIDB/00511/2020 and UIDP/00511/2020 (LEPABE), funded by national funds through FCT/MCTES (PIDDAC).

Abstract

With the rising of energy consumption and greenhouse gas emissions, it is of upmost importance to develop renewable energy-based technologies to replace fossil fuels. Particularly, hydrogen has emerged as the most promising option for the at-scale decarbonization of transportation, chemical and energy-intensive industries, since its utilization is essentially pollutant-free. Recently, water electrolysis has attracted much interest as the green-hydrogen producing method, owning to its suitability to be coupled with renewable energy resources, such as wind and solar. However, between 10 kg and 20 kg of pure water are required to produce 1 kg of hydrogen, which is a real concern since intense droughts have been shadowing the world. Therefore, it is of great interest to assess the feasibility of using alternative water sources (such as wastewater and seawater) for green-hydrogen production since the use of fresh water as feed for a water electrolyser is not a sustainable approach for long-term operation. However, to date, there has been no study examining the influence of real wastewater feeding to a water electrolysis cell.

Herein, it is reported the performance and stability of an electrolysis cell when fed with treated municipal and industrial wastewaters; both proton exchange membrane (PEM) and anion exchange membrane (AEM) water electrolysis were considered. Accelerated stress tests were performed for evaluating the stability of the electrolysers during long-term operation and fluctuations of the electrical power, which mimics the green power produced from renewable sources. Besides, a tertiary treatment unit, consisting of media-filtration and ion-exchange resins was assembled to further purify the wastewater sources. Relevant water quality parameters - conductivity, total solid content - were measured before and after feeding the water to the ion exchange column. The advanced treatment allowed a 99.8 % reduction in the wastewater's conductivity, resulting in water characteristics like those of ultrapure water.

The performance and stability of both PEM and AEM electrolysers using directly treated wastewaters are remarkably similar to those obtained when using ultrapure feed water. In fact, negligible overpotentials could be obtained in PEM and AEM electrolysis cells after performing intensive potential cycling for over 15 h, when using feed wastewater treated upon low-complexity, flexible and energy-efficient ion exchange methods. The obtained results are a significant advance over the state-of-the-art on using seawater and direct industrial/municipal wastewater for feeding electrolysers, making the electro-production of green hydrogen even more sustainable.

Keywords (theme): Water electrolysis, green-hydrogen production, wastewater treatment

Resumo

Com o aumento do consumo de energia e das emissões de gases com efeito de estufa, é de grande importância desenvolver tecnologias baseadas em energias renováveis para substituir os combustíveis fósseis. Em particular, o hidrogénio surgiu como a opção mais promissora para a descarbonização à grande-escala das indústrias do transporte e química, uma vez que a sua utilização não produz poluentes gasosos. Recentemente, a eletrólise da água tem atraído muito interesse como método de produção de hidrogénio verde, devido à sua facilidade em ser associada a recursos energéticos renováveis, como energias eólica e solar. No entanto, são necessários entre 10 kg e 20 kg de água para produzir 1 kg de hidrogénio, o que é preocupante devido às secas intensas têm vindo a assolar o mundo. Por conseguinte, é de grande interesse avaliar a viabilidade da utilização de fontes de água alternativas (como as águas residuais industriais e a água do mar) para a produção de hidrogénio verde, uma vez que a utilização direta de água doce como reagente para eletrólise não é uma abordagem sustentável a longo prazo. No entanto, até à data, não houve nenhum estudo que examinasse a influência da alimentação real das águas residuais para uma célula de eletrólise de água.

Aqui, relata-se o desempenho e estabilidade de uma célula de eletrólise quando alimentada com águas residuais municipais e industriais tratadas. Esta abordagem foi estudada tanto para membranas de troca protónica (PEM) como para eletrólise com membranas de permuta aniónica (AEM). Foram realizados testes de stress acelerados para avaliar a estabilidade da célula de eletrólise durante o funcionamento a longo prazo e também para imitar indiretamente a natureza intermitência das fontes renováveis. Além disso, foi desenvolvida uma unidade de tratamento terciário, constituída por resinas de permuta iónica e sistemas de filtração, com o objetivo de purificar as fontes de águas residuais. Parâmetros relevantes da qualidade da água - condutividade, teor de sólidos - foram medidos antes e depois da alimentação da água residual à coluna de resina de permuta iónica. O tratamento terciário permitiu uma redução de 99,8 % da condutividade das águas residuais, resultando em características semelhantes às da água ultrapura.

Tanto o desempenho como a estabilidade para ambas as tecnologias (PEM e AEM) são semelhantes quando a alimentação feita é com água ultrapura ou água residual tratada. Assim, esta dissertação traz novo conhecimento sobre a produção de hidrogénio através do eletrólise da água, preservando os escassos recursos de água doce.

Palavras-chave: Eletrólise da água, produção de hidrogénio verde, tratamento de águas residuais

Declaration

I hereby declare, under word of honour, that this work is original and that all non-original contributions are indicated, and due reference is given to the author and source

Maria Inês de Oliveira Romão

(Maria Inês de Oliveira Romão)

04/07/2022

Index

List of Figures

List of Tables

Notation and Glossary

a	Chemical activity	
C	Concentration	$\mathrm{mol\,m^{-3}}$
E	Potential	V
F	Faraday constant	$96\,485.31\,\mathrm{C\,mol^{-1}}$
G	Gibbs free energy	$\mathrm{J\,mol^{-1}}$
H	Enthalpy	$\mathrm{J\,mol^{-1}}$
I	Current	A
i	Current density	$\mathrm{A\,cm^{-2}}$
K	Selectivity	
n	number of electrons	$\mathrm{J\,mol^{-1}}$
P	Pressure	bar
p	Partial pressure	bar
$\mathcal{R}$	Universal gas constant	$8.314\,\mathrm{J\,mol^{-1}\,K^{-1}}$
R	Resistance	Ω
T	Temperature	K
Z	Specific impedance	$\Omega\,\mathrm{cm^2}$

Greek Letters

Δ	Difference operator	
σ	Conductivity	$\mathrm{S\,cm}$
ρ	Resistivity	$\Omega\,\mathrm{cm^{-1}}$

Indexes

act	activation
an	anode
cat	cathode
conc	concentration
i	variable
^{o}	standard conditions
OCP	open circuit potential
ohm	Ohmic
R	reaction
ref	reference
rev	reversible
th	thermoneutral

List of Acronyms

AEM	Anion exchange membrane
AEMWE	Anion exchange membrane water electrolysis
ASR	Area specific resistance
AST	Accelerated stress test
CCM	Catalyst coated membrane
CCS	Catalyst coated substrate
CER	Chlorine evolution reaction
EIS	Electrochemical impedance spectroscopy
ETS	Emissions trading system

EU	European Union
FTIR	Fourier-transform infrared
GDL	Gas diffusion layer
GHGE	Greenhouse gas emissions
HER	Hydrogen evolution reaction
IX	Ion exchange
LDL	Liquid diffusion layer
MEA	Membrane electrode assembly
OER	Oxygen evolution reaction
PEM	Proton exchange membrane
PEMWE	Proton exchange membrane water electrolysis
PFSA	Perfluorosulfonic acid
PGM	Platinum group metal
PSF	Polysulfone
PTFE	polytetrafluoroethylene
PTL	Porous transport layer
RO	Reverse osmosis
RO	Reverse osmosis
SEM	Scanning Electron Microscopy
SHE	Standard hydrogen electrode
TDS	Total dissolved solids
TGA	Thermogravimetric analysis
WWTP	Wastewater treatment plant

1 Introduction

1.1 Framing and Presentation of the Work

With a growing population and expanding industrialization, the extremely high consumption rate of fossil fuels led to a tremendous increase in carbon dioxide (CO_2) emissions which, in turn, has been a major responsible for dangerous climate change. European Union (EU) is, therefore, committed to reach carbon neutrality by 2050 [9]. In fact, there is a great interest in reducing fossil fuel utilization, by developing a global-scale sustainable system, which includes investing in renewable energy-based (solar, wind, hydro, biomass), emission-free technologies and energy storage systems, while financially encouraging industries to cut down pollutant emissions. In fact, the EU had to limit the amount of greenhouse gases emissions (GHGE), thus establishing the EU Emissions Trading System (EU ETS) - the world's first major carbon market. EU ETS is a key EU's policy for reducing GHGE effectively. Essentially, pollutant emissions are limited, and companies receive or buy emission allowances, which they can trade as needed. In April 2022, the average cost of a tone of equivalent CO_2 in this trading market was 81 € [10]. Considering the sectors covered by the EU ETS, the GHGE registered a reduction of 35 % between 2005 and 2019. Nevertheless, the overall volume of pollutant gases emitted by power plants, industry factories and aviation sector must decrease by 45 % by 2030 for limiting global heating to 1.5 °C, which in turn is a call to move towards decarbonization [11]. In Portugal, for instance, energy audits are mandatory in industries with an annual energy consumption of 500 tones of oil equivalent or higher, following the Decreto-Lei nº 71/2008, which foresees the reach of a 4 % to 6 % reduction in primary energy consumption over time.

Hydrogen (H_2) has emerged as the most promising option for the at-scale decarbonization of transportation, chemical and other energy-intensive industries since its combustion or oxidation does not produce pollutant emissions. Moreover, due to its flexibility and remarkable energy density (120 $MJ\,kg^{-1}$), its demand has been increasing in recent decades – Figure 1.1, particularly for chemical refining processes and methanol and ammonia production. However, carbon emissions associated with hydrogen production are closely linked to the type of technology and energy source used. Currently, about 96 % of hydrogen is produced by fossil fuels, mostly by steam methane reforming [12] – grey-hydrogen. Unless it is combined with a carbon capture technology, this approach is responsible for a substantial production and emission of carbon monoxide and carbon dioxide. Only when hydrogen is produced through water electrolysis, using electricity from renewable sources, or through biomass gasification [13], it can be considered green-hydrogen – in other words, clean-hydrogen without pollutant emissions associated. Green-hydrogen market is expected to exceed 100 million tones by 2050 [14] and,

therefore, the strategic EU objective is to install at least 40 GW electrolysers by 2030, ensuring the production of at least 10 million tones of renewable hydrogen in European countries [9].

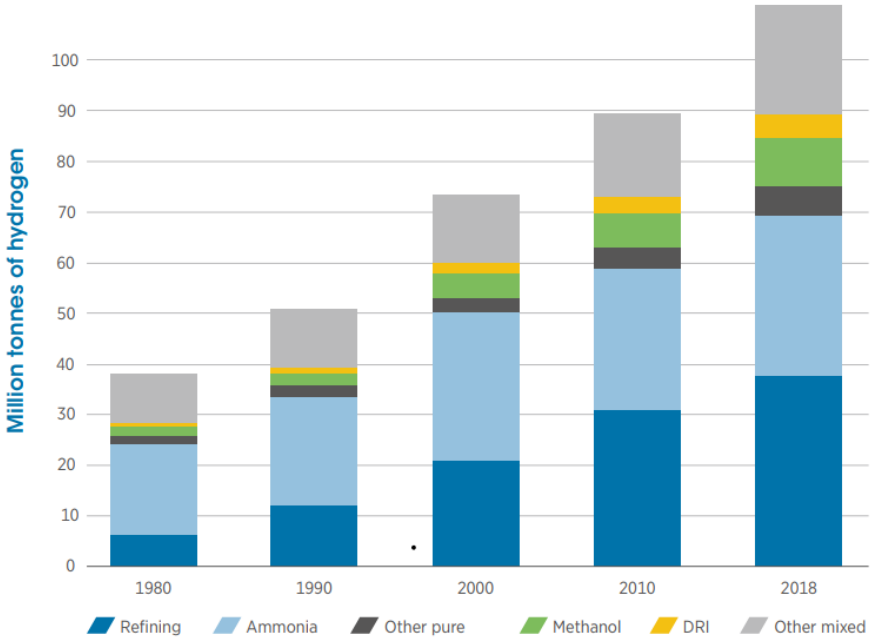

Figure 1.1 - Global annual demand for hydrogen since 1980 [4].

Water electrolysis is an energy-intensive process, since 51.2 kWh of energy are required to produce one kilogram of hydrogen [6]. Thus, the expected exponential growth of green-hydrogen production also implies significant efforts towards renewable energy production. In fact, when it comes to natural resources, Portugal has a unique potential to become a leading energy provider, which in turn, is crucial to tackle the challenges ascribed to green-hydrogen production. In 2021, approximately 60 % of electricity was produced from renewables [15] and the Portuguese Government has the objective of increasing renewable electricity production up to 80 % by 2026 [16]. In April of 2022, it was reached, in Portugal, 0.24 TWh of photovoltaic solar energy, 1.15 TWh of wind energy, and 0.51 TWh of hydro energy [17]. Annex M shows the photovoltaic power potential and the mean wind power potential for Portugal; many projects are already being developed regarding the installation of solar and wind farms, including offshore platforms, such as the EDP's floating solar farm in Alqueva [18] and the WindFloat Alantic Project [19], which, in turn, aims at producing offshore wind power in the MW-scale. Offshore platforms do not require valuable real estate and overall, wind energy density tends to be higher offshore (*ca.* 400 W m^{-2}) than inland (*ca.* 200 W m^{-2}) (see annex M).

To produce 1 kg of hydrogen, between 10 kg and 20 kg of pure water are necessary depending on the system [20]. Currently, the H_2 market is considering the use of freshwater, with only a purifying step, to be fed into the electrolysers. This approach is not sustainable since intense droughts have been shadowing the world. In Portugal, for example, January 2022 was considered as the second driest month since 2000 and every municipality was at least in

moderate drought [21]. Nevertheless, in Portugal, seawater is readily accessible along the coast and therefore, the national strategy for green-hydrogen production aims at taking advantage of the interesting geographic location of the country [16]. However, the use of seawater or other water sources, such as wastewater, can be a great challenge since it is essential to guarantee certain characteristics in the water fed to an electrolyser, namely in terms of purity, to allow long term operation. The presence of contaminants (i.e., heavy metals, ammonia compounds or chlorine), even if at low concentration levels, in the feeding water may compromise the performance of the electrolysers, and lead to shortened lifetimes [22]. Therefore, for maximizing the sustainability of the green-H_2 production process, without compromising the electrolyser's performance, the development of integrated solutions is of great interest, namely by considering wastewater and seawater as water sources, coupled with specific treatment [16].

1.2 Presentation of the Institution/Company

SEA+TECH is a spin-off company founded in 2021 at the University of Porto, Portugal.
The company focuses mainly on the smart management of renewable energy sources with advanced water treatment systems to produce fresh water from urban/industrial wastewaters or seawater, in order to fight the emerging water scarcity problem.
Currently, SEA+TECH is supporting the development of smart grid modelling tools to be coupled to photovoltaic panels, water purification systems and electrolyser systems to forecast hydrogen production rates and the premature failure of such systems. The main objective of this project is the development of an intelligent interface for screening the performance and stability of integrated solutions for green-hydrogen production.
Besides, the company R&D fields include the development of customized water purification and recirculation systems to assist the operation of proton exchange membrane (PEM) and anion exchange membrane (AEM) water electrolysers at kW (laboratorial) and MW (industrial) ranges for the production of green-hydrogen. The ultimate purpose of SEA+TECH at this level is to assemble efficient seawater treatment plants with water recycling circuits to and from electrolysers, guaranteeing that the overall water consumption is minimal. The company also delves onto the valorisation of the brine stream, namely by extracting high-value minerals.

1.3 Author's contribution to the work

This dissertation aims at introducing a unique vision for water electrolysis by using alternative water sources for green-hydrogen production via PEM or AEM water electrolysis, while correlating the long-term performance of the electrolysers with the quality of feed water upon performing distinct purifying steps. Furthermore, the water electrolysis units' operation was optimised, setting the most proper temperature conditions, water feed flow rate, liquid electrolyte concentration, among other parameters, with the aim of decreasing the overall water consumption while maximizing the hydrogen rate production/purity and lifetime of the devices. Several water qualities ranging from industrial wastewater, municipal wastewater and seawater followed by advanced water treatment strategies were fed into the hydrogen-producing devices. Then, the electrolysers were submitted to accelerated stress tests for evaluating their long-term stability and efficiency, while using treated wastewater or saltwater (mimicked seawater).

1.4 Organization of the Dissertation

This dissertation is divided into six chapters. In the first chapter, Introduction, it is given context on the importance of the work. The second chapter, State of the Art, provides a theoretical background into water electrolysis and brings to light to the recent development in non-pure water electrolysis and water treatment methods. The third chapter exhibits the MEA preparation methods, describes the electrolysis and water treatment units used, and the electrochemical and physical characterization of the materials used. Chapter four demonstrates the results obtained for pure and treated wastewater electrolysis and those results are discussed considering the existing literature. Finally, chapters five and six show the main conclusions and suggest future work.

2 State of the Art

2.1 Water Electrolysis

Water electrolysis refers to the splitting of water molecules (H_2O) into hydrogen and oxygen by applying electrical current. The overall reaction is represented in Equation (1).

In an electrolysis cell, the oxygen is oxidized (from an oxidation state of -II to 0) at the anode and the hydrogen is reduced (from +I to 0) at the cathode [23].

$$H_2O \rightarrow H_2 + \frac{1}{2}O_2 \quad (1)$$

There are four main types of water electrolysers: alkaline electrolysers, proton exchange membrane water electrolysers (PEMWE), anion exchange membrane water electrolysers (AEMWE) and solid oxide electrolysers. Alkaline and PEM water electrolysers are already at a commercial level, while the last two are emerging technologies [6]. The ion exchange media of both PEM and AEM electrolysers, the membrane, is solid and non-porous, and therefore, the design of the electrolysers is compact, which in turn ensures the possibility of operating at higher differential pressures, guaranteeing the high-grade purity of hydrogen and greater efficiencies, when compared to more mature alkaline electrolysers. This is economically advantageous because it can result in cost savings and plant process simplification by eliminating the hydrogen compression step. Contrarily, alkaline electrolyser operation considers the use of corrosive liquid electrolytes (up to a mass fraction of 30 % potassium hydroxide - KOH - solutions), a porous diaphragm as separator of both electrodes [24], and lower pressures, thus requiring purification and compression steps, as well as a high balance of plat cost, due to metal corrosion from the concentrate KOH solutions.

2.1.1 Components of an Electrolysis Cell

Membrane electrolysers – PEM and AEM - follow a standard symmetrical design, which is illustrated in Figure 2.1. The oxygen evolution reaction (OER) takes place at the anode side, and the hydrogen evolution reaction (HER) happens at the cathode side.

The endplates provide mechanical support to all the components. Bipolar plates allow the water to effectively reach the catalytic active sites and to remove the gaseous products. They must be corrosion resistant, to withstand the strongly acidic or alkaline environment, and have high electrical conductivity, since they are part of the electrical current transfer mechanism in the

cell (the electrons travel from the catalytic layer, through the bipolar plate to an outer circuit, reaching then the cathode side) [25].

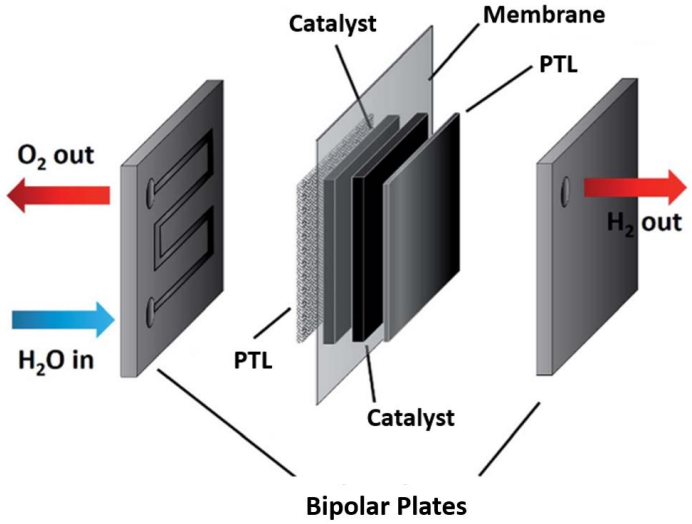

Figure 2.1 - Design of a membrane electrolyser.
Adapted from [7].

The porous transport layer (PTL), also known as the gas or liquid diffusion layer (GDL and LDL respectively), provides the required microstructure for improving transportation of reactants and products to and from the catalyst layer. In addition, it electrically connects the catalyst layer and the bipolar plate [26]. The membrane must transport solvated ions (protons in acidic media or hydroxyl ions in alkaline media) while acting as a barrier for electrons and the produced gases. Typically, the membrane consists of a polymer backbone, which is responsible for mechanical and thermal stability, and a functional group, which in turn is accountable for the ion exchange capacity [24]. The three joint parts (PTL, catalyst layer, and membrane) form the membrane electrode assembly (MEA).

The catalyst layer may be dispersed directly onto the PTL, or directly applied to the membrane, resulting in a catalyst coated substrate (CCS) or in a catalyst coated membrane (CCM), respectively. Typically, prior to catalyst deposition, it is crucial to optimize the catalyst ink composition, which consists of a suspension containing the catalyst powder, ionomer, and a solvent (or mixture of solvents) [27]. The ionomer is typically made of the same or similar material as the membrane used, and it aids in lowering the contact resistance between the catalytic layer and the membrane. The required ink rheology depends mainly on the type of coating method used and it is typically governed by the properties of solvents used and the solids' content. There are several alternatives for coating the catalyst layer, though doctor blade, screen printing, and spraying are particularly well-developed deposition processes. For doctor blade techniques, the solids' content is considerably high (between 20% and 30%, in mass fraction) [28], and solvents with a higher viscosity (such as ethylene glycol) are used [29],

resulting in a viscous ink, which in turn results in medium-thick catalyst layers, about 20 µm. When working with a doctor blade, several parameters must be considered and optimized (*e.g.* solid content, solvents used, blade velocity, amount of ink needed). This method is preferable when a high catalyst loading is required, but it results in a high loss of catalyst material, which raises the cost. In spraying methods, the ink is less viscous – a solid mass content of less than 1 % is typically considered - and the process is simple and easily automated. However, there is a risk of membrane swelling with this deposition method, which can result in preferential paths during operation [30].

The costs of a membrane electrolyser, namely a PEM electrolyser, Figure 2.2, are divided between the balance of the plant and the costs associated with the stacks. Each stack consists of two compartments – anode and cathode - separated by a membrane. Each compartment is constituted by a PTL and a catalyst layer, and all materials are compressed by bipolar plates. It is of notice the costs of the bipolar plates which, for PEM electrolysers, are typically made of bulk titanium, being responsible for about 24 % of the total cost of the electrolyser.

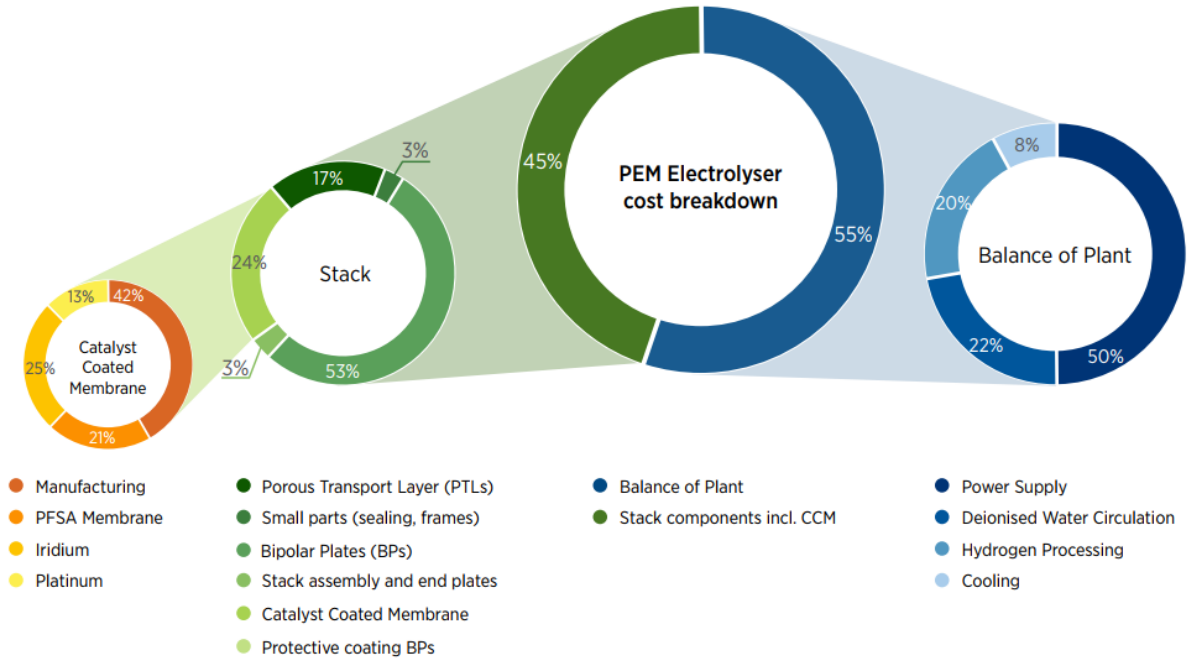

Figure 2.2 - Cost breakdown for a 1 MW PEM electrolyser (extracted from [6]).

2.1.2 General Principles

Under standard pressure (P) and temperature (T) conditions ($P = 1$ atm and $T = 298.15$ K), the water splitting reaction is not spontaneous, and the Gibbs Free Energy of the overall reaction (ΔG_R^0) is 236.483 kJ mol^{-1}. The reversible cell potential (E_{rev}^0) is given by equation (2), in which F is the Faraday constant ($F = 96\,485.309$ C mol^{-1}) [31], n is the number of moles of electrons transferred in the reaction (in the case of this reaction, $n = 2$) [32]. If no external energy is

supplied, the electric energy to be supplied is related to the reaction enthalpy ($\Delta H_{\mathrm{R}}^{0} = 285.83\,\mathrm{kJ\,mol^{-1}}$), which equates to a thermoneutral potential (E_{th}) of 1.481 V.

$$E_{\mathrm{rev}}^{0} = \frac{\Delta G_{\mathrm{R}}^{0}}{n \cdot F} = 1.229\ \mathrm{V} \tag{2}$$

The open circuit potential (E_{OCP}) refers to the potential difference when there is no current circulating between the terminals, and it is dependent on pressure and temperature [33]. E_{OCP} can be calculated using the Nernst equation (3) [34]:

$$E_{\mathrm{OCP}} = E_{\mathrm{rev}}^{0} + \frac{\mathcal{R} \cdot T}{2 \cdot F} \cdot \ln\left(\frac{p_{\mathrm{H_2}} \cdot \left(p_{\mathrm{O_2}}\right)^{1/2}}{a_{\mathrm{H_2O}}}\right) \tag{3}$$

where, $\mathcal{R}$ is the universal gas constant ($\mathcal{R} = 8.314\,\mathrm{J\,mol^{-1}\,K^{-1}}$), p is the partial pressure of the gas, in bar, and $a_{\mathrm{H_2O}}$ the activity of pure liquid water ($a_{\mathrm{H_2O}} = 1$).

There are several sources of performance loss in an electrolyser cell, meaning there is a deviation of ideal conditions, referred to as overpotentials. Such operation inefficiencies can be categorized as: activation overpotential (ΔE_{act}), ohmic overpotential (ΔE_{ohm}) and concentration overpotential (ΔE_{con}).

The activation overpotential may be calculated using the Butler-Volmer equation, (4). The overpotential is influenced by the kinetic characteristics of the process in both electrodes, which in turn are influenced by the catalyst's structure and materials.

$$\Delta E_{\mathrm{act}} = \frac{\mathcal{R} \cdot T_{\mathrm{an}}}{2 \cdot \alpha_{\mathrm{an}} \cdot F} \ln\left(\frac{i}{2\, i_{0,\mathrm{an}}}\right) + \frac{\mathcal{R} \cdot T_{\mathrm{cat}}}{2 \cdot \alpha_{\mathrm{cat}} \cdot F} \ln\left(\frac{i}{2 \cdot i_{0,\mathrm{cat}}}\right) \tag{4}$$

The exchange current density (i_0) is calculated using the Arrhenius expression, equation (5), which relates i_0 with the temperature. In this equation, $i_{0,\mathrm{ref}}$ is the exchange current density at a reference temperature T_{ref}, and H_{act} (J mol^{-1}) is the activation energy at the respective electrode [35].

$$i_0 = i_{0,\mathrm{ref}} \cdot \exp\left[-\frac{H_{\mathrm{act}}}{\mathcal{R}}\left(\frac{1}{T} - \frac{1}{T_{\mathrm{ref}}}\right)\right] \tag{5}$$

The ohmic overpotential is related to the resistance (*R*) of the different components of the electrolyser to the flow of ions and electrons, as well as the resistance at the interface between the components [35]. The overall ohmic overpotential is given by equation (6) (Ohm's law), and *I* is the current of the circuit, in A.

$$\Delta E_{\mathrm{ohm}} = R \cdot I \tag{6}$$

Concentration overpotential is mainly relevant at high current density and is represented by equation (7) [36]. The concentration overpotential depends on the concentration of products

(hydrogen or oxygen) in the catalyst active centres, at the membrane surface ($C_{O_2,an}$ and $C_{H_2,cat}$) and it is deeply influenced by the inefficient circulation of water and gaseous product throughout the PTL.

$$\Delta E_{con} = \Delta E_{con,an} + \Delta E_{con,cat} = \frac{\mathcal{R} \cdot T}{4 \cdot F} \ln\left(\frac{C_{O_2,an}}{C_{O_2,an,0}}\right) + \frac{R \cdot T}{2 \cdot F} \ln\left(\frac{C_{H_2,cat}}{C_{H_2,cat,0}}\right) \quad (7)$$

2.1.3 Electrochemical characterization methods

The performance of a water electrolyser can be measured using a polarization curve which is, typically, the most important characterization technique (Figure 2.3.a). This polarization method relates the potential difference with the current density: for a water electrolyser, as the current density increases the overpotential, associated with the different resistance sources, also increases. The different types of performance loss in a cell, as detailed above, may be easily distinguished in the polarization curve: at lower current densities, the activation overpotential, related to the electrochemical reactions that happen at the electrodes, is the most relevant phenomena; then, the ohmic overpotential, which corresponds to the linear region of the *i-v* curve, depends mainly on the type and properties (roughness factor, electrical resistivity, among others) of the used materials, specially the membrane; lastly, the mass transport overpotential region, at high current densities. Polarization curves can be obtained through chronoamperometry or chronopotentiometry techniques, which involve applying a set potential or current, respectively, to measure the potential or current response of an electrochemical reaction. The response is, then, recorded *vs.* time. These methods are of utmost prominence for analysing the stability of the components used in the cell over time and thus unveil the origin of the overpotentials. Moreover, the polarization curves may be related with the results obtained through electrochemical impedance spectroscopy (EIS – Figure 2.3.b).

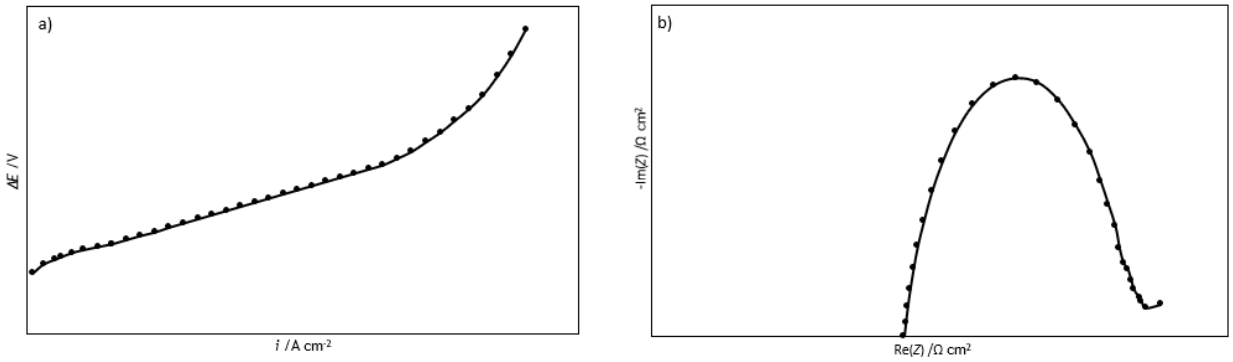

Figure 2.3 – a) Typical polarization curve and b) Nyquist plot of a water electrolysis cell.

Through EIS analysis, represented by Nyquist or Bode plots, it is possible to distinguish and quantify the contributions of each type of losses to the measured overpotential. The spectra reveals information about the behaviour of electrochemical reactions and unveils the dominant phenomena. Figure 2.3.b) is an example of a Nyquist plot, in which the ohmic resistance and the resistance associated with the reaction can be measured in the horizontal axis. Since impedance is a function of frequency, different ranges of frequencies must be examined. The high-frequency region (typically, >100 Hz) reflects the charge transport in the catalyst layer, whereas the low-frequency region (< 0.01 Hz, in general) represents mass transport overpotentials.

2.1.4 Proton Exchange Membrane Electrolysers

On a PEM electrolyser, the OER (anodic reaction) and the HER (cathodic reaction) are represented by equations (8) and (9), respectively.

$$H_2O \longrightarrow 2H^+ + \frac{1}{2}O_2 + 2e^- \quad (8)$$

$$2H^+ + 2e^- \longrightarrow H_2 \quad (9)$$

Typically, the membranes employed in PEM electrolysis are made of polyfluorosulfonic acid materials such as Nafion and have thicknesses of 20 μm to 300 μm [25, 37]. Iridium or iridium-ruthenium oxides are commonly used as anode catalysts, with loadings ranging from 0.2 mg cm^{-2} to 1 mg cm^{-2}; at the cathode, platinum catalysts are usually employed. Nevertheless, the scientific community's efforts are driven towards decreasing these loadings. In fact, the use of platinum group metals (PGM), is one of the main disadvantages of PEM electrolysers due to their scarcity and high costs [38]. PGM catalysts are, however, the materials of choice to circumvent the sluggish kinetics of OER (involving a 4-electron transfer while being able to withstand the harsh anodic conditions at an acidic environment.

2.1.5 Anionic Exchange Membrane Electrolysers

Regarding the AEM electrolyser, the OER and HER are described by equations (10) and (11), respectively.

$$4OH^- \rightarrow O_2 + 2H_2O + 4e^- \quad (10)$$

$$4H_2O + 4e^- \longrightarrow 2H_2 + 4OH^- \quad (11)$$

Since AEM water electrolysis is an emerging technology, the materials for producing AEM stacks are still under development, mainly concerning the fabrication of defect-free and stable AEMs and highly conductive catalyst layers. Only Enapter, an Italian company, has commercialized AEM stacks. Nevertheless, the possibility of using PGM-free materials such as iron or nickel-

based oxides as catalysts has sparked particular interest since these materials are much more abundant and inexpensive. Regarding AEM membranes, polysulfone (PSF), polystyrene cross-linked with divinylbenzene, or polystyrene cross-linked with divinylbenzene have been used as polymer backbones. These polymers are typically doped with functional groups composed of -$NH3^+$, –$RNH2^+$, –RN^+, =$R2N^+$, –$R3P^+$, –$R2S^+$ [39]. Moreover, PSF is normally used as ionomer due to its thermal and chemical stability [40].

Traditionally, a solution of KOH, with a concentration ranging from 0.1 M to 1 M is used as electrolyte. It is possible, with an electrolyte concentration of 1 M, to obtain current densities from 100 mA cm^{-2} to 500 mA cm^{-2} at 1.8 V [24].

2.1.6 Degradation Mechanisms

Accelerated stress tests (AST) are useful for determining the degradation mechanisms associated with a process, as well as the impact of various working conditions on those mechanisms. The main stressing phenomena in electrolysers are typically achieved by employing dynamic load operation using intensive cycling or steady-state operation at high current densities [41, 42]. The EU has developed protocols for testing of low temperature water electrolysis. In these protocols are present the reference conditions for single-cell and short stack testing, as well as protocols for accelerated stress testing [43]. Aßmann*et al*. [44] have also suggested an AST protocol divided into three sections: nominal current density operation, high current density operation, and load cycling between nominal and full load. Load cycling operation is of particular interest because it mimics current fluctuations which may occur when an electrolyser is directly coupled to renewable energy sources.

In PEM electrolysis, degradation occurs mainly at both catalyst layer level, especially at the anode compartment, and at the membrane. At the catalyst layer level, there is evidence of iridium dissolution in water, at potentials above 1.8 V, which has a negative impact on the electrolyser performance, particularly when the MEA comprises low catalyst loadings (below 0.2 mg cm^{-2}) [42]. Catalyst particles also suffer agglomeration, due to Ostwald ripening, reprecipitation and coalescence, especially when working at high potentials (2 V); this constant deposition and redissolution of the catalyst particles can promote catalyst porosity and activity, but it can also lead to detachment of the catalyst [22]. This effect is enhanced when working under intensive load cycling for long periods of time with fast ramp up and ramp down potential/current scans, and it may be attributed to a non-equilibrated process in the catalyst layer [45].

At the membrane level, the main concern in terms of degradation is poisoning by metallic cations, such as sodium (Na^+), lithium (Li^+), calcium (Ca^{2+}), coper (Cu^{2+}), nickel (Ni^{2+}) and iron

(Fe^{3+}) in PEMWE. These ions firstly dissolve and permeate through the membrane and then settle in its ion exchange sites, due to the higher affinity of the sulfonic groups to the cationic metals than to protons. These metallic ions may also deposit in the catalyst layer at the cathode – under potential deposition – and block active sites, lowering the activity of the catalyst at both PEM and AEM level. Also, when working with Nafion membranes, several authors detected the presence of fluoride ions in the exhaustion of the cell, suggesting the backbone polymer is degraded [22]. In AEMWE, quaternized polystyrene membranes have low stability in high alkaline environment. Besides, during OER, hydroxyl and hydroperoxyl radicals may be formed and trigger the degradation of the polymeric membrane.

The bipolar plate, which is normally composed of titanium, may suffer passivation, which in turns leads to a higher contact resistance. Besides, titanium particles may also deposit in the membrane, in the same mechanism described above for other metallic ions.

2.2 Hydrogen production using non-pure water feed

2.2.1 H_2 production coupled with water treatment systems

Several methods for hydrogen production coupled with wastewater treatment systems have been investigated. These hydrogen production methods can be classified as biological, electrical, electrochemical, photonic, and thermal. At the moment, the most promising processes seem to be dark fermentation, photo-fermentation and microbial electrolysis [46]. All these methods have the disadvantage of requiring pre-treatment of the wastewaters, specific for each wastewater and method used, to remove contaminants that may be toxic to the microorganisms (such as heavy metals) and the growth of other microorganisms, that compete for the substrate and generate undesired secondary products. In addition, the efficiency of this processes in terms of hydrogen production is very low and, therefore, these are unsustainable methods of hydrogen production from wastewater.

The use of conventional electrolysis cells for wastewater treatment has also been studied, in which the contaminant is oxidized on the anode side, with an appropriate catalyst, and hydrogen is produced on the cathode side. Hu*et al.* [47] used this method to oxidize solutions of ammonia, urea, and hydrazine. This method is still at lab scale, and, since specific potential conditions, as well as specific catalysts must be employed for each type of contaminant, the scalability of the process is difficult and requires further developments.

2.2.2 Seawater electrolysis

The hypothesis of using low-grade water, namely seawater, as feed in electrolysis has been studied over the years, due to its abundance. The chemical composition of seawater varies with its location, but regularly the main impurities are chlorine, sodium, magnesium and sulphur [48].

The competition between the oxidation of oxygen (OER) and chlorine (chlorine evolution reaction – CER) in PEM electrolysis is one of the main concerns in seawater electrolysis. Although the OER is thermodynamically favoured in acidic conditions, as shown in the Pourbaix diagram in Figure 2.3, the CER is kinetically favoured, since solely 2 electrons are involved in detriment of the 4 electrons required for the OER; therefore, both reactions overlap. Nonetheless, the production of chlorine gas (Cl_2) may lead to degradation in the cell [8]. There are other impurities for which the same might ensue, such as bromine, but since the bromine concentration in seawater is lower and the bromine evolution reaction kinetics' are slower, due to the transfer of 4 electrons, the concern with these is inferior. At a higher pH (above 7.5), the potential difference between the OER and CER is high enough (about 0.480 V versus 0.210 V at pH = 1) so that the parasitic reaction CER effect is minimal and, thus, the OER is the main reaction.

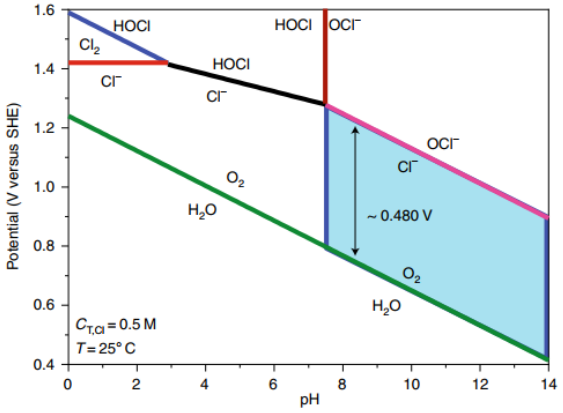

Figure 2.3 – Pourbaix diagram of an aqueous saline electrolyte [8].

In alkaline media (pH >9.5), the production of insoluble precipitates may happen at the cathode side, such as magnesium and calcium hydroxides, which may deposit in the catalyst active sites, creating a passive layer, whilst blocking the diffusion of water and reactants and increasing contact resistance [48].

Another parameter that must be considered refers to the presence of several microorganisms, which contribute to biofouling of the membranes used for electrolysis, similarly to the degradation mechanisms happening in nanofiltration/reverse osmosis membranes during

desalination. Despite, to the best of the author's knowledge, there are no studies that go in depth into this subject.

All these limitations suggest that, although solutions for the problems mentioned above are being studied, direct seawater electrolysis is not yet suitable for industrial applications. Several techno-economic studies suggest that it is economically beneficial to couple advanced filtration steps, *e.g.* reverse osmosis, with an electrolysis unit rather than using direct seawater electrolysis [49, 50]. So far, very little attention has been paid to the role of different advanced water treatment processes in the consequent electrolyser performance and thus hydrogen production. Each type of water source, whether municipal or industrial wastewater or seawater, requires different processing steps, and the optimization of a water purification plant and its economic analysis must be investigated.

2.3 Water Treatment

Contrarily to pure freshwater, industrial or municipal wastewaters or seawater may possess emerging pollutants and hard-to-remove molecules that condemn the long-term operation of water electrolysers. Thereafter, the main challenge for the incorporation of these alternative water sources for green-hydrogen production will be thus to apply the correct water treatment technology to remove them before feeding the water to the electrolyser.

Municipal or industrial wastewater must be submitted to water treatment processes prior to being delivered back into the environment or before reusing it. The purification treatment used is determined by the quality of the affluent wastewater and the end goal for its use. The requirements for water discharge into the environment are defined by Portuguese law – Decreto-Lei n.0 152/97. Most of the treated water in wastewater treatment plants (WWTP) is discarded to the environment; actually, in Portugal, only 1.2% of water treated on WWTPs is reused. Attending to the intense droughts lived in Iberian countries, proposing the reuse of industrial and municipal wastewaters as potential water sources for other water-intensive processes, namely green hydrogen production is of great interest. Moreover, there are already great examples of success in wastewater reuse. For example, in the NEWater project [52], in Singapore, after conventional water treatment processes, water goes through a series of filtration processes, from microfiltration to reverse osmosis, and an ultimate disinfection, resulting in high-grade water, suitable for industrial applications.

2.3.1 Conventional Wastewater Treatment

Water is typically treated in several stages at a wastewater treatment plant (WWTP) – Figure 2.4. In a preliminary stage, coarse solid particles and grease, which may cause operating issues

later, are removed through screening (steps 1 and 2). A mass fraction of about 50 % of the total pollutants are removed at this stage. In the primary treatment (step 3), most suspended solids and organic matter are removed from the wastewater. These steps are typically accomplished through flotation, in which the particles rise to the top of a tank with compressed air, and then are collected, or through mixing and flocculation followed by sedimentation. In the second process, a flocculant (usually a metallic salt) is added to the wastewater and the particles aggregate with the metallic ion due to electrostatic forces; the agglomerates are then separated through flocculent particle settling sedimentation. The secondary treatment (steps

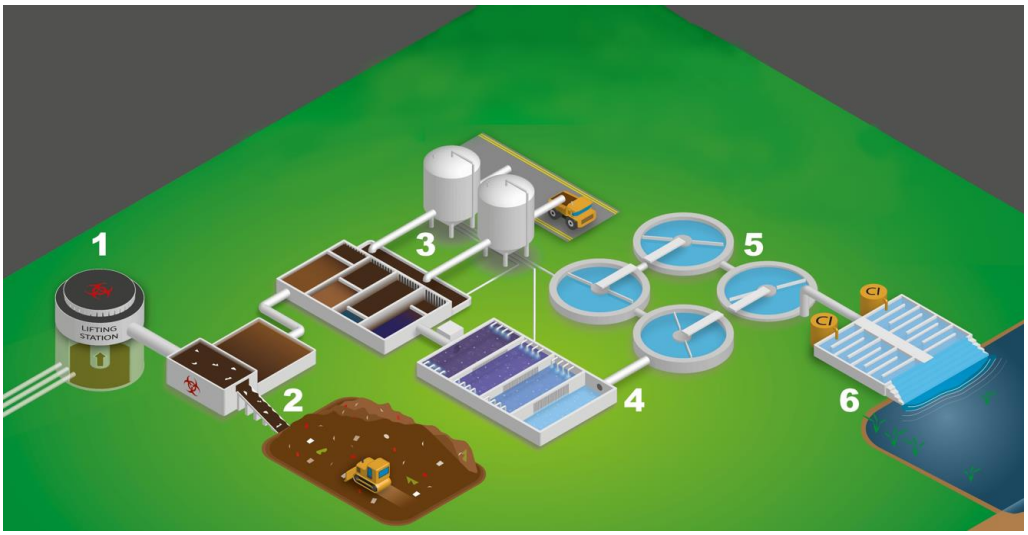

Figure 2.4 – Diagram of a wastewater treatment plant; 1) lifting station; 2) preliminary treatment; 3) primary setting basins; 4) bioreactors; 5) secondary clarifiers; 6) chlorine disinfection (adapted from [5]).

4 and 5) is typically a biochemical treatment, in which biodegradable organic matter, measured as biochemical oxygen demand, in solution or suspension is removed, as well as other nutrients. In this process, depending on the technology, either aerobic or anaerobic microorganisms are used to consume the organic matter. The wastewater is then separated into clarified water and sludge through sedimentation [53]. The final step in the wastewater treatment plant is disinfection by chlorination, ozonation or UV light (step 6), which aims to remove any pathogenic microorganisms and make the water safe to discharge.

Regarding industrial wastewater, prior to being sent to a WWTP, a preliminary treatment must be accomplished to remove specific organic compounds and heavy metals, which in turn might be difficult and costly to treat by conventional wastewater treatment processes. Furthermore, after treatment, some industrial facilities may reuse wastewater, reducing the utilization of this resource and lowering the water footprint [54]. For industries that consume hydrogen, it could be economically advantageous to treat and purify the produced wastewater in the plant, for subsequent hydrogen production through the treated water electrolysis. However, for obtaining water that can be fed into electrolysers, further, advanced treatment is required.

2.3.2 Advanced Water Treatment systems

Typically, advanced water treatment solutions are required to produce ultrapure water for industrial applications; the quality of water must obey to certain requisites for hydrogen production through water electrolysis, namely in resistivity terms (18.2 MΩ cm). The sequence of tertiary treatment steps to be considered varies depending on the water quality requirements for a certain application; however, a set of filtration steps, including ultrafiltration, nanofiltration and reverse osmosis are generally employed, with intermediate disinfection. These technologies encompass a membrane process to allow the separation of salts and minerals, micro-pollutants, and other suspended solids (reject stream or brine stream) from the purified water or permeate stream. In fact, reverse osmosis (RO) has emerged as the most promising technique for producing freshwater, having already attained a worldwide installed capacity of 95 million m^3 of freshwater per day [55]. Nevertheless, 50 % of the total costs associated with reverse osmosis plants are related to energy costs, due to the required high operating pressures. On the other hand, reverse osmosis is particularly attractive when the system is entirely and efficiently integrated with renewable energy sources, especially solar energy. Solar energy is considered to be the cheapest and most abundant energy source, having registered a cost reduction of about 90 % in the last decade [6]; thus, enabling the use of these filtration processes considering both the environmental and the economic aspects are indispensable. In these steps, water is pumped through membranes with several pore sizes, depending on the filtration type; generally, 0.1 µm for ultrafiltration and 0.1 nm for reverse osmosis.

Still, there are other alternatives for purifying water before feeding it into the hydrogen-producing devices. Ion exchange (IX) [56] resins are of particular interest due to their efficiency in the removal of trace metal ions from water. They normally consist of a styrene divinylbenzene copolymer and ion exchange group, that either possess acidic or alkaline properties, strong or weak, which are responsible for their cation exchange or anion exchange behaviour, respectively. Complexing groups are connected to mobile ions (H^+ or OH^-) that, during the process, are exchanged for the ions present in the affluent water – Figure 2.4. Ion exchange is a stoichiometric and reversible process. The selectivity and ion exchange rate of the resin for a specific ion is controlled by the selectivity coefficient (*K*), given by equation (12). B represents the mobile ion (H^+ or OH^-), which is present in the resin and A represent impurity ions in solution. A higher selectivity coefficient corresponds to a higher removal capacity, but also to a less efficient generation [57].

$$K = \frac{C_{B,resin} \cdot C_{A,solution}}{C_{A,resin} \cdot C_{B,solution}} \quad (12)$$

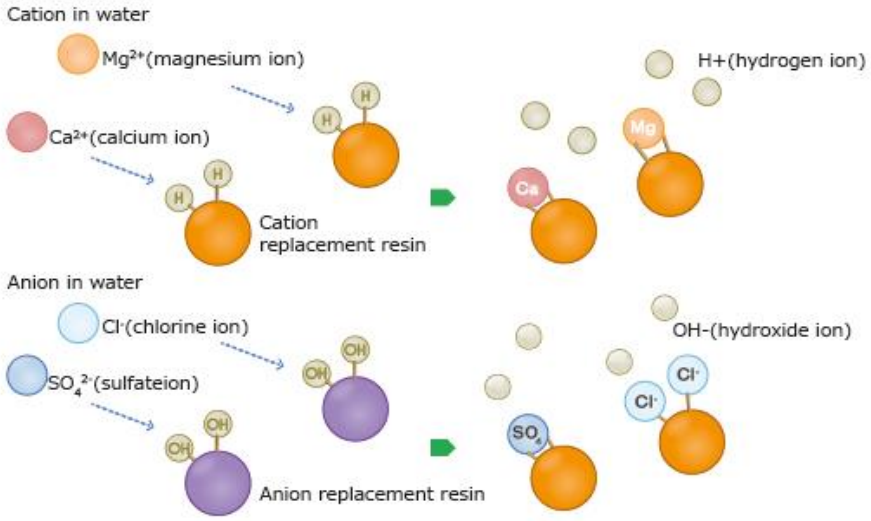

Figure 2.5 – Mechanism of ion exchange in strong acid (above) and alkaline (below) resins (extracted from [3]).

Ion exchange resins are often found inside a bed or a column through which the solution to be treated travels. Ions in solution generate bonds with ions in the resin's complexing group, until the resin is saturated, that is, until there are no more complexing groups available for bonding with the solution's ions and therefore there is no room to increase mass transfer. Thus, the resin must be regenerated using typically strong alkaline (sodium hydroxide - NaOH) or acidic solutions (sulphuric acid - H_2SO_4) to replace the impurity ions with H^+ and OH^- [57].

A common type of specialty resin are chelating resins. These resins are highly selective, and their affinity to a certain ion depends mainly on the chelating group. Though, the exchange process is slow and controlled by particle diffusion mechanisms [58]. This type of separation could be especially interesting if coupled with electrolysis considering a recycling step for the cell's exhausted water, since during long-term operation some metals may be leached out from the catalyst layers (such as iridium, platinum, or iron), as well as other impurities from the membrane or the PTL.

Overall, and comparing to advanced filtration technologies, such as RO, ion exchange resins are a reliable, proven technology for wastewater treatment; they have low power requirements, which results in lower operational costs in comparison to RO and lower CO_2 emissions and do not require water pre-treatment. Besides, the amount of water wasted in the process is lower (5% – 10% for IX versus 20% – 30% for RO) [59]. However, it is necessary the use of concentrated acidic and/or alkaline solutions for the regeneration of the resin, which must then be discarded.

These advanced water treatments are usually used for the production of industrial grade water from freshwater. However, they have not yet been tested for the production of pure water from treated wastewater, to be used as reactant in an electrolysis installation.

3 Materials and Methods

3.1 MEA Preparation

To prepare the membrane electrode assembly (MEA) for single-cell tests, several catalysts coated membranes (CCMs) and catalyst coated substrates (CCSs) were prepared using automatic spray deposition at a benchtop dispenser equipped with a robot FISNAIR F4300N. Since catalysts synthesis falls outside the scope of this work, commercial catalysts were used to prepare the MEAs, consisting namely of a platinum mass fraction of 40 % supported on Ketjenback EC 300 (Pt/C) as cathodic catalyst and IrO_2 powder to serve as anodic catalyst, both from Premetek Co.

3.1.1 Membranes Studied

Nafion® 115 and Nafion® 212 (Quintech) membranes were used for PEM electrolysis. These membranes are composed of a polytetrafluoroethylene (PTFE) backbone, which ensures mechanical and thermal stability, and by perfluorosulfonic acid (PFSA) as the proton exchange agent. These membranes are conditioned in the PEM cell, for 2 hours in ultrapure water at 1.8 V, for ensuring membrane hydration and and proper adaptation to the cell's conditions.

Fumasep® FAA-3-PK-130 (fumatech), Eurodia neosepta amx fg (Eurodia) and Sustainion X37-50 grade RT (Dioxide Materials) were used for AEM electrolysis. Studying the potential of the two latter is of particular interest since they are new in the market and these specific Sustainion membranes show great performance and stability; nevertheless, there is not much information available on their composition. For Eurodia membranes, as per the manufacturer's recommendation, the operating temperature must not exceed 60 °C for ensuring the membranes stability. On the other hand, Sustainion membranes have revealed the best results in the literature for AEM electrolysis and unveil a maximum working temperature of 80 °C, at which they present a conductivity of 140 $\mu S\,cm^{-1}$ in 1 M KOH [60].

3.1.2 Spraying Method

A catalyst ink was prepared by dispersing the catalyst powder in a water (Millipore) to isopropanol (VWR chemicals) 1:1 (V/V) solution, ensuring a total solids mass fraction of 0.4% The ratio between ionomer content and the total solids was set to 20 %, in mass. The loading of deposited catalyst was measured by mass difference obtained before and after deposition.

Considering PEM electrolysis, a Nafion solution with a mass fraction of 5 % (DuPont) solution was used as ionomer and the catalyst was directly deposited onto the membrane (resulting in a CCM) by spray deposition at 100 °C. After deposition on both sides, the membrane was hot-pressed for 5 minutes at 110 °C and 5 bar to stabilize both catalyst layers.

On the other hand, AEM membranes were firstly subjected to a pre-treatment, in which they were be kept in 1 M KOH solution for a minimum of 24 h to convert the membrane into the OH^- form. According to the manufacturer's instructions, the membranes must not be dried after the pre-treatment, because there is a strong risk of damaging the polymer backbone of the membrane. Therefore, for AEM single-cell tests, the CCS method was considered. Thus, at the anode side, a commercial hydrophilic GDE (ion powder, 0.4 $mg_{Pt}\,cm^{-2}$) was used at the anode side, IrO_2 catalyst ink was sprayed at 50 °C onto a copper foil (MTIcorp USA), used for improving water and gases mass transport, while being resistant to anodic potentials. The prepared ink had a solid mass fraction of 0.4 %, and the ionomer used was Sustainion XB-7 5 % (Dioxide Materials).

3.2 Electrolysis test bench

The electrolysis unit used consists of a 2-litter borosilicate tank, where water is heated to the working temperature of the cell, in a heating bath circulator, Julabo F25-MC. The bath is insulated to prevent water losses through evaporation. The water is then pumped to the cell by a peristaltic pump ISMATEC REGLO iCC, where the water flow can be controlled. The tubes are made of Perfluoroalkoxy alkane (PFA, Swagelok) and Polyuretane (Festo) and therefore can withstand the operating temperature of the circulating water. To maintain electrolysis working temperature, the single cell is placed in a Memmert UF 55 oven. The gas-saturated water that exits the electrolyser is sent to borosilicate glass closed vials which act as liquid-gas separators; the produced gases – H_2 and O_2 – are thus, sent to exhaustion, whereas the water is recycled for decreasing the overall water consumption. In some circumstances, water circulated through an column (with 20 cm height and 6 cm diameter) with an ion exchange resin Amberlite IRN150 before returning to the tank, in order to study the removal of contaminants from water exhausted from the cell. Figure 2.1 depicts the installation scheme, and Appendix A contains some images of the installation.

The electrolysis cell used (Quintech) had an active area of 5 cm^2. Figure 2.2 includes a diagram of the constructed cell as well as a breakdown of its various parts. The bipolar plates (a) were composed of bulk titanium, to prevent corrosion. The silicon-based gaskets (b), as well as titanium PTLs (c) were supplied with the cell. On the cathode side, carbon paper (f) SpectraCarb (Fuel Cell Store) was used as an additional diffusion layer; on the cathode side, for AEM membranes, copper foil (d) (MTIcorp USA) is used as a CCS. These components were sandwiched together, with the membrane (e), which was placed in the middle.

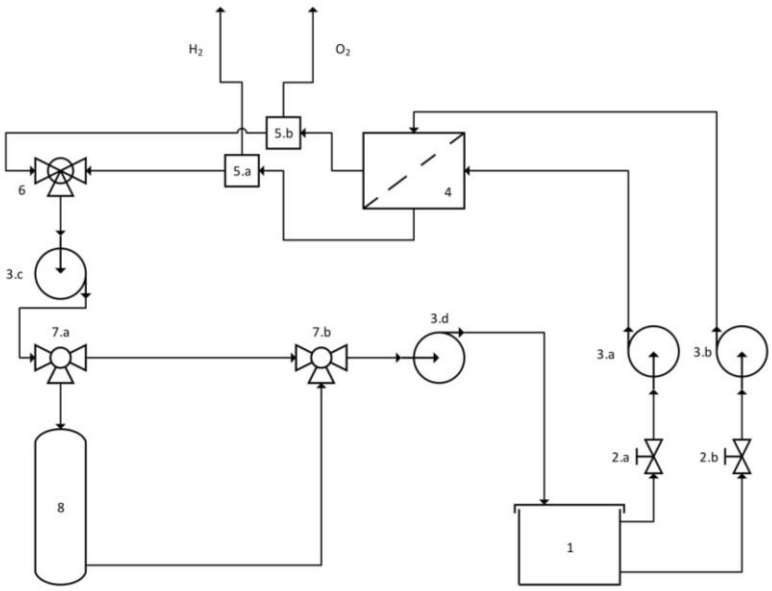

Figure 3.2 – Sketch of the electrolysis unit. 1) Feed tank; 2) On/off valve; 3) Peristaltic pump; 4) Electrolysis cell; 5) gas/liquid separator; 6) mixing valve; 7) 3-way mixing valve; 8) Ionic exchange resin column

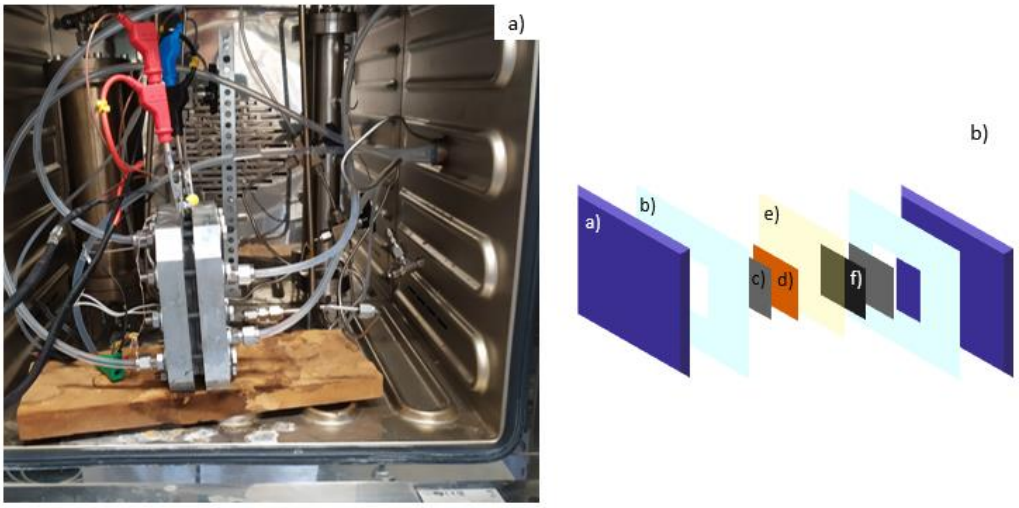

Figure 3.1 – a) Image of the assembled electrolysis cell; b) scheme of the cell assembly, with a) Bipolar plate, b) Gasket, c) Titanium PTL, d) copper CCS, e) membrane, f) carbon paper diffusion layer.

3.3 Filtration Unit Installation

A filtration unit installation was developed with the intent of further purifying wastewater. The installation consisted of a feed tank (1), a rententate tank (6) and a permeate tank (7). Water was fed into the Osmonics' high pressure RO cell (5) through a high-pressure pump. The pressure is measured and regulated through a pressure gauge (3) and a valve (4.a), respectively. The flow of retentate and, by consequence, of the permeate is controlled through valve (4.b). Images of the installation are present in appendix A.

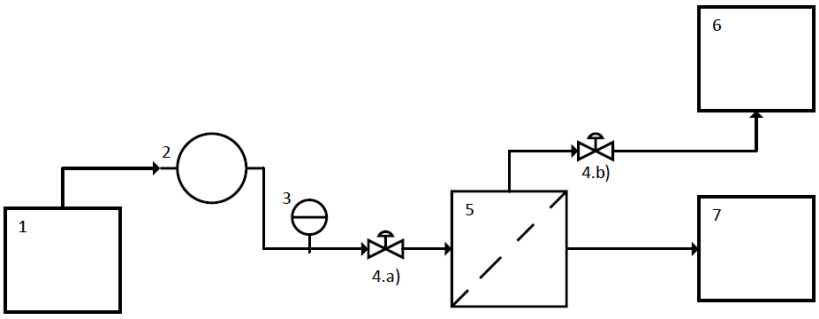

Figure 3.3 – Sketch of the filtration unit. 1) Feed tank; 2) Pump; 3) Manometer; 4) Valve; 5) Filtration module; 6) Retentate tank; 7) Permeate tank.

3.4 Electrochemical Characterization

3.4.1 Polarization Curve

All electrochemical characterization tests were performed using an Autolab PGSTAT204 potentiostat/galvanostat, equiped with a Booster of 10 A. Potential was measured at different values of applied current. The current varied between 0 A and the limiting current that ensures the cell stability, typically 6 A. Smaller increments of 0.10 A were made at lower currents between 0 A and 1 A, and then larger steps of 0.25 A were considered between 1 A and the limiting current. For each applied current, the dwell time was 30 s, for attaining the steady-state, and a potential value was retrieved at every 2 seconds. Solely the average of potential values measured at the last 10 s at each current step were considered to obtain the polarization curves, in order to achieve steady state.

3.4.2 Electrochemical Impedance Spectroscopy

Electrochemical Impedance Spectroscopy (EIS) was used for collecting information on the activation, ohmic and mass transport resistances on the cell. EIS was performed in galvanostatic mode, for 0.2 A, 1 A, 2 A and 4 A, considering frequencies ranging from 2500 Hz to 100 mHz. The amplitude of the perturbation was set up to 8 % of the current at which the test was performed. Each test was preceded by a conditioning period of 20 s.

3.4.3 Accelerated Stress Test

The accelerated stress tests (AST) were carried out to assess the degradation mechanisms occurring in the electrolysis cell over a long period of use, especially when using purified wastewater and seawater. The AST consisted of cycling the potential between 1.5 V and 2.5 V, with step times of about 1 min, for 15 hours. This AST is based on known high stressors for the membrane, like high potential difference, and square-type cycling potentials [43, 44].

3.4.4 Water characterization

Conductivity (σ), resistivity (ρ) and total solid content (TDS) in the wastewaters tested were measured by the conductivity meter pHenomenal (VWR).

Other water parameters were analyzed elsewhere. These parameters are: conductivity, chemical oxygen demand, biological oxygen demand, total nitrogen, nitrate, nitrite, sodium, potassium, iron, nickel, copper, magnesium, lead, calcium, zinc, sulfate and chlorite concentration.

The conductivity measured by the conductivity meter and measured elsewhere were consistent.

3.5 Physical Characterization

3.5.1 Fourier-Transform Infrared Spectroscopy

Fourier-Transform Infrared (FTIR) Spectroscopy was performed by a Bruker VERTEX70 apparatus in the 400 cm^{-1} – 4000 cm^{-1} range at room temperature using air as sweep gas at 8 $ml\,min^{-1}$ to analyse the composition of the different membranes used. Furthermore, it was used to analyse the presence of impurities in the tested wastewaters.

3.5.2 Thermogravimetric Analysis

Thermogravimetric analysis (TGA) was performed by thermal analyser STA 449 F3 Jupiter (NETZSCH). The analysis was made from 20 °C to 900 °C, with a heating ramp of 5 $°C\,min^{-1}$, under oxygen flow. The main objective was to understand thermal stability and the amount of volatile material present on the tested membranes.

3.5.3 Scanning Electron Microscopy

Scanning Electron Microscopy (SEM) makes use of an electron beam for scanning a sample and to produce a magnified image (in the micron range). SEM was used to examine the morphology of the catalyst layer and analyse its thickness, as well as the membrane's, using a field emission scanning electron microscope (PhenomPro XL). SEM images were obtained at different magnifications (up to 12500x) to decipher features at the nanoscale.

4 Results and discussion

4.1 Preparation of membrane electrode assemblies

Initially, both catalyst coated membranes (CCMs) and catalyst coated substrates (CCSs) were prepared using an automatic spray device. For both PEM and AEM water electrolysis, the catalysts used were IrO_2 for the anode side (OER) and platinum supported on carbon with a mass fraction of 40 % of platinum, for the cathode side (HER). Loadings of $0.30 \pm 0.05\,mg_{Pt}\,cm^{-2}$ for the cathode side and $0.50 \pm 0.05\,mg_{Ir}\,cm^{-2}$ for the anode were obtained. An example of a prepared CCM is represented in figure 4.1.

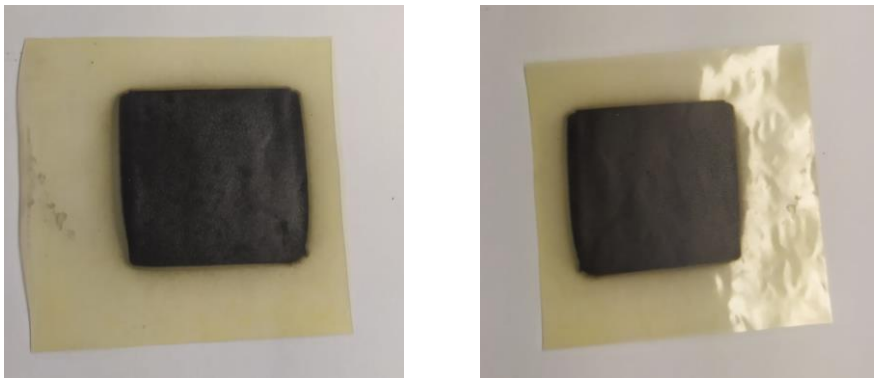

Figure 4.1 – Figure of a catalyst coated membrane with IrO_2 as anode and Pt/C as cathode, with $0.50\,mg_{Ir}\,cm^{-2}$ and $0.26\,mg_{Pt}\,cm^{-2}$, respectively.

4.2 Assessment of operating conditions for the water electrolysis test station

The main objective of the assembled test station, depicted in Figure 3.2 and in appendix A, is to mimic the operation of an industrial installation. It was thus necessary, and before running any characterization experiments, to unveil the most suitable operating conditions for the 25 W water electrolysis test station. The studied variables include temperature, inlet water flow rate at the anode and cathode and liquid electrolyte concentration. As the energy needed for the reaction varies with temperature, thermoneutral potential was calculated – appendix C; thermoneutral potential does not change significantly with the temperature: it has a value of 1.475 V at 60 °C and 1.474 V at 70 °C. The following subsections provide insights on the electrochemical evidence which underpin the most proper operating conditions for the used single-cell test bench, which are similar to that of a typical electrolyser plant.

4.2.1 Proton Exchange Membrane Water Electrolysis (PEMWE)

Ultrapure water (Millipore), with a resistivity of 201 kΩ cm at 23 °C, was fed to the PEM water electrolyser. Usually, water electrolysis occurs above 50 °C in order to reduce cell overall impedance and below 90 °C, to maintain the material's, mainly membrane's and ionomer's, chemical and mechanical integrity [23]. Two Nafion membranes, Nafion 115 and Nafion 212 were tested, and their performances were similar – appendix F. In this regard, the following tests were performed with a Nafion 115 membrane.

The cell was firstly tested, by feeding a water flow rate of 30 ml min^{-1} (*ca.* 536 times the stoichiometric flow, calculated in appendix D) to both electrodes at 60 °C and 70 °C. From the analysis of the polarization curve, shown in Figure 4.2, it can be concluded that the cell reaches the highest performance at higher temperatures, specifically at 70 °C. From the analysis of the Nyquist plot (Figure 4.2 b) the overall charge transfer resistance is similar for both cell assemblies; nevertheless, the ohmic resistance, associated mainly to the membrane and ionomer, decreases with raising temperatures. This finding is consistent with that of Silva*et al.* [61], who measured the conductivity of Nafion membranes and related it with their thickness and operating temperatures. Besides, at both temperatures, the resistance associated with the cathodic reaction is negligible compared to the resistance of the anodic reaction, evidenced by the single visible contribution in the Nyquist plot, as expected, attributed to OER.

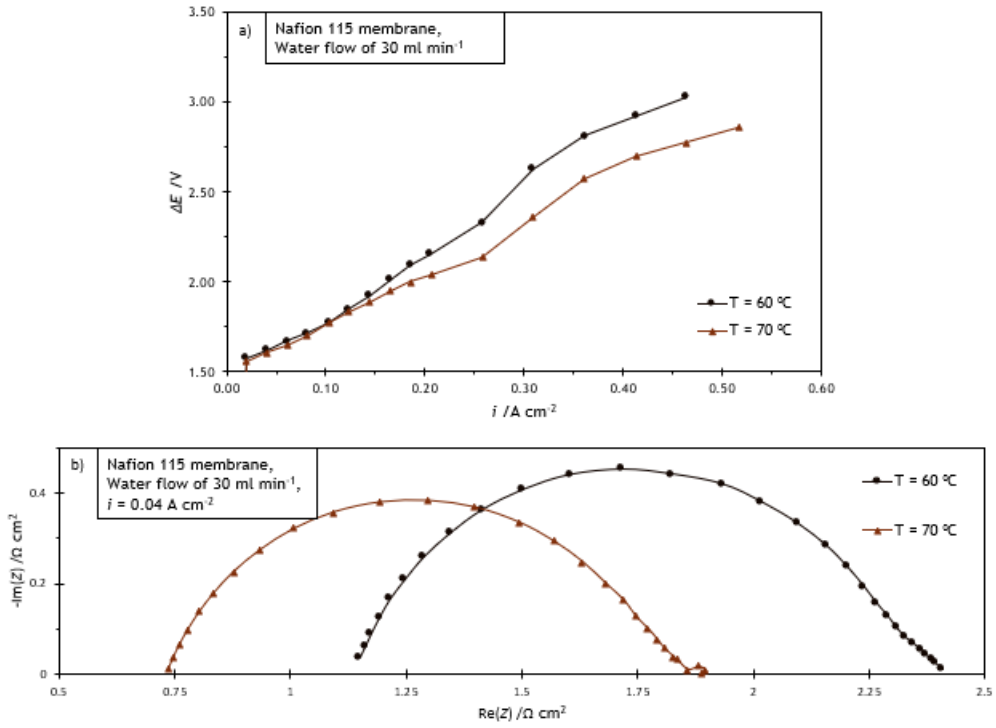

Figure 4.2 - a) Polarization curve and b) Nyquist plot at 0.04 A cm^{-2} for different temperatures, for a Nafion 115 membrane, with a pure water feed flow rate of 30 ml min^{-1}.

The performance of the electrolysis cell was then tested for different feed water flow rates, The stoichiometric flow of water, for a cell operating at a current density of 2 A cm^{-2}, is 0.056 ml min^{-1} (appendix D). Several water flow rates were tested, at 70 °C, from 5 times the stoichiometric flow (0.28 ml min^{-1}) to *ca.* 500-fold higher the stoichiometric flow (30.00 ml min^{-1}). The results are displayed in Figure 4.3.

The optimal water feed flow rate to each electrode was considered to be 5.60 ml min^{-1}, which corresponds to *ca.* 100-fold the stoichiometric flow. It was considered that most of the water fed to the anode side of the cell served as reactant to the OER, whilst the water supplied to the cathode served mainly as a drag fluid to aid on the exhaustion of the hydrogen gas. The reasons for such a high reactant demand are mainly the pressure drop associated with internal friction of the fluid (viscosity) and friction between fluid and walls of the tubes and other connections in in the hydraulic circuit, depending on their length, and material type (roughness); therefore it is expected that the flow rate reaching the cell will be smaller than the one imposed at the pump. Besides, the water is not only important as reactant for the electrolysis reactions, but also to keep the membrane hydrated, which boosts the ionic conductivity by enabling the proper solvation of protons that are transported through the membrane from the anode towards the cathode. These findings contradict the current trend on techno-economic studies [49, 62], in which it is commonly assumed that just 9 kg of water (the stoichiometric amount) is required to produce 1 kg of hydrogen.

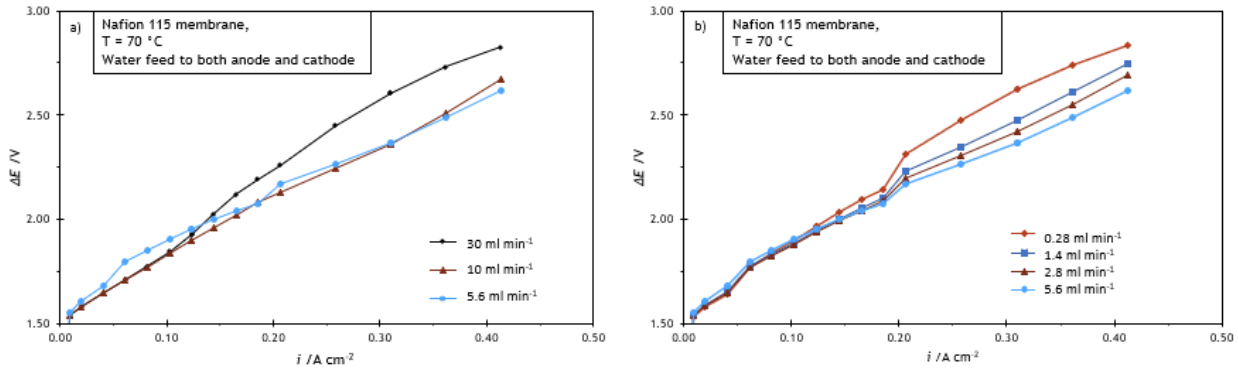

Figure 4.3 – Polarization curve for different water feed rates at both the anode and the cathode a) above the optimal feed flow rate and b) below, for a Nafion 115 membrane in an electrolysis cell working at 70 °C

In the activation region (until 0.04 A cm^{-2}), the amount of water required for the reactions to occur is minimal, and thus there is not an effect on efficiency loss due to starvation of reactant

since water is fed in surplus. In this region, the efficiency is dependent mainly on kinetic properties of the catalysts that perform both the OER and HER.

At the ohmic region (starting from 0.04 A cm^{-2}), varying flow rate of fed water begin to influence the cell potential difference. For lower water flow rates, even if higher than the stoichiometric flow, (*e.g.* at 0.28 ml min^{-1}, Figure 4.3.b), the proper hydration of the membrane may be compromised, leading to local drying, preferential paths and hot spots in the electrolysis membrane [63], which results in higher ohmic resistances, as can be observed in Figure 4.3.b). In fact, it was possible to observe this phenomenon when SEM analysis was carried out on catalyst coated Nafion membranes on the anode side (Figure 4.4), in which it is possible to discern various preferential paths in the uneven catalyst layer. These findings are consistent with those observed in previous works, where CCMs were tested in electrolysers under similar operating conditions and preferential paths in the catalyst layer are also reported [64, 65].

These preferential paths may explain the overpotential jump observed at greater current densities, around 0.20 A cm^{-2} in the polarization curve from Figure 4.3.b), as it gets steeper as the water flow rate decreases, and thus, there is shortage of water.

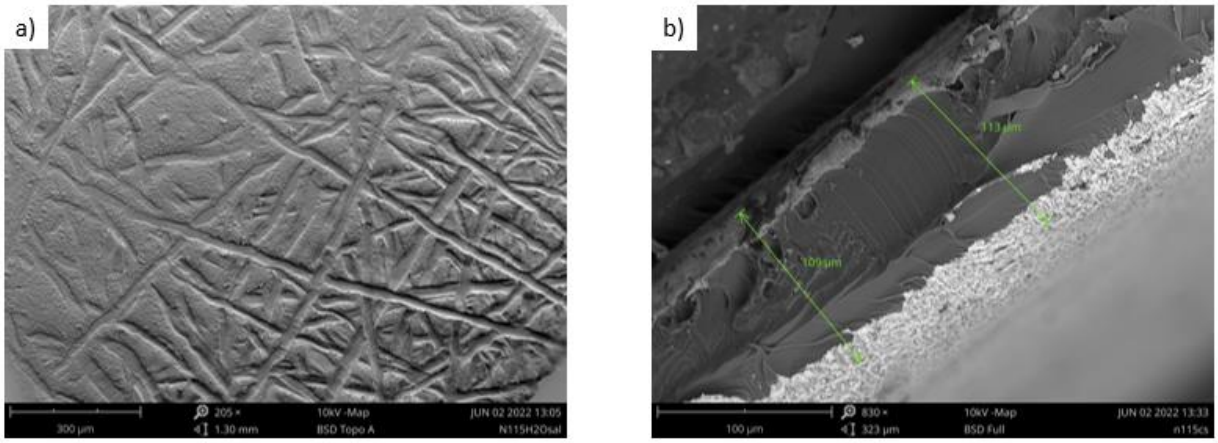

Figure 4.4 – SEM images of the anode side of a catalyst (IrO_2) coated Nafion membrane from a) top view and b) cross section.

On the other hand, at higher water feed flow rates (above 10 ml min^{-1}), the ohmic resistance increases, as seen in Figure 3.3.a); this may happen since the flow of inlet water is opposite to the gas exhaustion direction (H_2 and O_2), and thus an increase in water flow may prevent gas bubbles from leaving the catalyst layer and entering the flow channel.

Different water feed methods were also screened: water feeding to the anode side of the electrolysis cell, to the cathode side and to both the anode and cathode. The polarization curves obtained are represented in Figure 4.5.

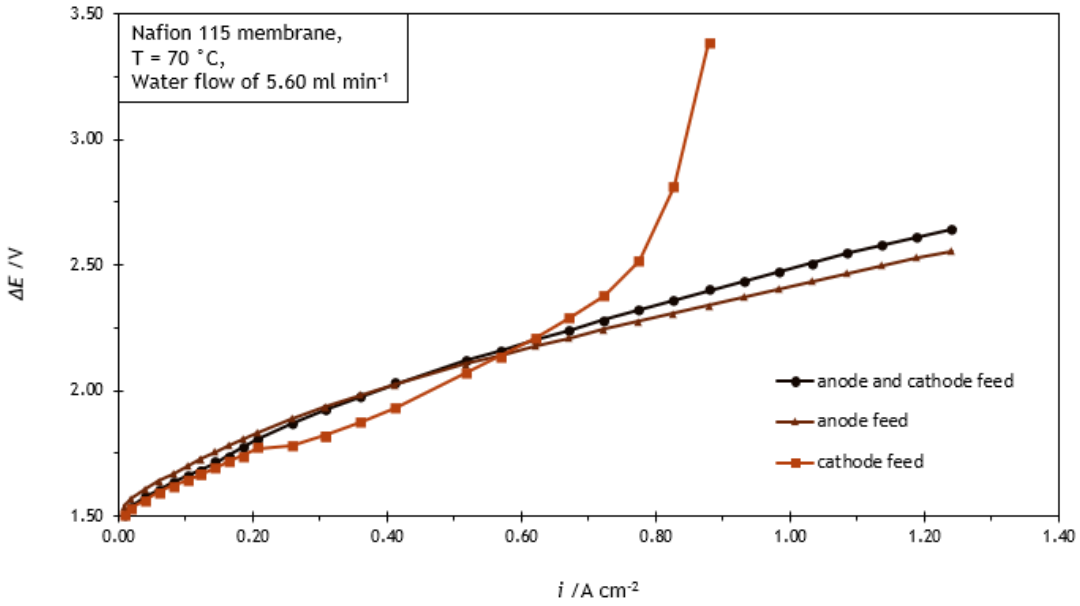

Figure 4.5 - Polarization curves for different circulation methods at the PEMWE cell with a Nafion 115 membrane, working at 70 °C and a feed flow of 5.60 ml min^{-1}.

The activation overpotential region (up to *ca.* 0.10 A cm^{-2}), Figure 4.5, is similar for all the systems, varying negligibly if the water is solely supplied to the anode, cathode or to both sides or even with varying flow rate, as seen previously - Figure 4.3. However, the same trend is not observed at higher current densities. When water is fed solely to the anode side, the cell efficiency is very similar to that of when water that is fed to both sides simultaneously. However, at the concentration overpotential region (> 1.00 A cm^{-2}), the performance is slightly enhanced when the water is solely fed to the anode, which suggests that the water fed to the cathode side serves not only to enable exhausting the product (H_2) but it is also transported from the cathode to the anode by diffusion mechanisms (due to concentration difference, since the water fed to the anode is consumed), causing additional water-gas management difficulties [35]. When water is fed only to the cathode side, while low current (below 0.40 A cm^{-2}) is applied, the potential is lower than expected and thus the performance appears to be enhanced. This indicates that diffusion is an efficient mechanism to transport water from the cathode to the anode, where the OER (limiting reaction in which water is consumed) takes place, at lower currents, while ensuring fully hydration of the membrane. Operating the PEM water electrolysis cell at higher currents, though, while supplying the cell via the cathode side is ineffective since the concentration of water molecules at the anode catalyst surface becomes insufficient, since the diffusion of water through the membrane becomes the limiting step. This

way, there is a steep decrease in the cell's efficiency, demonstrated as an increase in potential from 0.60 A cm^{-2} in the polarization curve for the cathode feed, in Figure 4.5.

For the best conditions considered, that is, 5.60 ml min^{-1} of ultrapure water fed to the anode, and a working temperature of 70 °C, it was obtained a current density of 0.18 A cm^{-2} at 1.8 V. García-Valverde, Espinosa [33] obtained, for the same temperature and potential, a current density of 1.20 A cm^{-2}.

An accelerated stress test (AST), consisting of 15 hours of cycling between 1.5 V and 2.5 V was performed. Figure 4.6 shows the polarization curves obtained before and after the AST.

There is no visible degradation after 15 h of continuous operation (Figure 4.6). In fact, the performance increases slightly in the activation region (*ca.* 29 % at 2 V), probably due to the rearrangement of the catalytic layer through Ostwald ripening, reprecipitation and coalescence, and the increase in porosity, that may have a positive effect on the availability of active sites, which increase in number [66].

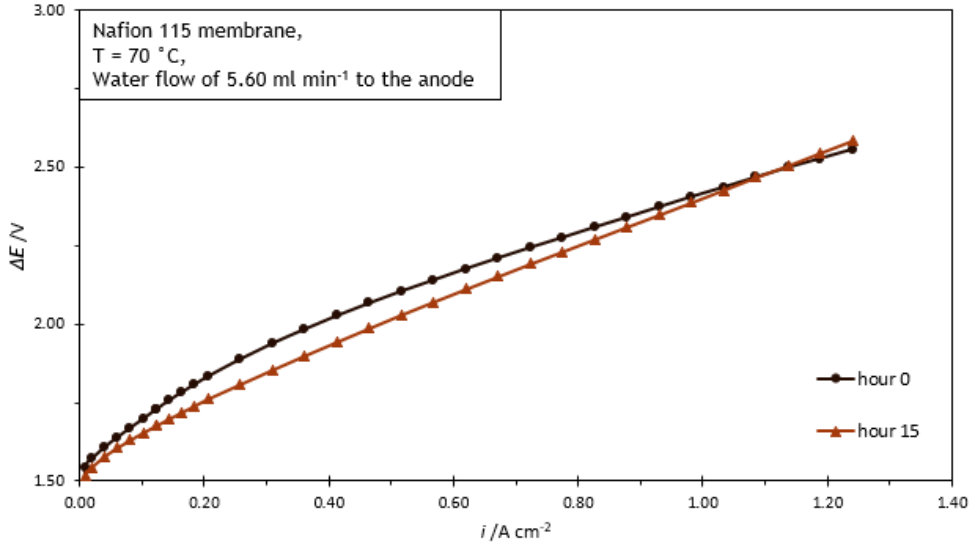

Figure 4.6 – Polarization curves obtained before and after a 15 h AST, for a Nafion 115 membrane in an electrolysis cell working at 70 °C, for a water feed flow rate of 5.60 ml min^{-1} to the anode.

4.2.2 Anion Exchange Membrane Water Electrolysis (AEMWE)

A similar approach was followed for screening the best operating conditions when using a AEMWE cell. Several solid electrolytes, of different chemical compositions, were tested, namely Eurodia neosepta amx fg (Eurodia), fumasep® FAA-3-PK-130 (fumatech) and Sustainion (Dioxide Materials) membranes (see appendix B and E for FTIR and TG analysis). Additional

information on the performance of the electrolysis cell for each membrane is detailed in appendix G.

Since AEMs have low electrical conductivity, typically an alkaline solution is supplied to the cell. Thereafter, the effect of electrolyte concentration on the cell performance was studied using, firstly Eurodia membranes. In this study, a KOH solution was used as an electrolyte, as it is the best liquid electrolyte reported in literature to date, due to its high conductivity, compared to other electrolyte solutions, such as sodium hydroxide (NaOH) and potassium bicarbonate ($KHCO_3$) [67, 68]. Different concentrations (0.2 M and 0.5 M) were studied in terms of cell performance and their effects on system degradation upon long-term operation (Figure 4.7).

The tests performed indicate that a higher concentration of electrolyte leads to a better performance of the cell (Figure 4.7.a), mainly by enhancing membrane conductivity (about an 81 % increment in current density at 2 V, for an electrolyte concentration of 0.5 M, in comparison to that of 0.2 M) and, therefore, decreasing the ohmic resistance.

However, potassium ions can react with dissolved CO_2, leading to the formation of potassium carbonate, which can be deposited at the active sites of the catalyst, leading to activity loss. Furthermore, the membrane may lose its ionic conductivity over time, leading to a higher ohmic resistance [67]; this can be observed in the polarization curves and Nyquist plots before and after the 15-hour AST – appendix G. The mentioned contributions, in Chapter 2.1.6, are responsible for a faster degradation on the cell performance when a higher electrolyte concentration is used – Figure 4.7.b). Besides, from the exhausted water analysis, when it is fed to the electrolysis cell working with an Eurodia membrane, the content of carbon is quite high (671.5 mg L^{-1}), which indicates that the carbon paper has degraded along the stress test.

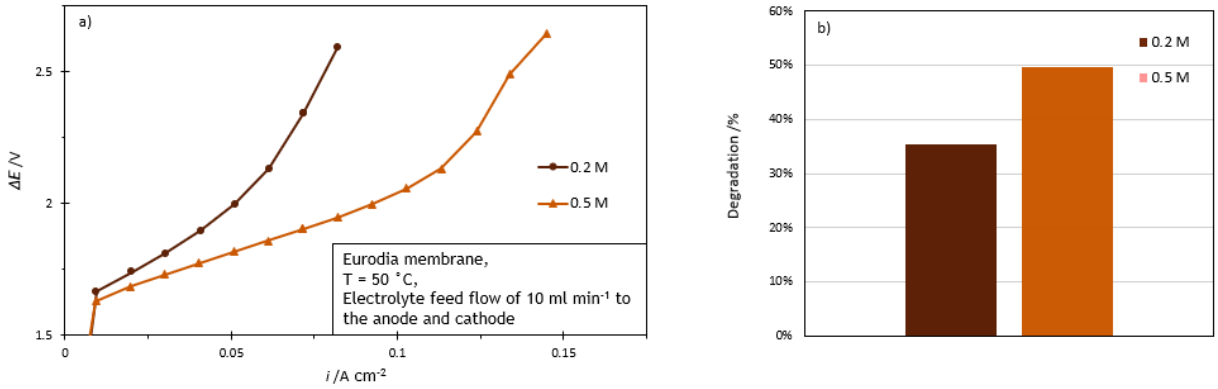

Figure 4.7 – a) Polarization curve for Eurodia membranes operating in an electrolysis cell at 50 °C for different liquid electrolyte concentration; b) Degradation ratio measured at 2.5 V after performing an AST for 15 h.

As a result, it was decided that subsequent tests with AEM membranes would be performed with an electrolyte concentration of 0.2 M. For subsequent tests, a Sustainion membrane was used due to its outstanding performance when compared with Eurodia or fumasep membranes – appendix G.

The performance of the AEMWE was investigated by varying the electrolyte feed flow rate and the feeding method when both Sustainion membranes and ionomer were employed, at 60 °C and while using a 0.2 M liquid KOH electrolyte, as seen in Figure 4.8. Similarly to PEM water electrolysis, the best feed flow rate is 5.60 ml min^{-1}. Contrarily to what happens in PEMWE, the best performance in not obtained when water is fed to the electrode where water spilling occurs (the cathode in the case of AEM), but rather when water is fed to the anode.

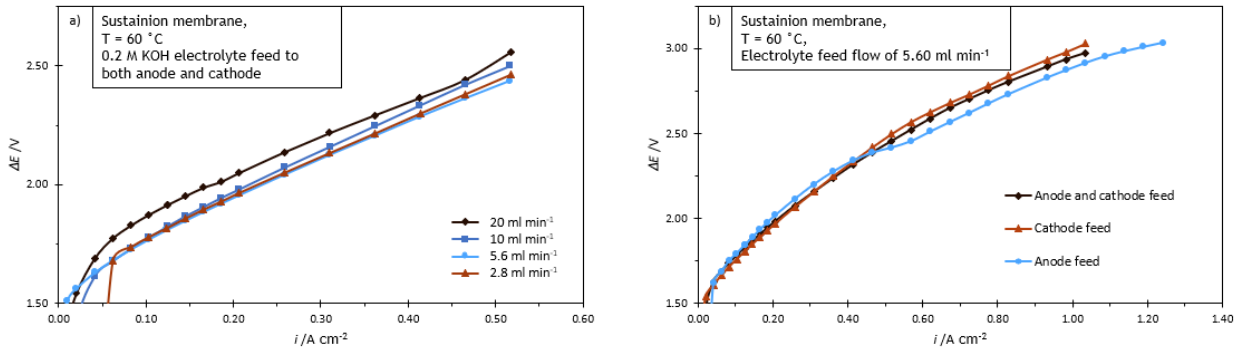

Figure 4.8 – a) Polarization curve for different electrolyte (0.2 M KOH) feed flow rate and b) different feed method with a feed flow rate of 5.60 ml min^{-1} to an electrolysis cell working with a Sustainion membrane at 60 °C.

Upon achieving the optimal operating conditions, namely a feed flow rate of 5.60 ml min^{-1} to the anode, using a 0.2 M KOH solution at 60 °C, an AST, consisting of potential cycling between 1.5 V and 2.5 V during 15 hours, was performed. The performance decay was practically negligible after performing the cycling steps (*ca.* 15 % at 2 V), until it short-circuited at around 10 hours of continuous operation under stress conditions.

Sustainion membranes are, at the moment, the highest performing AEMs reported in the literature. These membranes present an area specific resistance (ASR) of 0.045 Ω cm^2 and a conductivity of 115 µS cm^{-1} at 60 °C in 1 M KOH, due to its imidazolium functional groups, which improve its ion exchange capacity [60]. Pushkareva, Pushkarev [65] compared three different membranes (Sustainion, AEMION and A-201) and discovered that, for the same operating conditions, Sustainion membranes unveil the highest performance. Besides, Motealleh*et al.* [69] studied the membranes stability over periods of 11 000 hours at a steady current density of 1 A cm^{-2}, for an electrolyte (KOH) concentration of 1 M, and reported a minimal degradation of 8 mV in that time period. However, in this work, some limitations in the use of this membrane

for water electrolysis were found. Firstly, the membrane is extremely sensitive to higher cell potential differences; when potentials above 2.5 V are applied, the membrane short-circuits instantly. Secondly, this study has been unable to demonstrate the membrane's stability as showed in Motealleh, Liu [69] study, which may be linked to the nature of the degradation tests, which were of steady current in the case of Motealleh's study, but of cycling potential in this work. Overall, it seems that these membranes may be suitable for assembly in electrolysers which mostly operate under constant power conditions but, for electrolysers operating at varying potentials, as it may the case of ones connected to renewable, intermittent, energy sources (*e.g.* photovoltaic panels), these membranes may not be the most appropriate.

4.3 Wastewater Characterization

Three different wastewaters, two of them from municipal water treatment facilities (Arcos de Valdevez and Ave) and one from an industrial wastewater treatment plant (CIN) were tested as feed for both PEM and AEM electrolysers. Despite being treated in a municipal WWTP, Ave wastewater contains some textile industry effluent, which influences its composition. The results of the characterization made can be found in annex N.

Overall, all three wastewaters present high chemical oxygen demand and biological oxygen demand, which indicate the presence of biological matter and microorganisms, respectively. Besides, all show high content (above 100 mg L^{-1}) of sodium and chloride. FTIR analysis was also performed on all three wastewaters (appendix H), and, in comparison to an ultrapure water spectrum, some activity, namely between *ca.* 1000 cm^{-1} and 1500 cm^{-1} could be detected. This zone is characteristic of C-N, C-O, N-O and S-O bounds. The intensity of the transmittance spectra was higher for Arcos de Valdevez wastewater which is the one with a higher carbon and sulfate content.

Comparing the two municipal wastewaters, both with secondary treatment at the WWTP, there are considerable differences in the parameters studied. Overall, Arcos de Valdevez wastewater had a higher content in pollutants, namely in organic matter, potassium, calcium, and sulfates. The parameters from CIN industrial wastewater are comparable with the ones from both municipal wastewaters, with exception of the concentration of organic carbon and magnesium, that are about 10-fold higher than on the municipal wastewaters.

Among the considered pollutants, according to the potential (*vs.* SHE – Standard Hydrogen Electrode) at which their oxidation occurs (annex N), only chlorine is susceptible to oxidation (in an acidic environment). However, other impurities, such as sodium, calcium, copper, and iron may poison the membrane and catalyst layer. Besides, the high amount of organic matter may lead to fouling of the membrane and of the PTL, in a similar manner to what happens in RO membranes.

4.4 Performance and stability of PEM and AEM electrolysers using feed waters of several origins

4.4.1 Salt water (seawater)

In order to test the influence of a known contaminant, the electrolysis of a solution of 25 mg L^{-1} of sodium chloride (NaCl) was studied. This value is on *par* with the concentration of salts in the effluent of a tertiary water treatment when ultrafiltration and reverse osmosis are employed. The conductivity (σ), resistivity (ρ), and total dissolved solid content (TDS) of the fed water are presented in table 4.1.

PEMWE

Comparing the polarization curves of electrolysis of pure water and of the NaCl solution, represented in figure 4.9.a), it is observed that the activation region is different for each curve, which may indicate the presence of parasitic reactions, or that the Na^+ ion, present in the water, may be precipitating on the catalyst layer or inside the membrane, namely on the anode side, where the water is fed, interfering with the reaction and with the membrane's ion exchange capacity. After an accelerated stress test of 15 hours, a 6 % degradation in performance at 2 V can be observed. Besides, the solid content in the recycled water increased - Table 4.1 - which indicates leaching of the cell's components. Figure 4.9.b) contrasts the Nyquist plots before and after the 15-hour AST, for pure water and saltwater; it shows a second arc in the impedance spectra for saltwater, indicating that the cell, at 0.41 A cm^{-2}, reaches the mass transfer region (Re(Z) > 0.28 Ω cm^2), following the AST, when fed with saltwater. This suggests that the ions present in solution may be accumulating in the catalyst layer, preventing gaseous products from traveling through the PTL and exiting the cell [22].

Table 4.1 – Parameters of ultrapure water and NaCl solution

	T /ºC	σ /µS cm^{-1}	ρ /kΩ cm	TDS /mg
Pure water	69.9	3.4	205	6
NaCl solution at hour 0	74.6	61.7	16.15	122
NaCl solution at hour 15	75.3	76.8	13.16	135

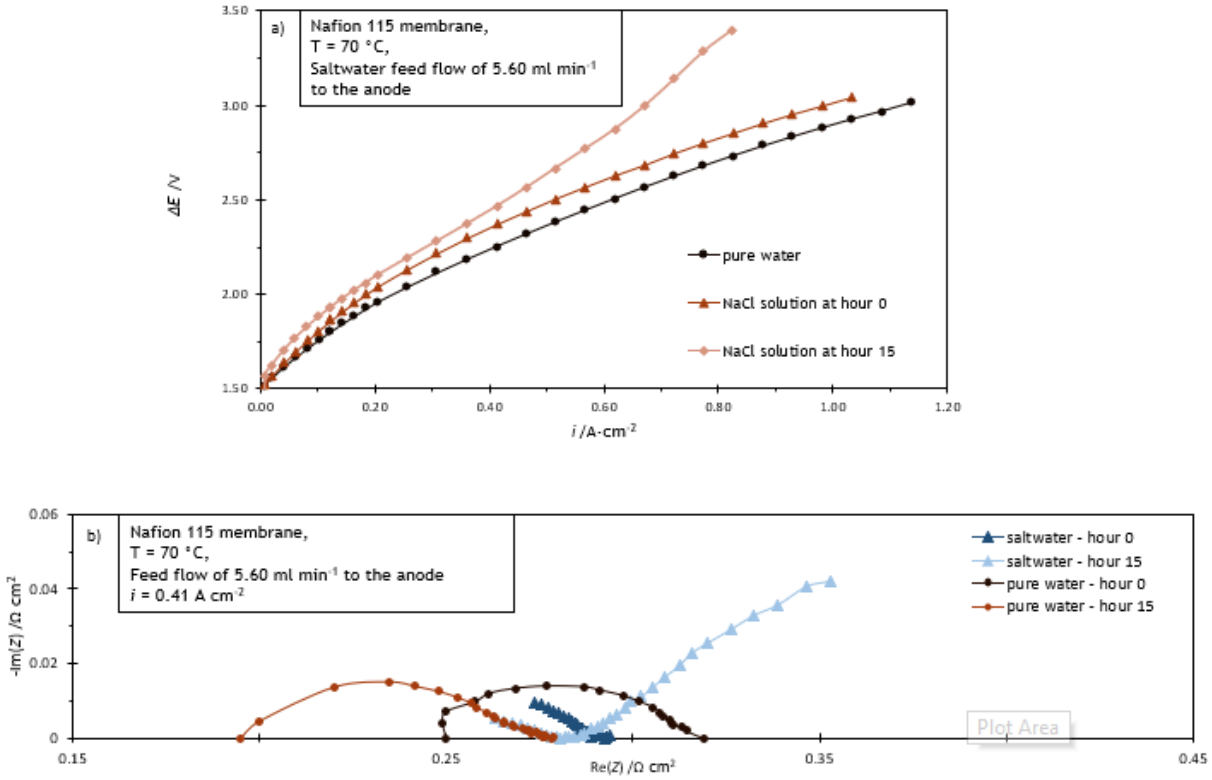

Figure 4.9 – a) Polarization curves of pure water and a solution of NaCl before and after an AST b) Nyquist plot at 0.41 A cm^{-2} of a 25 mg L^{-1} solution of NaCl, both fed at a feed flow rate of 5.60 ml min^{-1} to the anode, working at 70 °C.

AEMWE

The same tests were carried out for AEMWE, using a Sustainion membrane, while circulating a 0.2 M KOH electrolyte. *Per* the literature [70], AEMWE seems more promising than PEMWE for hydrogen production through direct saltwater electrolysis, since the potential difference between OER and CER is greater (about a 460 mV difference – Image 2.3) at a higher pH and, therefore, the OER seems to be favoured in detriment of the chlorine oxidation. However, in this work, it was concluded that the membrane suffered greatly by the addition of salt, leading to its short-circuit almost instantaneously, which may indicate that, in order to have a properly working electrolysis cell, with these specific Sustainion membranes, there must be a limit on solid content or on NaCl concentration fed to the electrolysis cell.

4.4.2 Non-treated wastewater

For both AEMWE and PEMWE, municipal wastewaters were fed to the electrolysis cell, with only a previous vacuum filtration, with filter paper (VWR) with a particle retentions size of 12 µm - 15 µm, to remove coarser solids present in the wastewater.

PEMWE

The degradation in 15 hours for PEMWE, with Arcos de Valdevez and Ave wastewaters as electrolysis cell feed, were tested. The difference between electrolyser performance working with ultrapure water and Arcos de Valdevez and Ave wastewater, at 2.5 V, is 88 % and 53 %, respectively (appendix I). In the 15 h of AST, for Ave and Arcos de Valdevez wastewater, cell degradation of 70 % and 82 % at 2.5 V was obtained, respectively.

From the TG analysis - Figure 4.10 – where the evolution of the sample with rising temperature is evaluated, there is a slower degradation between 300 °C and 400 °C for the membranes used in wastewater electrolysis in comparison to that used in pure water electrolysis, which implies that the membranes were doped with metallic ions. For higher temperatures (>500 °C) the solid residue content, that did not degrade with the temperature, is significantly higher (11 % for Arcos de Valdevez and 7 % for Ave). This correlates to the contaminant content in the studied wastewaters: Arcos de Valdevez water has a much higher content in calcium and potassium, which settle in the ion exchange groups inside the membrane, due to Nafions´ sulfonic group affinity with these contaminants, increasing in the charge transfer resistance [22, 71].

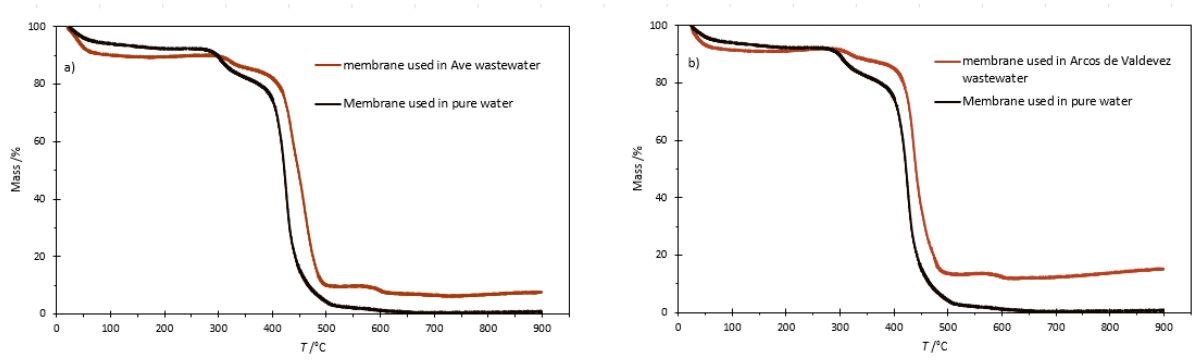

Figure 4.10 – TG analysis of the Nafion membranes used in a) Ave and b) Arcos de Valdevez wastewaters in comparison of with that used in ultrapure water.

AEMWE

For AEMWE, Arcos de Valdevez wastewater was tested. There is little to no difference in performance between ultrapure water and Arcos de Valdevez water – Figure 4.11. The degradation during the AST was minimal (*ca.* 10 %), and it happened mainly on the first hour of operation. However, at around the fourth hour of operation, the membrane short-circuited (appendix J).

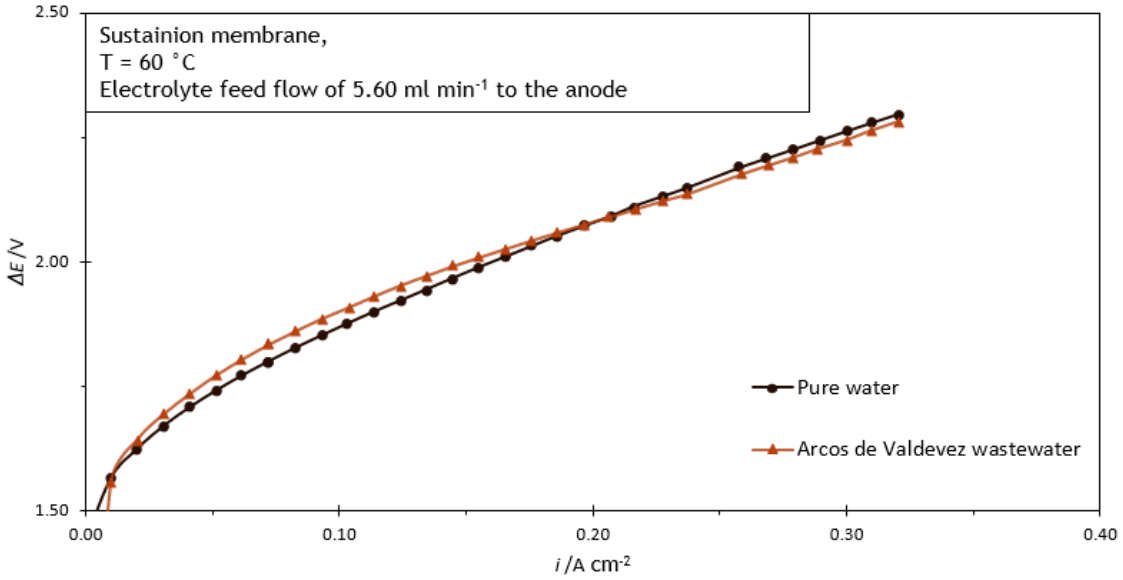

Figure 4.11 – Polarization curve of a AEM water electrolysis cell, for ultrapure water and Arcos de Valdevez untreated wastewater, for a feed flow rate of 5.60 ml·min^{-1} to the anode of a cell with a Sustainion membrane, working at 60 °C.

Therefore, it was concluded that it is not possible to directly use wastewater to produce hydrogen.

4.5 Effects of treatment with an ionic exchange resin

4.5.1 Working in series with the electrolysis cell

The presence of contaminants, even at low levels, negatively impacts the performance of hydrogen-producing devices, especially considering continuous operation; therefore, high-quality waters are usually used for green-hydrogen production. Among the various water treatment solutions available, the implementation of ion-exchange resins as part of seawater/wastewater treatment procedures has become common, particularly for the removal of impurities such as inorganic contaminants. Indeed, ion-exchange resins ensure a considerable decrease in the use of chemical compounds, and their high selectivity allows the meeting of strict water discharge specifications. Therefore, to understand the effects of applying an ion-exchange resin-based treatment on the studied seawater-quality parameters and thus on the overall performance of the electrolysers, the above-performed stability protocols were repeated, using an IX resin - Amberlite IRN150 (Supelco). This resin was chosen due to its stability in a great range of pH and temperatures; besides, it is able to exchange both positive and negative ions that are present in the wastewaters. The tests were made with a saltwater (25 mg L^{-1} NaCl) feed flow of 5.60 ml min^{-1} to the anode, for PEM electrolysis, with a Nafion 115 membrane and a working temperature of 70 °C.

A column filled with the ion exchange resin, was introduced in the water-recycling line after the electrolysis cell. Essentially, during the long-term operation, after being fed to the electrolyser, the water was treated by passing through the ion-exchange column and it was continuously recirculated back to the electrolyser – Figure 3.1.

Upon stability test, the degradation suffered by the electrolysis cell was higher when no ion-exchange resin-based treatment step is added to the water circuit – 4% *vs.* 6% degradation at 2 V for operation with and without the IX resin column, respectively – Figure 4.12.a). Moreover, the treatment with the ion-exchange resin slightly reduces the ohmic and mass transfer resistance in the cell (Figure 4.12.b).

Moreover, relevant water-quality parameters – conductivity and TDS – were evaluated during the stability test; their values remarkably decreased over time (Table 4.2). This preliminary test applied to the mimicked seawater indicates the effectiveness of implementing the ion-exchange resin technique for ensuring proper water-quality parameters on the water-recycling step. This insight is of paramount importance for minimizing the hydric stress associated with the green-hydrogen production, without compromising the stability and long-term performance of the electrolysers.

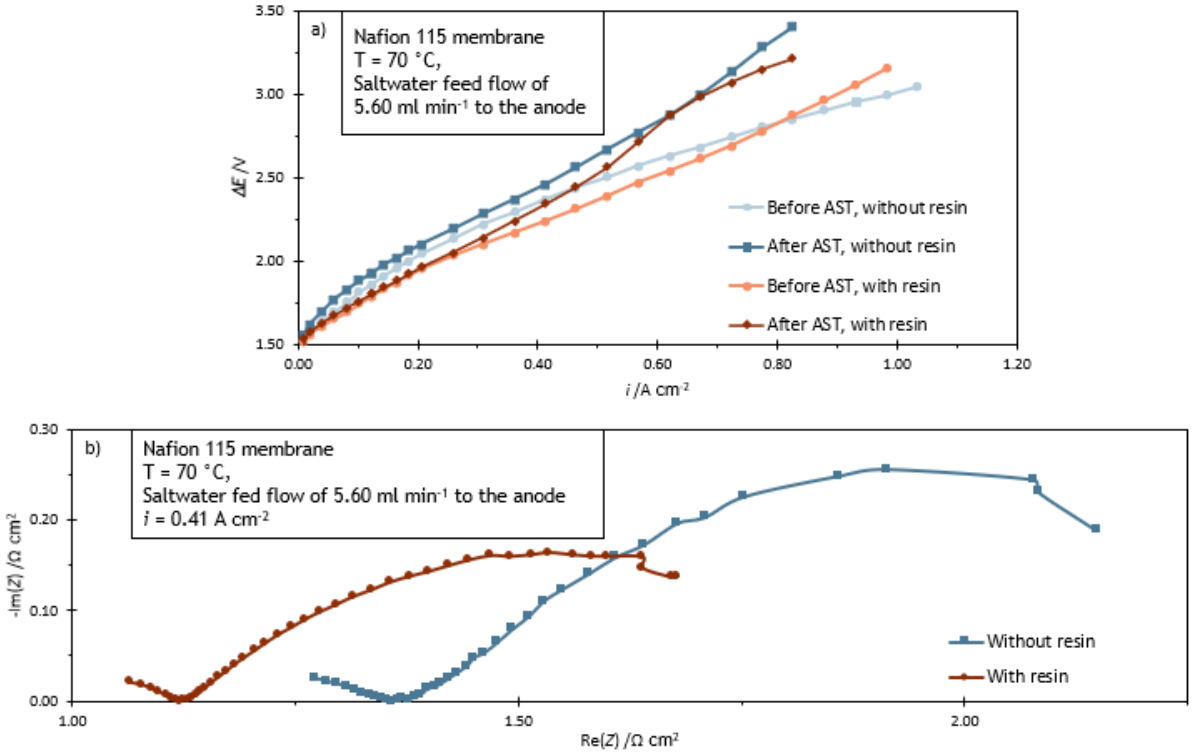

Figure 4.12 - a) Difference in potential before and after a 15 h AST with and without an ion exchange resin in the hydraulic circuit; b) Nyquist Plots at 0.41 A cm^{-2} after an AST, for a Nafion 115 membrane, with a saltwater flow of 5.60 ml min^{-1} to the anode, with a working temperature of 70 °C.

Table 4.2 – Parameters of a NaCl solution over time, fed to an electrolysis cell and treated with an IX resin in series.

	T /ºC	*σ* /μS cm^{-1}	*R* /kΩ cm	TDS /mg
NaCl solution at hour 0	79.6	60.3	17.5	128
NaCl solution at hour 15	80.7	45.7	22.4	86
NaCl solution at hour 30	78.8	14.1	71.8	15

4.5.2 Ionic exchange resin as a preliminary advanced wastewater treatment

Moreover, the Amberlite IRN50 resin was also applied as preliminary water treatment technique to the studied wastewaters – Ave, Arcos de Valdevez and CIN.

Firstly, the wastewaters were treated using a closed circuit consisting in a buffer tank and an ion-exchange column. Ave water was continuously fed to the column, using a flow rate of 100 ml min^{-1}. The water-quality parameters measured during the wastewater treatment can be found in table 4.3. The wastewater had a residence time of *ca.* 45 s in the ion exchange column. Upon two hours, the conductivity and solid content were constant, assuming values similar to those of ultrapure water, and therefore the treated wastewater was considered ready to be fed to the electrolyser. Indeed, after 2 hours of treatment, it was possible to decrease the solid content by 99.8 %, which corresponds to a tremendous improvement in water-quality.

Table 4.3 – Water parameters along time with IX resin treatment, for Ave water.

	T /ºC	*σ* /μS cm^{-1}	*R* /kΩ cm	TDS /mg L^{-1}
hour 0	40.1	2170	0.46	2160
hour 1	52.1	69.0	14.67	69
hour 2	44.8	4.3	257	4
hour 3	42.1	4.1	262	4

Then, the three wastewaters tested were treated, in batches of 1.5 L, in the IX column for two hours. Thus, the studied wastewaters were properly treated using the ion-exchange column and then, the performance and stability of both PEM and AEM electrolysis were evaluated by performing ASTs.

PEMWE

Considering PEMWE, table 4.4 shows the water quality parameters of the treated wastewaters fed to the electrolysis cell, alongside the degradation suffered during a stability test consisting of 15-hour AST. In terms of performance at 2 V, it increased (as shown by the negative degradation in Table 4.4), as it does in operation with ultrapure water.

Table 4.4 – Conductivity and solid content of the treated wastewaters fed to the electrolysis cell, along with the degradation after a 15-hour AST, for specific potentials.

	σ /µS cm^{-1}	TDS /mg L^{-1}	Degradation at 2 V /%	Degradation at 3 V /%
Ave treated wastewater	4.5	5	-50	12
Arcos de Valdevez treated wastewater	5.9	6	-25	4
CIN treated wastewater	3.1	3	-24	9

For the three treated wastewaters tested, the solid content is very similar, which resulted in a similar degradation. The polarization curves before and after the AST are very similar to the ones obtained for circulating ultrapure water (Figure 4.6), with a slight increase in performance at a lower current density (< 0.50 A cm^{-1}). Figure 4.13 shows the polarization curves and Nyquist plots before and after the AST, for Arcos de Valdevez treated wastewater, and the corresponding information for the other treated wastewaters tested can be found in appendix K.

The similarities between the polarization curves obtained with treated wastewater circulation in comparison to that of ultrapure water indicate that the degradation mechanisms were similar in both cases. However, looking at the curve correspondent to the hour 15 in the Nyquist plot at 0.41 A cm^{-2} – Figure 4.13.b) – and comparing it to the one in Figure 4.9.b), it can be inferred that the main resistance in the cell is the mass transfer resistance: the rate at which the gaseous products (H_2 and O_2) are being produced exceeds the rate at which they exit the cell. This is probably due to metallic poisoning in the catalyst layer [22]. It would be interesting, as future work, to connect the gas exhaustion from the electrolyser cell to a gas analysis device, to understand if any parasitic reaction is taking place.

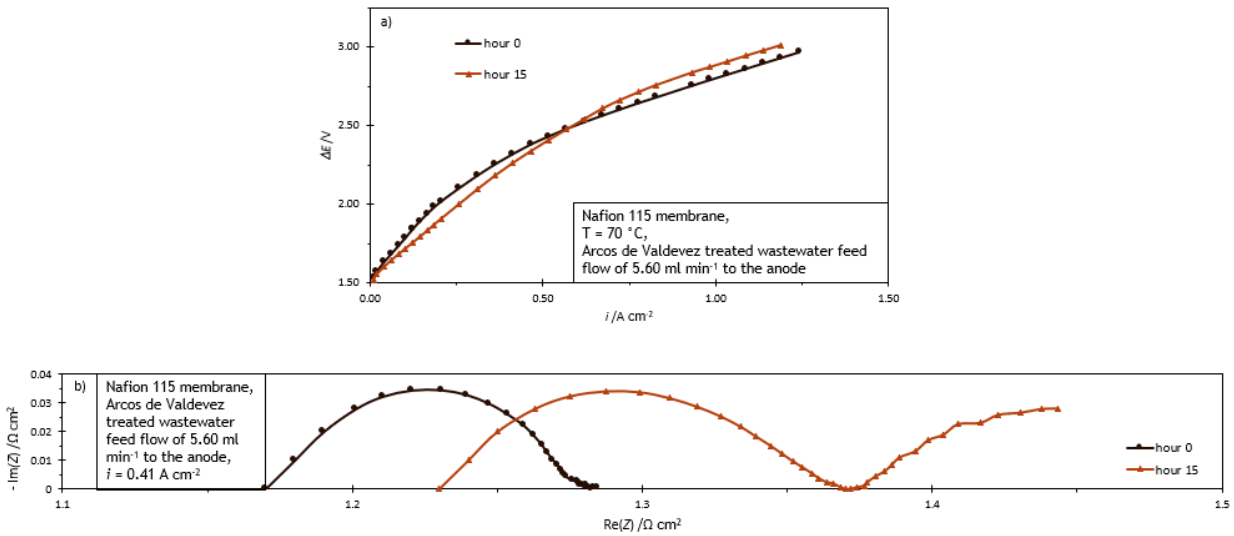

Figure 4.13 – a) Polarization curves and b) Nyquist plot at 0.41 A cm^{-1} before and after a 15-hour AST, with a water feed flow of 5.60 ml min^{-1} to the anode, at a temperature of 70 °C, for Arcos de Valdevez treated wastewater.

AEMWE

For AEMWE tests, potassium hydroxide was added to the treated wastewaters before feeding them to the electrolyser, to obtain an electrolyte concentration of 0.2 M. The treated wastewaters' quality parameters are depicted in table 4.5.

Table 4.5 - Conductivity and solid content of the different treated wastewaters fed to the AEM electrolysis cell.

	σ /μS cm^{-1}	**TDS /mg L^{-1}**
Ave treated wastewater	10.3	10
Arcos de Valdevez treated wastewater	28.2	28
CIN treated wastewater	523.8	526

For both Ave and Arcos de Valdevez treated wastewaters, the electrolysis performance was similar to the one obtained with pure water – Appendix L. For Arcos de Valdevez treated wastewater, the performance increased about 21 % at 2 V in the first 3 hours of operation and then was constant – Figure 4.13. Considering Ave water, the performance was stable during the entire AST, until the short-circuit.

Comparing ultrapure water *versus* treated wastewater feed, the performance of the electrolyser was extremely similar, and the stability greatly improved when using treated wastewater. When using ultrapure water, the performance decreases by 15 % at 2 V in the first 2 hours of operation and the membrane short-circuits upon 10-hour of test. Contrarily, when treated wastewater was fed to the cell, the performance increased (for Arcos de Valdevez treated wastewater feed) or was stable (for Ave treated wastewater feed). Besides, for pure water feed, a short-circuit occurs around the tenth hour of continuous operation, while for treated wastewater feed, the short-circuit happened upon 14.5 hours of operation.

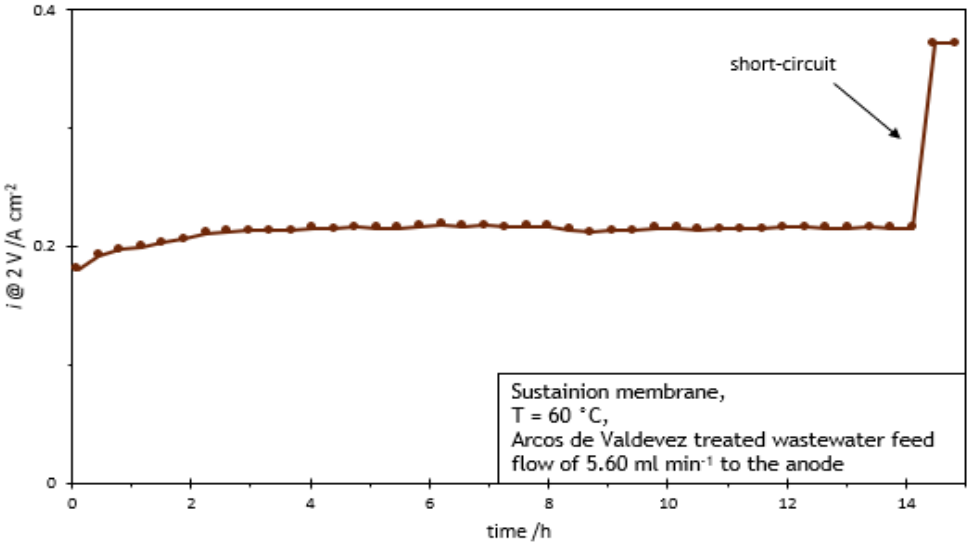

Figure 4.14 – Evolution of the current density at 2 V along the 15-hour AST, for Arcos de Valdevez treated wastewater feed flow rate of 5.60 ml min^{-1} to the anode of an electrolysis cell with a Sustainion membrane and a working temperature of 60 °C.

In the case of the tested CIN treated wastewater, its solid content was above the desired – Table 4.5 - due to the saturation of the IX resin. However, the treated wastewater was nonetheless fed to the electrolyser, resulting in immediate short-circuiting. This is on par with the results obtained when the electrolysis cell was fed with a 25 ml L^{-1} NaCl solution and from that, one could conclude that the solid content in the water is damaging the membrane, thus leading to short-circuit. However, when the electrolysis cell was fed with Arcos de Valdevez wastewater without treatment, the cell only short-circuits at around 4.5 hours of the AST, and the system, until the short-circuit, suffered a smaller degradation than when fed with ultrapure water (both in a 0.2 M KOH solution) – 10 % *vs.* 15 % at 2 V, respectively. Therefore, due to these contradictory results, no conclusions can be inferred in terms of cell degradation when working with feed waters with a solid content of 25 mg L^{-1} or higher.

Overall, and in conclusion, these tests support the hypothesis that it is, indeed, possible to use treated wastewater as a water resource for hydrogen production through water electrolysis.

5 Conclusions

The main objective of this work was to study the possibility of using treated municipal and industrial wastewaters as feed to electrolysers for green hydrogen production through both PEM and AEM water electrolysis. The work was divided into two main parts: firstly, an electrolysis setup was developed and properly optimized, considering working temperature, water feed flow rate, water feed method (water feeding to the anode, cathode or to both electrodes) and electrolyte concentration, in the case of AEMWE. Secondly, an advanced water treatment step, consisting of an ultra-filtration and reverse osmosis unit, followed by an ion exchange resin column was created, with the objective of treating the considered wastewaters. The treated water was then fed into the electrolyser and the performance and stability of the system was studied.

Considering PEMWE, the best working conditions were obtained using a water feed flow rate of 5.60 ml min^{-1} (about 100 times the stochiometric flow) fed to the anode, combined with a working temperature of 70 °C. For these conditions, with a Nafion 115 membrane, a current density of 0.38 A cm^{-2} at 2 V was obtained. For AEMWE, the optimal conditions were achieved using a concentration of 0.2 M KOH supporting electrolyte solution, at a feed flow rate of 5.60 ml min^{-1} to the anode and a working temperature of 60 °C. Under these conditions, using the best-performing AEM membranes - Sustainion X37-50 grade RT -it was obtained a current density of 0.14 A cm^{-2} at 2 V.

Regarding electrolysis cell operation with wastewater, it was concluded that the feed of wastewaters with only secondary treatment to the electrolyser for hydrogen production was not possible for neither PEM nor AEM electrolysis. With a tertiary treatment, consisting of an ion exchange resin column, it was possible to obtain a decrease of 99.8 % in terms of solid content. The beginning of life performance of both PEM and AEM electrolysis, working with the treated wastewater, was similar to the performance when working with ultrapure water. The cell degradation was also comparable: considering PEM, there was a performance increase at lower potentials (25 % for Arcos de Valdevez water versus 29 % for ultrapure water at 2 V), which was mainly attributed to the rearrangement in the catalytic layer. For AEM, the performance improved when treated wastewaters were used instead of ultrapure water. In fact, for treated Arcos de Valdevez treated wastewater, there was a 21 % increase in performance, at 2 V, during the AST until the short-circuiting of the membrane at the 14.5-hour mark, in contrast to the 15 % decrease in performance for ultrapure water and short-circuit at 10 hours.

There is, however, still a difference in performance and stability of the Nafion and Sustainion membranes. Both the ohmic and charge transfer resistance are higher when the electrolysis

cell uses a Sustainion membrane, in comparison with using Nafion membranes, for the best conditions for each (ohmic resistance of 0.66 Ω cm^2 *vs*.1.16 Ω cm^2 and charge transfer resistance of 0.67 Ω cm^2 *vs*. 1.61 Ω cm^2 at 0.04 A cm^{-2} for a system with Nafion and Sustainion membranes, respectively). Besides, Sustainion membranes, specifically, still exhibit low stability when working at higher potential differences (> 2.5 V) and cycling operation, which results in a short-circuit of the system.

It shows that the use of treated municipal wastewater, industrial wastewater and seawater as feed for an electrolyser is feasible and, with the appropriate advanced treatment, feasible for long term operation.

Overall, this work presents a novel approach regarding the production of green-hydrogen, without depleting scarce freshwater resources. The operating conditions of a packed column with an ion exchange resin were optimized to be used as an advanced treatment for industrial/municipal wastewaters and to be directly coupled upstream PEM and AEM water electrolysers. This technique was shown to be robust and efficient for preventing the passage of chlorine ions which cause chloride corrosion mainly at the anode of the electrolysis cell, and thus guarantee high efficiencies and the stability, in comparison to conventional approaches, where ultra-pure water is used. This integration is shown to be promising for allowing both capital and operation cost reduction for green-hydrogen production while saving energy and hydric resources.

6 Assessment of the Work Done

6.1 Objectives Achieved

This work comprised of two main objectives: firstly, the optimization of a single-cell test bench and, secondly, studying the performance and stability of a single-cell when operating with treated wastewater or saltwater, in contrast with those of ultrapure water operation.

An optimum regarding working temperature, Water feed flow rate, water circulation type and electrolyte concentration was achieved for both PEMWE and AEMWE.

An advanced water treatment setup, consisting of ultrafiltration, reverse osmosis and an ion exchange resin column was built, but it was only possible to carry out the ion exchange treatment, due to issues in the delivery of filtration membranes. The treated wastewater was then fed to the electrolysis cell, and the performance and stability was studied, in comparison with the ones in ultrapure water feeding.

6.2 Limitations and Future Work

It is of utmost importance to understand the influence of the tertiary treatment in the performance of the cell, and the advanced filtration unit, already developed, may be used for future works to remove pollutants from wastewaters. The characteristics of the water fed to the electrolysis cell, and respective electrolysis performance must be studied. This way, the overall efficiency of the tertiary treatment can be optimized. Furthermore, the possibility of including water treatment solutions (through ion exchange resin, for example) in series after the electrolysis cell, to remove contaminants arising from the cell's degradation (mainly during long-term operation) may also yield interesting results.

Besides, PGM-free catalysts may be employed when working in alkaline media, and the single-cell performance and stability evaluated using ultrapure water and treated wastewater for feeding the electrolysis cell. This work may be interesting due to current evolution in reducing PGM utilization, which is possible in AEMWE.

Finally, it would be interesting to further understand the mechanisms of degradation due to water impurities in the electrolysis cell, namely by performing thorough physicochemical characterization of CCMs to investigate the presence of metallic impurities or organic matter.

6.3 Final Assessment

This work allowed me to further explore and understand different areas of chemical engineering, such as electrochemistry and water treatment and provided me an overall insight on numerous topics ranging from catalyst ink formulation and deposition to water electrolysis process and its optimization. Furthermore, all the knowledge on different techniques used, from electrochemical to physical characterization were fundamental to attain great tools for my future career.

It is of critical importance to continue the investigation regarding hydrogen production through water electrolysis, with treated wastewater feed. This dissertation demonstrates the possibility of using advanced water treatment technologies to purify wastewater, followed by its feeding to an electrolyser, obtaining overall great performance and stability. This work serves, therefore, as a steppingstone for the development of a novelty process for hydrogen production through wastewater electrolysis.

7 References

1. Data, E. *Global Wind Atlas*. 2022; Available from: https://globalwindatlas.info/.
2. Data, E. *Global Solar Atlas*. 2022; Available from: https://globalsolaratlas.info/map?c=39.427707,-9.228516,6&m=site&a=-10.195313,36.5626,-10.195313,42.617791,-5.932617,42.617791,-5.932617,36.5626,-10.195313,36.5626.
3. Kurita. *Deionization Technologies*. 2022 16/06/2022]; Available from: https://www.kurita.co.jp/english/technology/core_technology/deionized.html.
4. Gielen, D., E. Taibi, and R. Miranda, *Hydrogen: A renewable energy perspective*. 2019, International Renewable Energy Agency: Abu Dhabi.
5. Scutt, G. *Waste Water and Sewage Treatment Process*. 2012 04/06/2022]; Available from: https://visual.ly/community/Infographics/environment/waste-water-and-sewage-treatment-process.
6. Taibi, E., H. Blanco, R. Miranda, and M. Carmo, *Green Hydrogen Cost Reduction: Scaling up Electrolysers to Meet the 1.5ºC Climate Goal*. 2020, International Renewable Energy Agency: Abu Dhabi.
7. Chisholm, G., P.J. Kitson, N.D. Kirkaldy, L.G. Bloor, and L. Cronin, *3D printed flow plates for the electrolysis of water: An economic and adaptable approach to device manufacture*. Energy and Environmental Science, 2014. **7**(9): p. 3026-3032.
8. Dionigi, F., T. Reier, Z. Pawolek, M. Gliech, and P. Strasser, *Design Criteria, Operating Conditions, and Nickel-Iron Hydroxide Catalyst Materials for Selective Seawater Electrolysis*. ChemSusChem, 2016. **9**(9): p. 962-972.
9. COMMISSION, E., *A hydrogen strategy for a climate-neutral Europe*. 2020.
10. EMBER. *Carbon pricing*. 2022 04/06/2022]; Available from: https://ember-climate.org/data/data-tools/carbon-price-viewer/.
11. Fecht, S. *It's totally possible to limit global warming to 1.5 degrees*. 2018 05/06/2022]; Available from: https://phys.org/news/2018-10-totally-limit-global-degrees.html.
12. Blank, T.K. and P. Molloy, *Hydrogen's Decarbonization Impact for Industry: Report*. 2020.
13. Energy, O.o.E.E.R. *Hydrogen Production: Biomass Gasification* 2022; Available from: https://www.energy.gov/eere/fuelcells/hydrogen-production-biomass-gasification.
14. Cornelissen, B. *The potential of hydrogen for the chemical industry* 2021; Available from: https://www2.deloitte.com/xe/en/pages/energy-and-resources/articles/the-potential-of-hydrogen-for-the-chemical-industry.html.
15. APREN. *Balanço da Produção de Eletricidade de Portugal Continental*. 2022 [cited 2022 28/02/2022]; Available from: https://www.apren.pt/pt/energias-renovaveis/producao.
16. Governo, X., *Estratégia Nacional para o Hidrogénio*, A.e.A. Climárica, Editor. 2020.
17. EMBER. *Data Explorer*. 2022; Available from: https://ember-climate.org/data/data-explorer/.
18. Gonçalves, S. and M. Pereira, *Portugal set to start up Europe's largest floating solar park*. World Economic Forum, 2022.
19. EDP, *Floating offshore wind-power generating platform*. 2022.
20. Simoes, S.G., J. Catarino, A. Picado, T.F. Lopes, S. di Berardino, F. Amorim, F. Gírio, C.M. Rangel, and T. Ponce de Leão, *Water availability and water usage solutions for electrolysis in hydrogen production*. Journal of Cleaner Production, 2021. **315**: p. 128124.
21. Barros, R. and C.C. Silva, *Como a seca afecta Portugal e o seu concelho*, in *Público*. 2022.

22. Feng, Q., X.Z. Yuan, G. Liu, B. Wei, Z. Zhang, H. Li, and H. Wang, *A review of proton exchange membrane water electrolysis on degradation mechanisms and mitigation strategies.* Journal of Power Sources, 2017. **366**: p. 33-55.
23. Millet, P., *Chapter 2 - Fundamentals of water electrolysis*, in *Electrochemical Power Sources: Fundamentals, Systems, and Applications*, T. Smolinka and J. Garche, Editors. 2022, Elsevier. p. 37-62.
24. Vincent, I. and D. Bessarabov, *Low cost hydrogen production by anion exchange membrane electrolysis: A review.* Renewable and Sustainable Energy Reviews, 2018. **81**: p. 1690-1704.
25. Carmo, M., D.L. Fritz, J. Mergel, and D. Stolten, *A comprehensive review on PEM water electrolysis.* International Journal of Hydrogen Energy, 2013. **38**(12): p. 4901-4934.
26. Doan, T.L., H.E. Lee, S.S.H. Shah, M. Kim, C.-H. Kim, H.-S. Cho, and T. Kim, *A review of the porous transport layer in polymer electrolyte membrane water electrolysis.* International Journal of Energy Research, 2021. **45**(10): p. 14207-14220.
27. Zhang, H., X. Wang, J. Zhang, and J. Zhang, *Conventional Catalyst Ink, Catalyst Layer and MEA Preparation*, in *PEM Fuel Cell Electrocatalysts and Catalyst Layers: Fundamentals and Applications*, J. Zhang, Editor. 2008, Springer London: London. p. 889-916.
28. Park, I.-S., W. Li, and A. Manthiram, *Fabrication of catalyst-coated membrane-electrode assemblies by doctor blade method and their performance in fuel cells.* Journal of Power Sources, 2010. **195**(20): p. 7078-7082.
29. Wang, W., S. Chen, J. Li, and W. Wang, *Fabrication of catalyst coated membrane with screen printing method in a proton exchange membrane fuel cell.* International Journal of Hydrogen Energy, 2015. **40**(13): p. 4649-4658.
30. Lim, B.H., E.H. Majlan, A. Tajuddin, T. Husaini, W.R. Wan Daud, N.A. Mohd Radzuan, and M.A. Haque, *Comparison of catalyst-coated membranes and catalyst-coated substrate for PEMFC membrane electrode assembly: A review.* Chinese Journal of Chemical Engineering, 2021. **33**: p. 1-16.
31. Daintith, J., *fatty acid*, in *Dictionary of Chemistry (6th Edition)*. Oxford University Press. p. 220.
32. Falcão, D.S. and A.M.F.R. Pinto, *A review on PEM electrolyzer modelling: Guidelines for beginners.* Journal of Cleaner Production, 2020. **261**.
33. García-Valverde, R., N. Espinosa, and A. Urbina, *Simple PEM water electrolyser model and experimental validation.* International Journal of Hydrogen Energy, 2012. **37**(2): p. 1927-1938.
34. Abdin, Z., C.J. Webb, and E.M. Gray, *Modelling and simulation of a proton exchange membrane (PEM) electrolyser cell.* International Journal of Hydrogen Energy, 2015. **40**(39): p. 13243-13257.
35. Maier, M., K. Smith, J. Dodwell, G. Hinds, P.R. Shearing, and D.J.L. Brett, *Mass transport in PEM water electrolysers: A review.* International Journal of Hydrogen Energy, 2022. **47**(1): p. 30-56.
36. Marangio, F., M. Santarelli, and M. Calì, *Theoretical model and experimental analysis of a high pressure PEM water electrolyser for hydrogen production.* International Journal of Hydrogen Energy, 2009. **34**(3): p. 1143-1158.
37. Ayers, K., N. Danilovic, R. Ouimet, M. Carmo, B. Pivovar, and M. Bornstein, *Perspectives on Low-Temperature Electrolysis and Potential for Renewable Hydrogen at Scale.* Annual Review of Chemical and Biomolecular Engineering, 2019. **10**(1): p. 219-239.
38. Yu, F., L. Yu, I.K. Mishra, Y. Yu, Z.F. Ren, and H.Q. Zhou, *Recent developments in earth-abundant and non-noble electrocatalysts for water electrolysis.* Materials Today Physics, 2018. **7**: p. 121-138.
39. Pavel, C.C., F. Cecconi, C. Emiliani, S. Santiccioli, A. Scaffidi, S. Catanorchi, and M. Comotti, *Highly Efficient Platinum Group Metal Free Based Membrane-Electrode*

Assembly for Anion Exchange Membrane Water Electrolysis. Angewandte Chemie International Edition, 2014. **53**(5): p. 1378-1381.

40. Zeng, L. and T.S. Zhao, *High-performance alkaline ionomer for alkaline exchange membrane fuel cells*. Electrochemistry Communications, 2013. **34**: p. 278-281.
41. Lettenmeier, P., R. Wang, R. Abouatallah, S. Helmly, T. Morawietz, R. Hiesgen, S. Kolb, F. Burggraf, J. Kallo, A.S. Gago, and K.A. Friedrich, *Durable Membrane Electrode Assemblies for Proton Exchange Membrane Electrolyzer Systems Operating at High Current Densities*. Electrochimica Acta, 2016. **210**: p. 502-511.
42. Alia, S.M., S. Stariha, and R.L. Borup, *Electrolyzer Durability at Low Catalyst Loading and with Dynamic Operation*. Journal of The Electrochemical Society, 2019. **166**(15): p. F1164-F1172.
43. Tsotridis, G. and A. Pilenga, *EU harmonised protocols for testing of low temperature water eletrolysers*. 2021, European Commision Join Research Centre: Luxembourg.
44. Aßmann, P., A.S. Gago, P. Gazdzicki, K.A. Friedrich, and M. Wark, *Toward developing accelerated stress tests for proton exchange membrane electrolyzers*. Current Opinion in Electrochemistry, 2020. **21**: p. 225-233.
45. Cherevko, S., S. Geiger, O. Kasian, A. Mingers, and K.J.J. Mayrhofer, *Oxygen evolution activity and stability of iridium in acidic media. Part 1. – Metallic iridium*. Journal of Electroanalytical Chemistry, 2016. **773**: p. 69-78.
46. Aydin, M.I., A.E. Karaca, A.M.M.I. Qureshy, and I. Dincer, *A comparative review on clean hydrogen production from wastewaters*. Journal of Environmental Management, 2021. **279**: p. 111793.
47. Hu, S., Y. Tan, C. Feng, H. Wu, J. Zhang, and H. Mei, *Synthesis of N doped NiZnCu-layered double hydroxides with reduced graphene oxide on nickel foam as versatile electrocatalysts for hydrogen production in hybrid-water electrolysis*. Journal of Power Sources, 2020. **453**: p. 227872.
48. Maril, M., J.-L. Delplancke, N. Cisternas, P. Tobosque, Y. Maril, and C. Carrasco, *Critical aspects in the development of anodes for use in seawater electrolysis*. International Journal of Hydrogen Energy, 2022. **47**(6): p. 3532-3549.
49. Khan, M.A., T. Al-Attas, S. Roy, M.M. Rahman, N. Ghaffour, V. Thangadurai, S. Larter, J. Hu, P.M. Ajayan, and M.G. Kibria, *Seawater electrolysis for hydrogen production: a solution looking for a problem?* Energy & Environmental Science, 2021. **14**(9): p. 4831-4839.
50. Hausmann, J.N., R. Schlögl, P.W. Menezes, and M. Driess, *Is direct seawater splitting economically meaningful?* Energy & Environmental Science, 2021. **14**(7): p. 3679-3685.
51. Português, G., *Decreto-lei 152/97, de 19 de Junho*, M.d. Ambiente, Editor. 1997.
52. Agency, S.N.W. *NEWater* 2022; Available from: https://www.pub.gov.sg/watersupply/fournationaltaps/newater.
53. Santos, C., *Tratamento de Água e de Águas Residuais*. 2021, Universidade do Porto.
54. Têxtil, P., *«A nossa meta é conseguir reaproveitar entre 60% e 70% da água»*, in *Portugal Têxtil*. 2022.
55. Jones, E., M. Qadir, M.T.H. van Vliet, V. Smakhtin, and S.-m. Kang, *The state of desalination and brine production: A global outlook*. Science of The Total Environment, 2019. **657**: p. 1343-1356.
56. Tikkanen, A., *ion-exchange resin*, in *Encyclopaedia Britannica*. 2022.
57. Cheremisinoff, N.P., *Chapter 10 - Ion exchange and carbon adsorption*, in *Handbook of Water and Wastewater Treatment Technologies*, N.P. Cheremisinoff, Editor. 2002, Butterworth-Heinemann: Woburn. p. 372-445.
58. Schmuckler, G., *Chelating Resins - Their Analytical Properties and Applications*. Talanta, 1965. **12**: p. 9.

59. SamCo. *Ion Exchange vs. Reverse Osmosis: Choosing the Best Treatment System for Your Needs*. 2017; Available from: https://www.samcotech.com/ion-exchange-vs-reverse-osmosis-choosing-best-treatment-system-needs/.
60. Liu, Z., S.D. Sajjad, Y. Gao, H. Yang, J.J. Kaczur, and R.I. Masel, *The effect of membrane on an alkaline water electrolyzer*. International Journal of Hydrogen Energy, 2017. **42**(50): p. 29661-29665.
61. Silva, R.F., M. De Francesco, and A. Pozio, *Tangential and normal conductivities of Nafion® membranes used in polymer electrolyte fuel cells*. Journal of Power Sources, 2004. **134**(1): p. 18-26.
62. Dresp, S., F. Dionigi, S. Loos, J. Ferreira de Araujo, C. Spöri, M. Gliech, H. Dau, and P. Strasser, *Direct Electrolytic Splitting of Seawater: Activity, Selectivity, Degradation, and Recovery Studied from the Molecular Catalyst Structure to the Electrolyzer Cell Level*. Advanced Energy Materials, 2018. **8**(22): p. 1800338.
63. Sun, S., Y. Xiao, D. Liang, Z. Shao, H. Yu, M. Hou, and B. Yi, *Behaviors of a proton exchange membrane electrolyzer under water starvation*. RSC Advances, 2015. **5**(19): p. 14506-14513.
64. Niaz, A.K., J.-Y. Park, and H.-T. Lim, *Operational parameters correlated with the long-term stability of anion exchange membrane water electrolyzers*. International Journal of Hydrogen Energy, 2021. **46**(62): p. 31550-31562.
65. Pushkareva, I.V., A.S. Pushkarev, S.A. Grigoriev, P. Modisha, and D.G. Bessarabov, *Comparative study of anion exchange membranes for low-cost water electrolysis*. International Journal of Hydrogen Energy, 2020. **45**(49): p. 26070-26079.
66. Frensch, S.H., F. Fouda-Onana, G. Serre, D. Thoby, S.S. Araya, and S.K. Kær, *Influence of the operation mode on PEM water electrolysis degradation*. International Journal of Hydrogen Energy, 2019. **44**(57): p. 29889-29898.
67. Li, D., A.R. Motz, C. Bae, C. Fujimoto, G. Yang, F.-Y. Zhang, K.E. Ayers, and Y.S. Kim, *Durability of anion exchange membrane water electrolyzers*. Energy & Environmental Science, 2021. **14**(6): p. 3393-3419.
68. Miller, H.A., K. Bouzek, J. Hnat, S. Loos, C.I. Bernäcker, T. Weißgärber, L. Röntzsch, and J. Meier-Haack, *Green hydrogen from anion exchange membrane water electrolysis: a review of recent developments in critical materials and operating conditions*. Sustainable Energy & Fuels, 2020. **4**(5): p. 2114-2133.
69. Motealleh, B., Z. Liu, R.I. Masel, J.P. Sculley, Z. Richard Ni, and L. Meroueh, *Next-generation anion exchange membrane water electrolyzers operating for commercially relevant lifetimes*. International Journal of Hydrogen Energy, 2021. **46**(5): p. 3379-3386.
70. Tong, W., M. Forster, F. Dionigi, S. Dresp, R. Sadeghi Erami, P. Strasser, A.J. Cowan, and P. Farràs, *Electrolysis of low-grade and saline surface water*. Nature Energy, 2020. **5**(5): p. 367-377.
71. Khatib, F.N., T. Wilberforce, O. Ijaodola, E. Ogungbemi, Z. El-Hassan, A. Durrant, J. Thompson, and A.G. Olabi, *Material degradation of components in polymer electrolyte membrane (PEM) electrolytic cell and mitigation mechanisms: A review*. Renewable and Sustainable Energy Reviews, 2019. **111**: p. 1-14.
72. Baehr, H.D., *Thermochemical properties of inorganic substances*. Forschung im Ingenieurwesen, 1992. **58**(4): p. 103-103.
73. Rumble, J., *CRC Handbook of Chemistry and Physics*. 102 ed. 2021: Taylor&Francis. 1624.

Appendix A – Images of the Installations and Devices Used

Here, are depicted images of the different devices (Figure A.1) and installation (Figures A.2 and A.3 used in this work.

Automatic Spray Dispenser

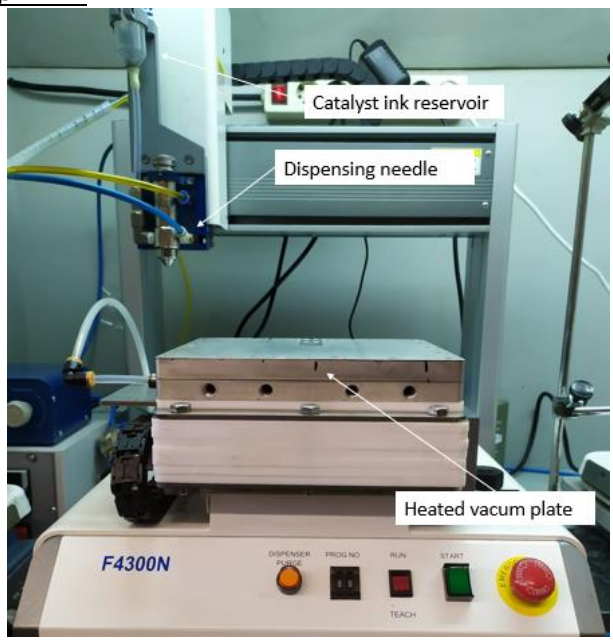

Figure A.1 – Image of the Automatic dispensing robot Fisnair.

Tertiary water treatment unit

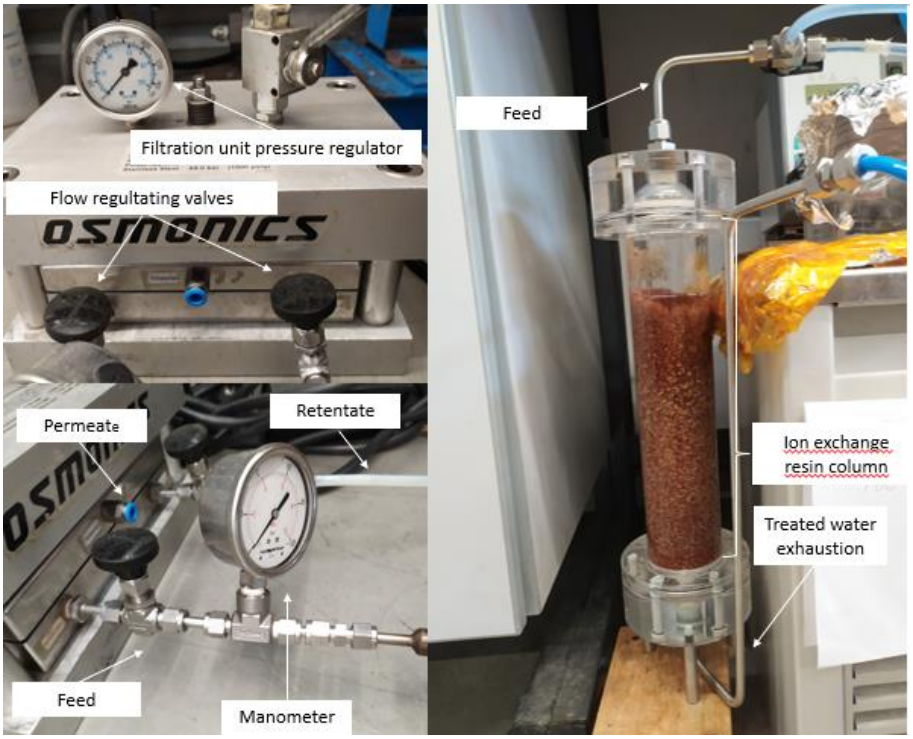

Figure A.2 – Tertiary water treatment installation, consisting of an advanced filtration and an ion exchange resin units.

Electrolysis Installation

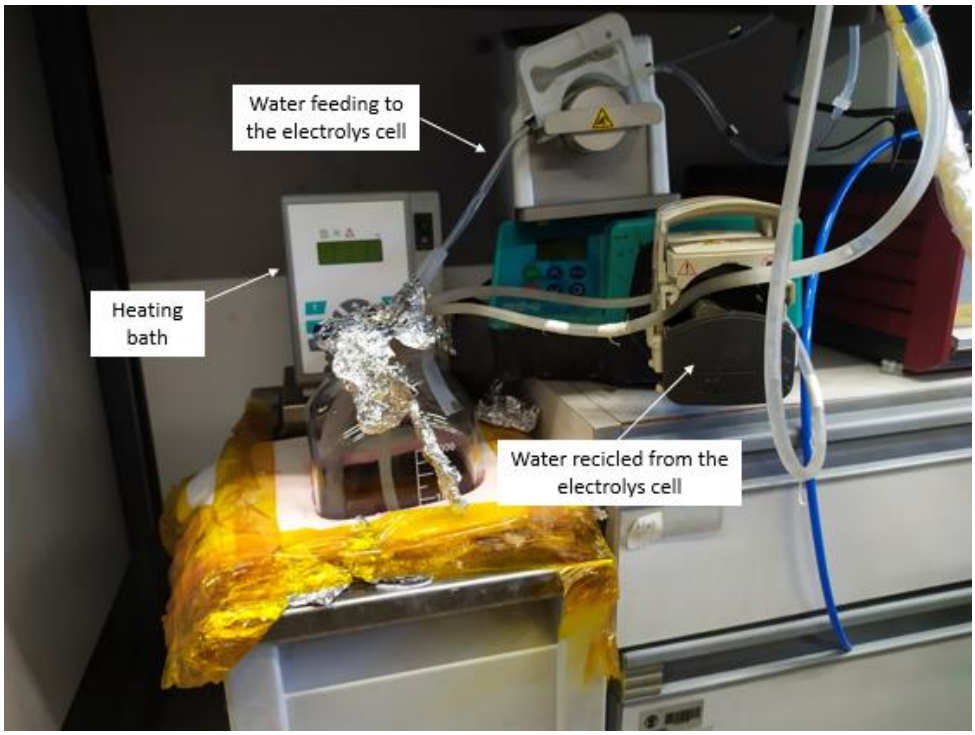

Figure A.3 – Pumping system to and from the electrolysis cell.

Appendix B - Thermogravimetric analysis of the used membranes

With the intent of understanding the thermal stability of the different membranes tested, a thermogravimetric analysis was made. Image B.1 shows the evolution of sample's mass as a function of the temperature. According to Figure B.1.a), the catalyst layer aids the membrane's thermal stability: when the analysis is performed on a membrane without catalyst coating, the volatilization (represented by the decrease in mass percentage) occurs at a higher rate, between 300 °C and 400 °C, than when the membrane was coated with catalyst on both sides.

Nafion 115 and Sustainion membranes – Figure B.1.c) – behave similarly: the mass remains constant until around 300 °C, after which it drops abruptly. Sustainion membranes have slightly higher thermal stability; steeper degradation starts around 320 °C, whereas Nafion membranes start around 270 °C. Water evaporation causes the mass loss that occurs until 100 °C.

Thermal stability of the Eurodia membrane is lower than that of Nafion 115 and Sustainion membranes. The mass decrease begins at around 200 °C and continues at a slow rate until around 400 °C; after that, it decreases at a higher rate. The degradation begins at a significantly lower temperature than both Nafion 115 and Sustainion membranes. This is consistent with the supplier's recommendation of a maximum working temperature of 50 °C, while this limit in both Sustainion and Nafion membranes is around 80 °C

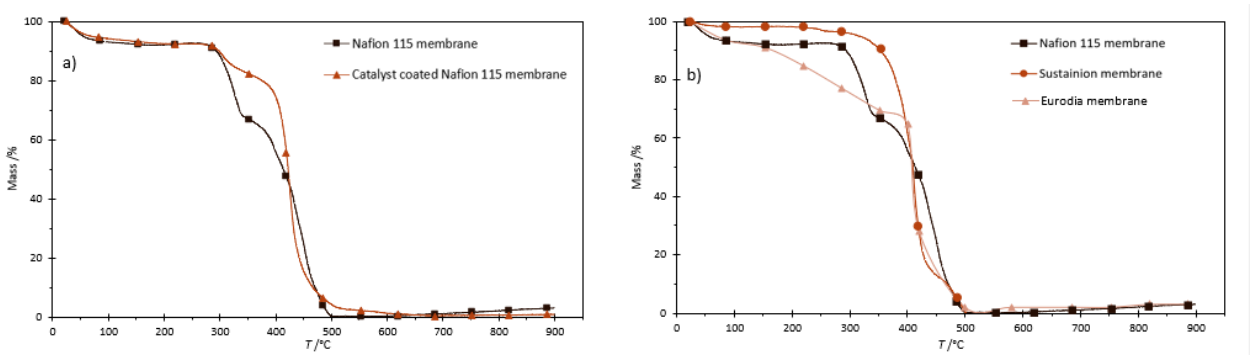

Figure B.1 -TG comparison between a) coated and non-coated with catalyst Nafion 115 membranes; b) Nafion 115, Sustainion and Eurodia membranes, without catalyst coating.

Appendix C - Thermoneutral potential at the considered temperatures

As explained in chapter 2.1, thermoneutral potential (E_{th}) for the water splitting reaction is 1.481 V at standard conditions (25 °C and 1 bar). The electrolysis cell operates, however at different temperatures: 70 °C for PEMWE (with Nafion membranes) and 60 °C for AEMWE (With Sustainion membranes). Here, thermoneutral potential is calculated for those temperatures.

The enthalpy of reaction (ΔH_{R}) is related to the enthalpy of formation (ΔH_{i}) of the products and reactants, and their respective stoichiometry in the reaction. For water splitting, ΔH_{R} is given by equation (C.1) and E_{th} may be calculated by equation (C.2):

$$\Delta H_{\mathrm{R}} = \Delta H_{\mathrm{H_2}} + \frac{1}{2}\Delta H_{\mathrm{O_2}} - \Delta H_{\mathrm{H_2O}} \qquad \text{(C.1)}$$

$$E_{\mathrm{th}} = \frac{\Delta H_{\mathrm{R}}}{n \cdot F} \qquad \text{(C.2)}$$

Where n is the number of electrons changed in the reaction and F is the Faraday constant (F = 96 485 C mol^{-1})

The enthalpy of formation of different substances is dependent on the temperature and it is normally calculated in relation the enthalpy at 25 °C – T_1 - by equation (B.3). The parameters a, b, c, d, and H_{i}^0 are present in Table B.1.

$$\Delta H_i^{T_2} - \Delta H_i^{T_1} = \int_{T_1}^{T_2} (a + b \cdot T + c \cdot T^{-2} + d \cdot T^2) dT \qquad \text{(C.3)}$$

Table C.1 – Thermodynamic parameters for enthalpy of formation calculation [72].

	H_2O	H_2	O_2
H_i^0 /J mol^{-1}	-285829	0	0
a	20.355	26.882	29.154
b 10^3	109.198	3.586	6.477
c 10^{-6}	2.033	0.105	-0.184
d 10^6	0	0	-1.017

From these parameters and equations, it is possible to calculate the thermoneutral potential at the working temperatures of the electrolysis cell. It is, thus, 1.475 V and 1.474 V for 60 °C and 70 °C, respectively.

Appendix D – Stoichiometric water flow

Water is split per equation (D.1):

$$H_2O \rightarrow H_2 + \frac{1}{2}O_2 \quad \text{(D.1)}$$

The goal of the single cell operation was to achieve a current density of 2 A cm^{-2}, which, for a 5 cm^2 cell, corresponds to a current (I) of 10 A.

For each mol of reactant water, 2 electrons are exchanged in the reaction. Therefore, the stoichiometric water flow (Q_{H_2O}), in mol s^{-1} is given by equation (D.2):

$$Q_{H_2O} = \frac{I}{2 \cdot F} \quad \text{(D.2)}$$

Where F is the Faraday constant (F = 96 485 C mol^{-1}). From water's specific weight (18 g mol^{-1}) and density (0.997 g ml^{-1}), water flow can be calculated as 5.18 10^{-5} mol s^{-1}, or 0.056 ml min^{-1}.

Appendix E - FTIR analysis of the membranes studied

Figures E.1 and E.2 show the FTIR spectra of the different membranes studied in this work: Sustainion and Eurodia for AEMWE and Nafion 115 for PEMWE.

Comparing the transmittance spectra of Sustainion and Eurodia membranes, it is possible to observe some similar peaks (dashed lines in Figure E.2). The peaks at around 450 cm^{-1} and 1480 cm^{-1} indicate the presence of amine groups, while peaks around 990 cm^{-1} and 710 cm^{-1} suggest the presence of substituted aromatic rings. Otherwise, no similar peaks are observed. This suggests that the compositions of these membranes are not particularly similar, even though both appear to contain amines in their functional, ion exchange group.

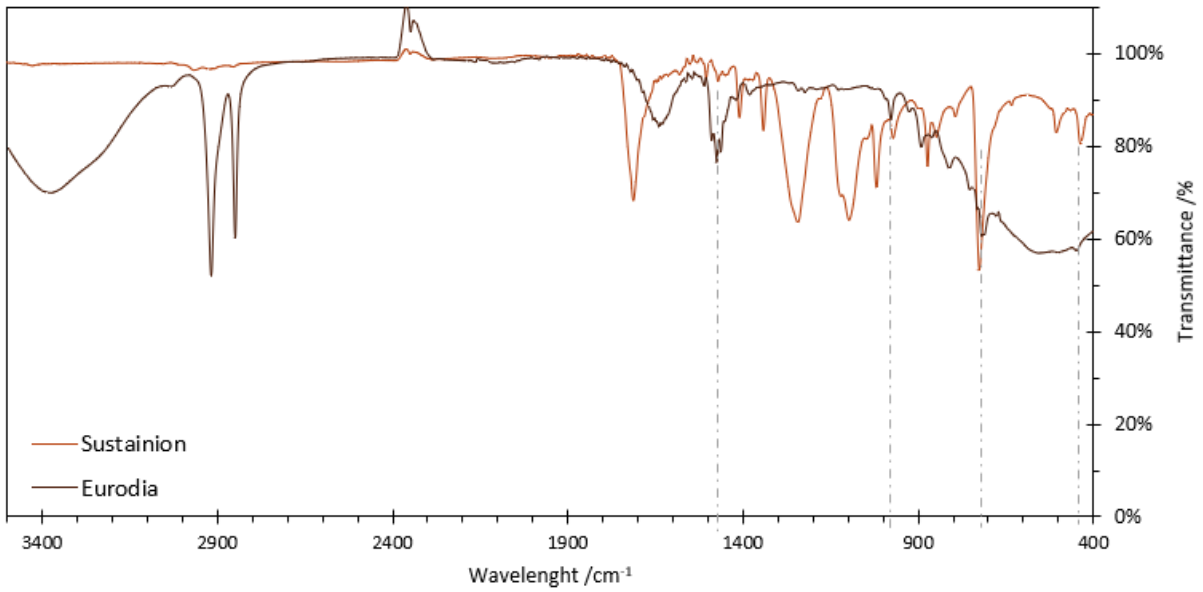

Figure E.1 - FTIR spectra of Sustainion and Eurodia membranes, used in AEMWE.

For Nafion 115 membranes, the respective FTIR spectra – Figure E.2 – show the presence of a polymer backbone (peaks between 900 cm^{-1} and 1000 cm^{-1}) and the peaks between 1100 cm^{-1} and 1250 cm^{-1} show the presence of fluorine functional groups (CF_2) – functional groups.

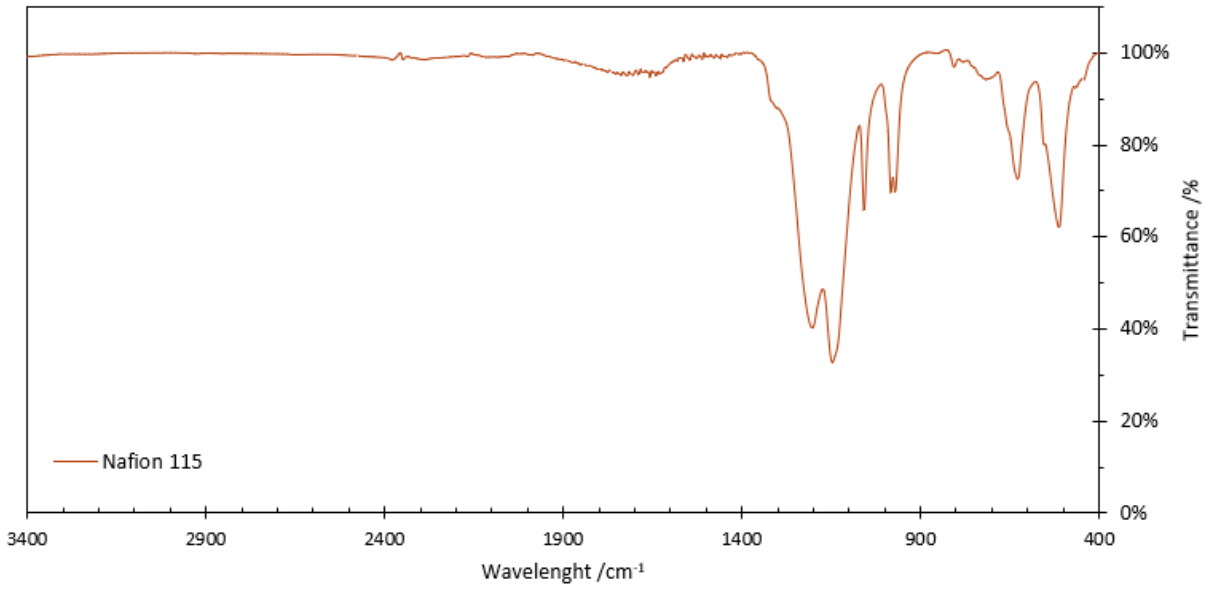

Figure E.2 – FTIR spectra of Nafion 115 membranes, used in PEMWE.

Appendix F - Comparison between the PEM membranes tested

In the best conditions considered for the Nafion 115 membrane, a Nafion 212 membrane was also tested. The comparison in performance of the electrolysis cell working with the two membranes is represented by the polarization curves in Figure F.1. As the Nafion 212 membrane is much thinner (about 51 µm) than Nafion 115 (127 µm), its ohmic resistance should be much smaller, as the ohmic resistance in the membrane is proportional to its thickness [61].

However, it is possible to conclude, from Figure F.1.b), that the ohmic resistance in the cell is very similar for both membranes – Figure F.1. This may indicate that the main resistance ohmic resistance can be attributed to the ionomer content. Furthermore, the resistance associated with the cathodic and anodic reactions seems to be higher in the tests performed with the Nafion 212 membrane, which may be due to some small difference in the catalyst ink deposition in the membrane.

As the performance is better for the tests made with Nafion 115 membrane, and it has less tendency for short-circuits comparing with Nafion 212, this membrane was the one used for the remainder of the tests.

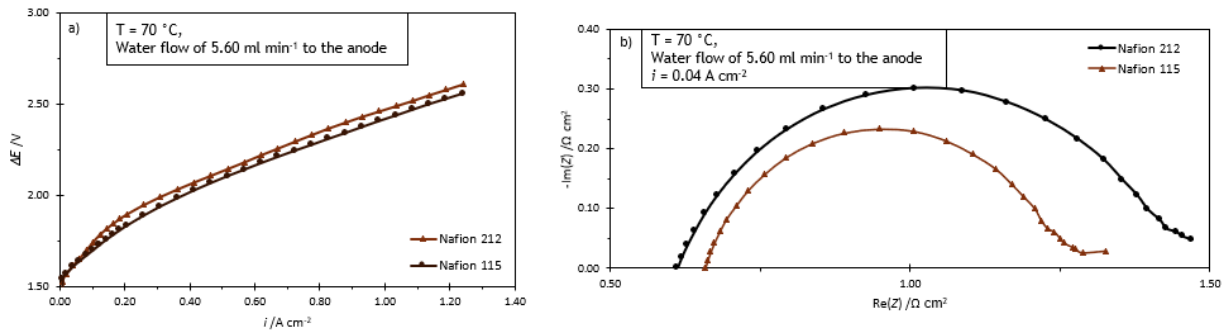

Figure F.1 – a) Polarization curve and b) Nyquist plot at 0.04 A cm^{-2} for Nafion 212 and Nafion 115 membranes, for a water flow rate of of 5.60 ml min^{-1} to the anode and a working temperature of 70 °C.

Appendix G - Comparison between AEM membranes studied

For AEM, unlike PEM, there is still no standard membrane used. Therefore, several membranes from different manufacturers were tested. Figure G.1 shows the polarization curves for 3 different membranes: fumasep FAA-3-PK-130, Eurodia AMX-fg and Sustainion® X37-50 Grade RT. The deposition methods used are described below, and the best conditions obtained for each membrane and deposition method are represented in table G.1.

For fumasep membranes, a commercial Platinum coated GDE was used as an electrode for the cathode side. For the anode side, an IrO_2 catalyst was deposited into the membrane by doctor blade method.

In the case of Eurodia membranes, two deposition methods were studied. Firstly, the catalyst was deposited directly into the membrane on both sides (CCM), through a spray method. Secondly, the catalyst was deposited into carbon paper electrodes (CCS), also through a spray method. The second method was tested because it was considered that the membrane drying process done in order to the catalyst deposition happen was damaging the membrane structure and, consequently, its performance.

When using Sustainion membranes, the catalyst layer was deposited in the electrode, both at the anode and cathode. For the anode, a commercial Pt/C coated GDE was used. For the anode, catalyst ink was deposited into a copper electrode (MTIcorp USA) through a spray method.

Table G.1 – Best working conditions for different membranes studied

	Temperature /°C	Feed flow /ml min^{-1}	Feed type	KOH concentration /M
fumasep	30	10	Anode and cathode	0.5
Eurodia CCS	50	10	Anode and cathode	0.5
Eurodia CCM	50	10	Anode and cathode	0.5
Sustainion	60	5.60	Anode	0.2

G.1 - Performance

From the analysis of the graphics from Figure G.1, it is possible to conclude that the Sustainion membrane is, by far, the one in which the electrolysis cell exhibits better performance. The system presents very similar ohmic resistances for the different membranes, with exception of the catalyst coated Eurodia membrane. The main source of overpotential difference stems from the resistance at the electrodes.

Contrary to expectation, for the same conditions, the ohmic resistance is higher when the catalyst is coated into the membrane than when is coated into the substrate. This suggests that the catalyst ink, even with the ionomer, does not adhere to the membrane and, therefore, the contact resistance between the catalyst layer and the membrane is higher. In the case of the catalyst coated electrode, the ink is well coated into the carbon paper electrode, which leads to smaller ohmic resistances. In the case of CCS the electrode resistance is also much smaller, which also indicates the better adherence of the catalyst into the overall cell system.

For fumasep membranes, it is expected that the electrode resistance is smaller compared with other membranes, not only because the quality of the membrane, but also due to the lower operation temperature. This temperature is, however, necessary for the operation of this membrane, as the maximum working temperature of the membrane is 40 °C.

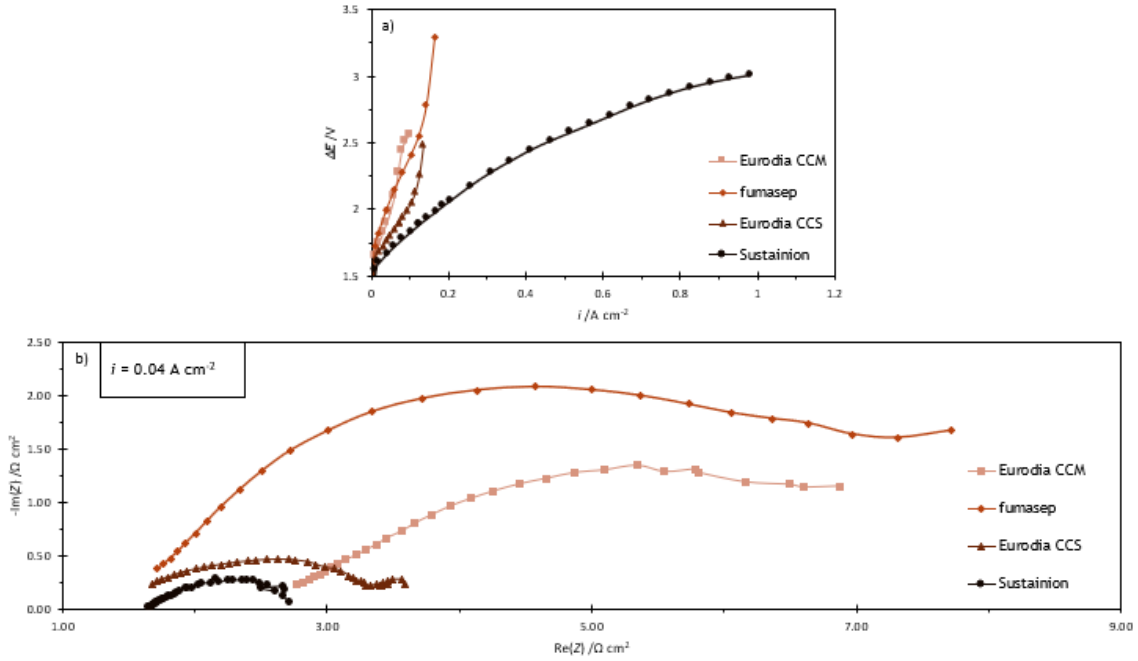

Figure G.1 – a) polarization curves and b) Nyquist diagram at 0.04 A cm^{-2} for different AEM membranes tested, for the conditions referenced in table G.1.

G.2 - Stability

Stability, through accelerated tests, was tested for the different membranes. Here are presented the polarization curves and Nyquist plots before and after the ASTs for the electrolysis cell with a Eurodia membrane, with the catalyst coated into a carbon paper substrate, and with a fumasep membrane. For the system with both membranes, a solution of 0.2 M KOH was fed into the electrolysis cell, and in both cases the performance decreased: 53 % for Eurodia and 61 % fumasep.

In the case of Eurodia membranes – Figure G.2 – it is of notice the increase of the ohmic resistance, which may indicate a loss in the ionic conductivity of the cell.

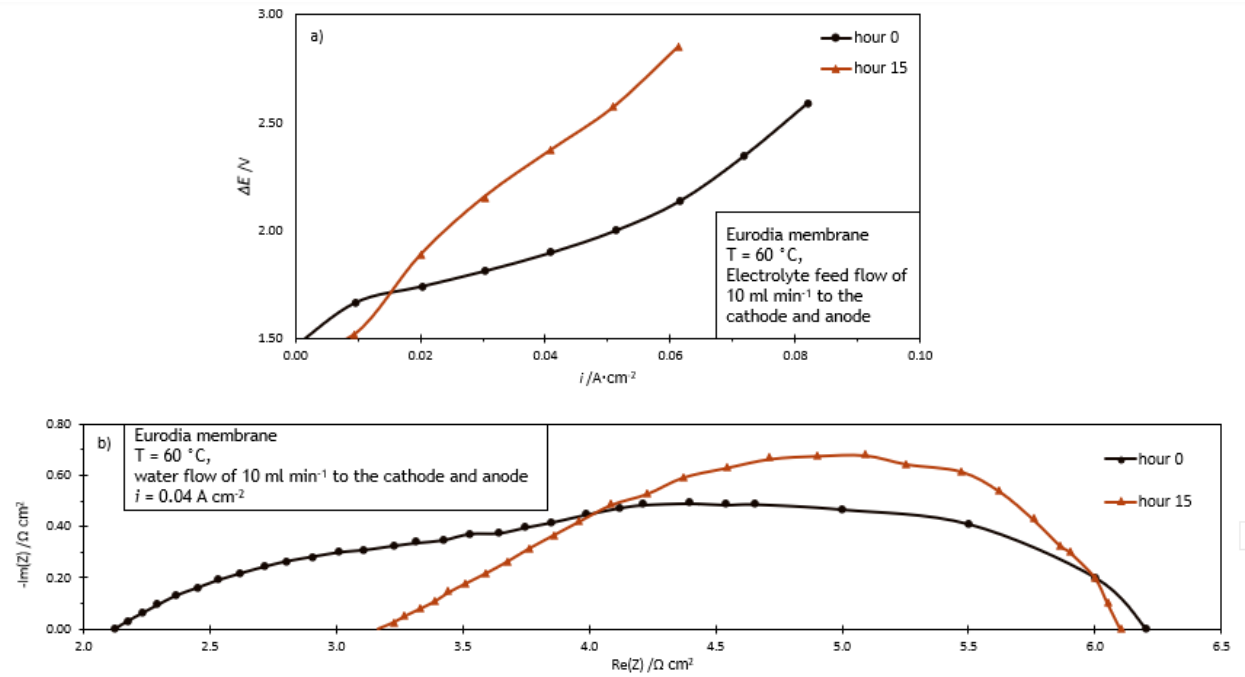

Figure G.2 – a) polarization curves and b) Nyquist diagram at 0.04 A cm^{-2} for an electrolysis cell working with an Eurodia membrane, at 60 °C and a 0.2 M KOH solution feel flow of 10 ml min^{-1} to both the anode and cathode.

For fumasep membranes – Figure G.3 – the ohmic resistance is similar to both before and after the AST; the main difference resides in the charge transfer resistance, that increases about 1 Ω cm^2 during the AST, which can be consequence of the degradation of the catalyst layer.

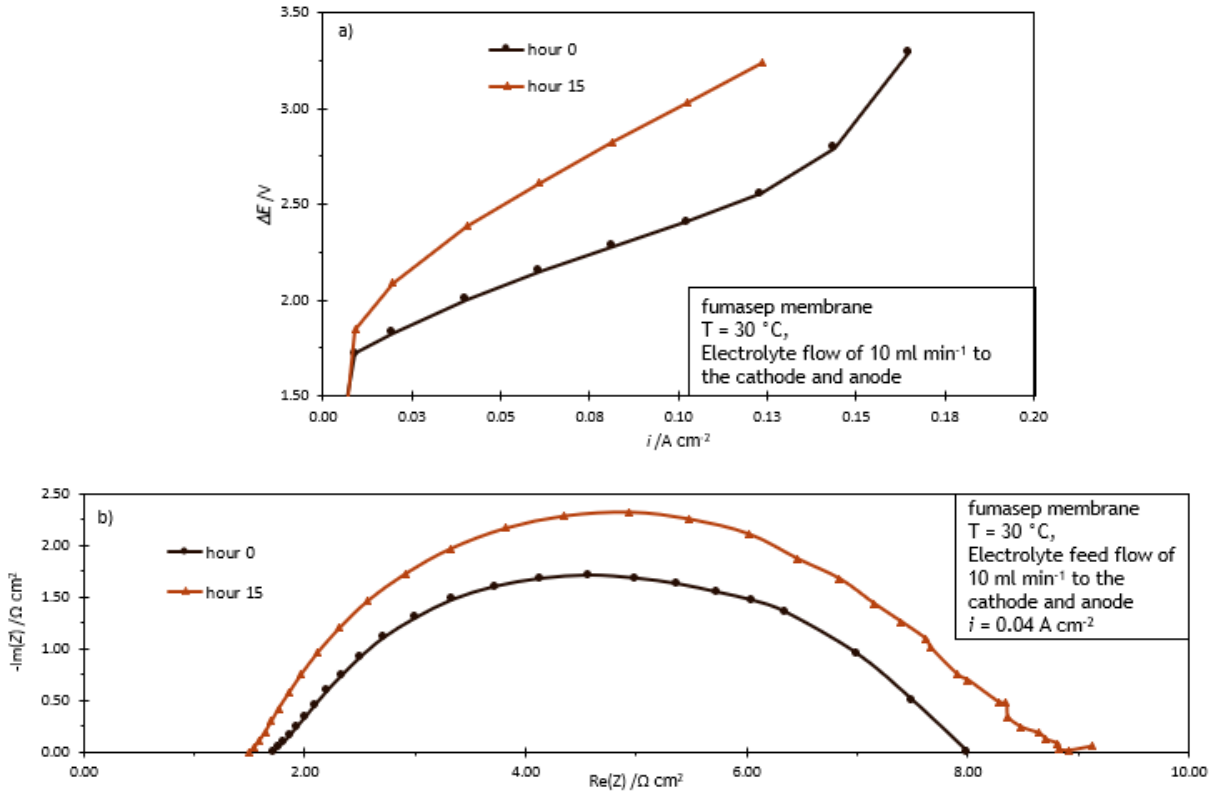

Figure G.3 – a) polarization curves and b) Nyquist diagram at 0.04 A cm^{-2} for an electrolysis cell working with a fumasep membrane, at 30 °C and a 0.2 M KOH solution feel flow of 10 ml min^{-1} to both the anode and cathode.

Appendix H - FTIR analysis of the used wastewaters

Figures H.1.a), H.1.b) and H.1.c) show the FTIR spectra of CIN, Ave and Arcos de Valdevez wastewater, respectively, in comparison to the spectra obtained for ultrapure water. It is possible to conclude, from the FTIR spectra, that all wastewaters present various peaks in the 1000 cm^{-1} to 1500 cm^{-1}; this phenomenon is specifically prominent in the Arcos de Valdevez wastewater. This zone in the spectra is characteristic of C-O, C-N and N-O bonds. In this specific situation, it probably indicates the presence of organic matter. The ionic metallic bonds cannot be observed at this wavelength.

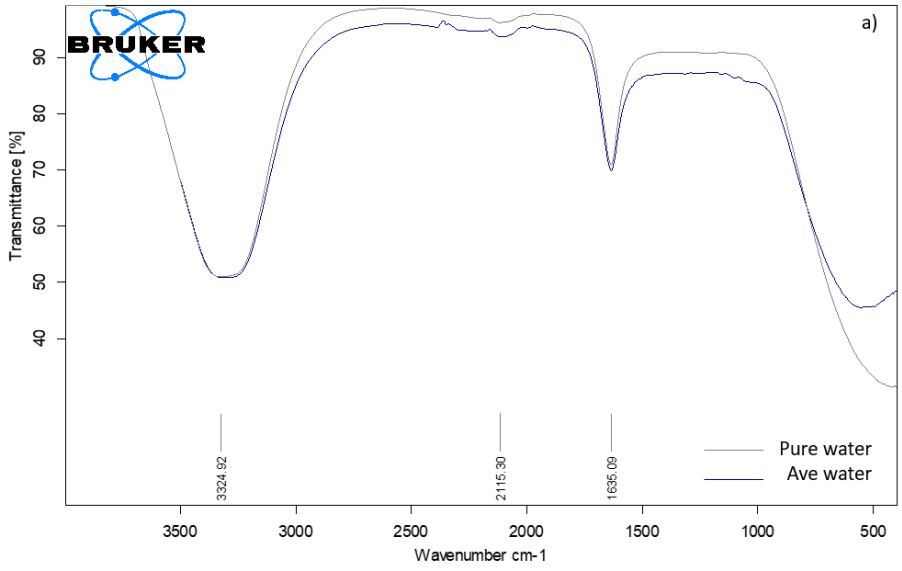

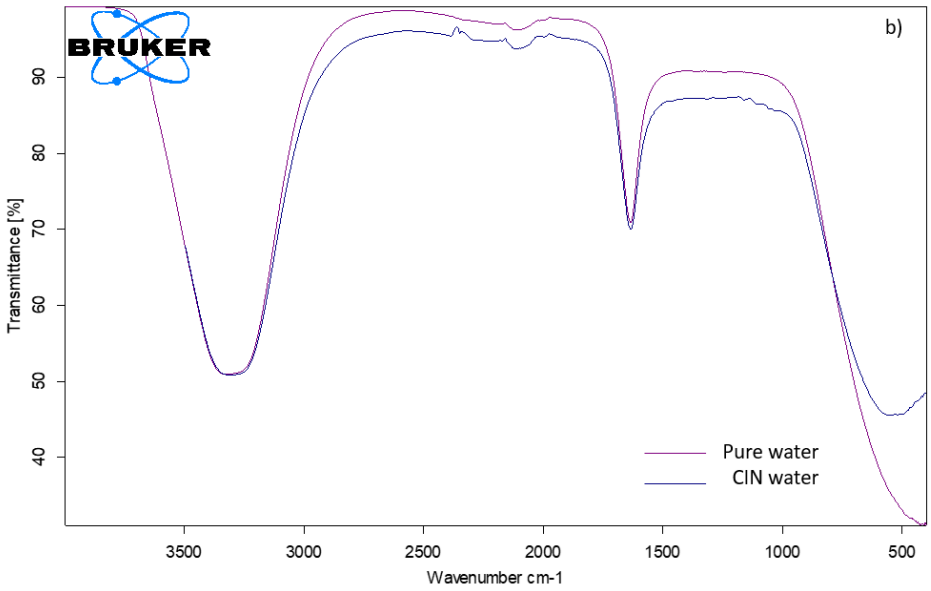

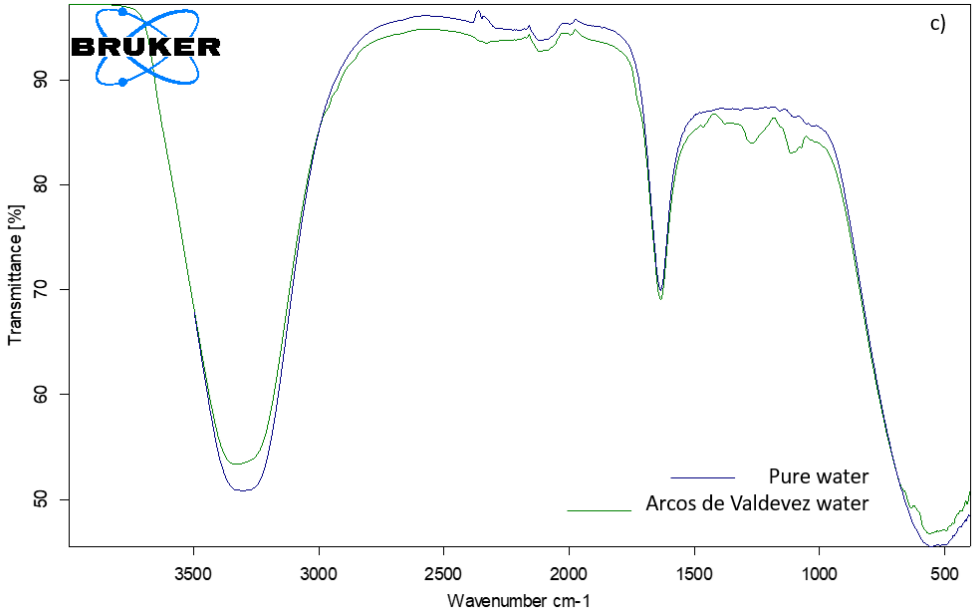

Figure H.1 – FTIR spectra comparison between ultrapure water and a) Ave wastewater; b) CIN wastewater; c) Arcos de Valdevez wastewater.

Appendix I – PEM AST analysis with untreated wastewater

For PEM untreated wastewater electrolysis, two of the three wastewaters were tested: Ave and Arcos de Valdevez water. Arcos de Valdevez wastewater presented a higher conductivity (2.14 mS cm) in comparison with Ave wastewater (0.92 mS cm), which, in turn, correlates to a higher solid content in the water, that, as seen before, jeopardizes the proper cell's operation.

Figure I.1 shows the polarization curves for pure water feed, and Arcos de Valdevez feed at beginning of life and after a 15-hour AST. A great difference between the performance with pure water and Arcos de Valdevez water at beginning of life is observed (*ca.* 53 % at 2.5 V) – Figure I.1.a). *Per* the analysis of the Nyquist plot – Figure I.1.b) - this performance loss is primarily due to charge transfer resistance, which may be caused by metallic poisoning of the

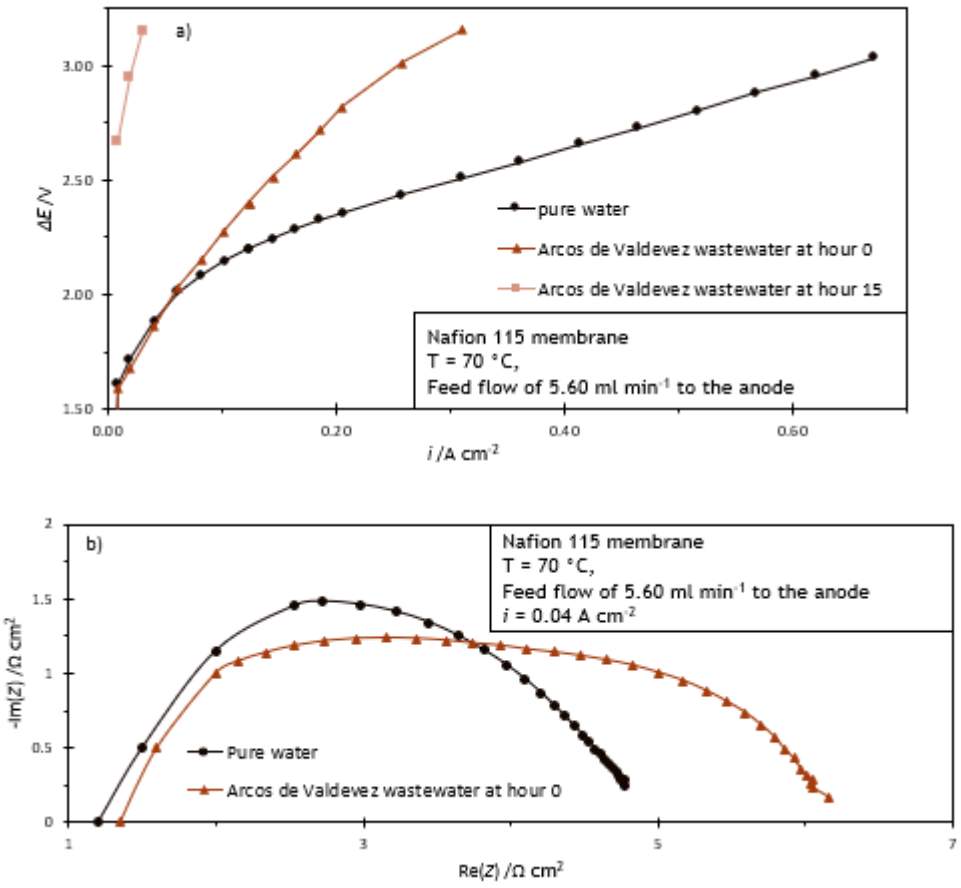

Figure I.1 – a) Polarization curve for pure water and Arcos de Valdevez wastewater feed, at beginning and end of life; b) Nyquist plot at 0.04 A cm^{-2} for pure water and Arcos de Valdevez water at beginning of life, for a cell working with a Nafion 115 membrane at 70 °C, with a water feed flow rate of 5.60 ml min^{-1} to the anode.

catalyst layer [22]. Between the beginning of life and end of life there is also a great loss in performance (58 % at 3 V).

For operation with Ave wastewater, similar results were obtained to those with Arcos de Valdevez wastewater. When Ave wastewater is used instead of ultrapure water, performance decreases about 42 % and the ohmic resistance in the cell increases about 0.60 Ω cm^2, indicating deposition of impurities in the membrane's ion exchange sites. In comparison to beginning of life, the performance, with Ave wastewater feeding to the cell, decreases 74 % at 3 V, after a 15-hour AST – Figure I.2. It can be inferred form the Nyquist plot at 0.04 A cm^{-2} – Figure I.2.b) – that the cell enters in the mass transport region at very low currents, and the charge transfer resistance increases in comparison to that beginning of life, which in turn indicates metallic poisoning of the catalyst layer [22].

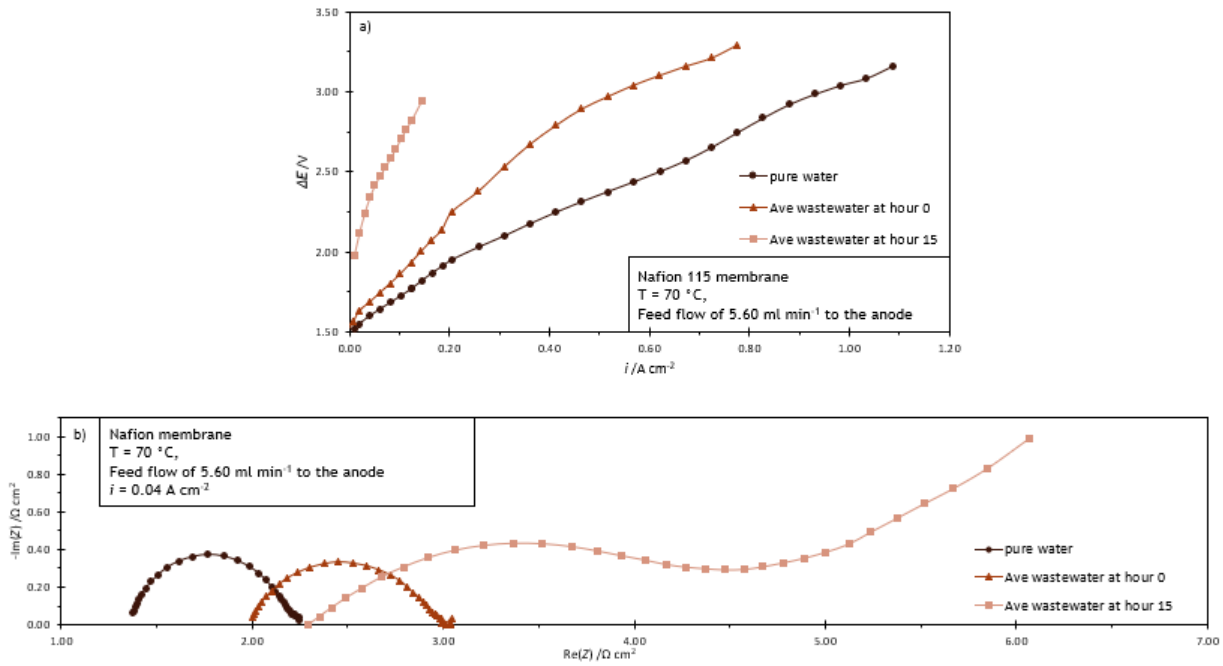

Figure I.2 - a) Polarization curve and b) Nyquist plot at 0.04 A cm^{-2} for pure water and Ave wastewater feed, at beginning and end of life, for a cell working with a Nafion 115 membrane at 70 °C, with a water feed flow rate of 5.60 ml min^{-1} to the anode.

Appendix J - AEM AST analysis with untreated wastewater

For AEMWE, Arcos de Valdevez wastewater, without any further purification, was tested. In contrast with PEMWE, the performance at beginning of life with Ave wastewater compared with that of pure water feeding, is extremely similar – Figure J.1.

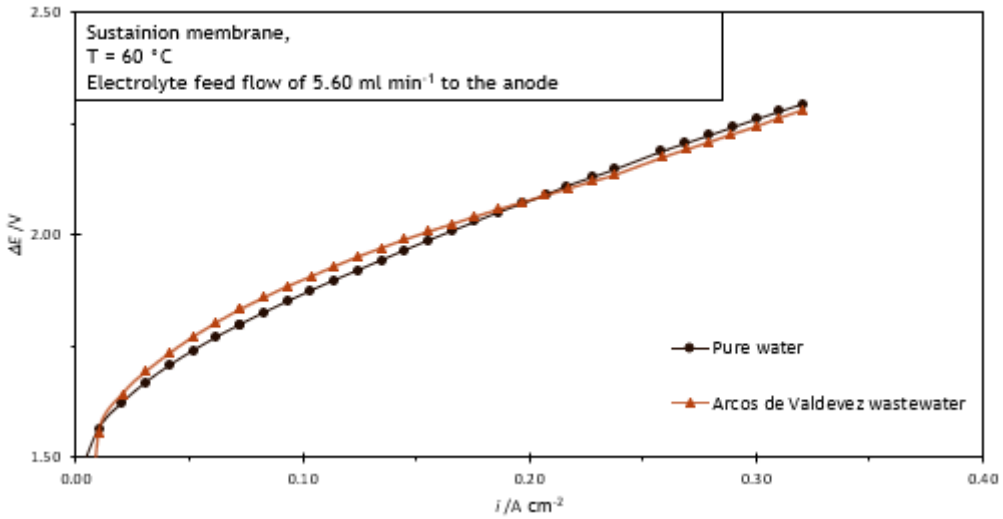

Figure J.1- Polarization curve of a AEM water electrolysis cell, for ultrapure water and Arcos de Valdevez wastewater, for a feed flow rate of 5.60 ml min^{-1} to the anode of a cell with a Sustainion membrane, working at 60 °C.

During the cyclic accelerated stress test, the performance decreases about 10 % at 2 V in the first hour of operation. The performance, then, kept constant until around 4 hours of operation, moment when the membrane short-circuited – Figure J.2. From that moment beyond, the short-circuit grew, shown by represented by the growth in current density at 1.4 V; at this potential, the current density should be zero, because it is below thermoneutral potential. The current density at 2 V shows the same trend to that 1.4 V; therefore, the increased in current potential along time is attributed to the short-circuit.

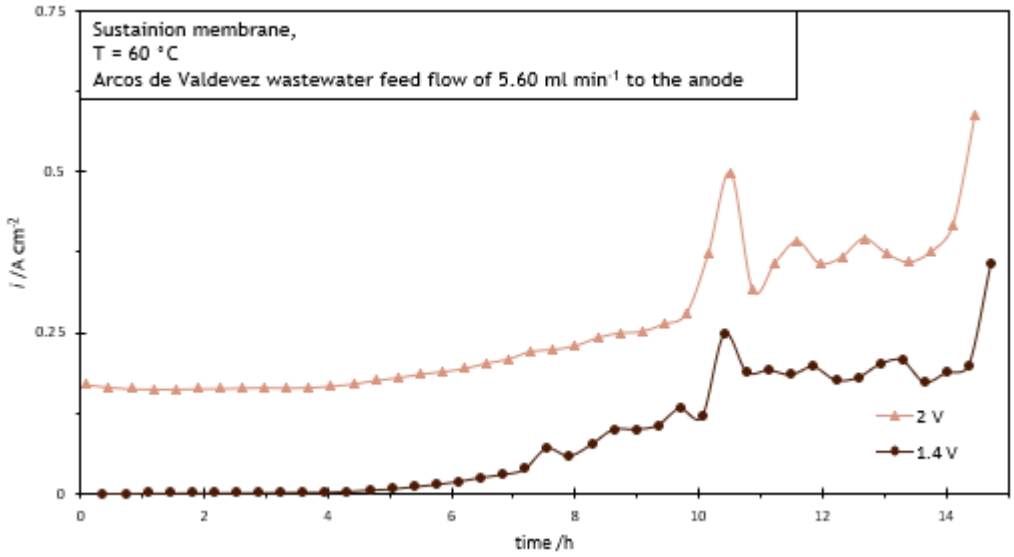

Figure J.1 – Evolution of the current density along time, at 1.4 V and 2 V, for Arcos de Valdevez wastewater feed flow rate of 5.60 ml min^{-1} to the anode of a electrolysis cell with a Sustainion membrane, working at 60 °C.

Appendix K - PEM AST analysis with treated wastewater

Considering PEM water electrolysis, with treated wastewaters feeding, the degradation occurred in the 15-hour AST is very similar to that of pure water feeding - Figure K.1:

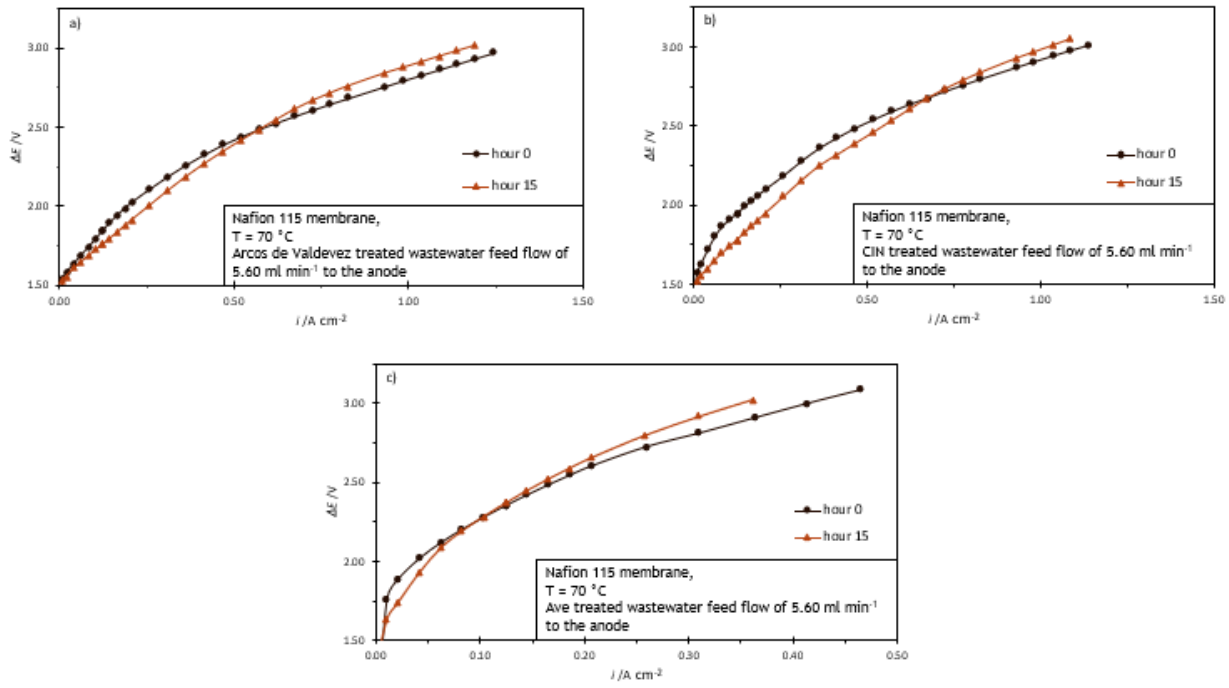

Figure K.1 - Polarization curve of a AEM water electrolysis cell, for a) treated Arcos de Valdevez wastewater; b) treated CIN wastewater; c) treated Ave wastewater, for a feed flow rate of 5.60 ml min^{-1} to the anode of a cell with a Sustainion membrane, working at 60 °C.

Appendix L - AEM AST analysis with treated wastewater

For the treated wastewaters, regarding AEMWE, the performance is similar to both ultra-pure water, Arcos de Valdevez treated wastewater and Ave treated wastewater – Figure L.1. Potassium hydroxide was added to all the waters fed to the electrolyser, to obtain a 0.2 M KOH solution. The electrolysis cell presented a worse performance for Arcos de Valdevez treated wastewater than for Ave treated wastewater feed (0.07 A cm^{-2} *vs.* 0.17 A cm^{-2} at 2 V, respectively).

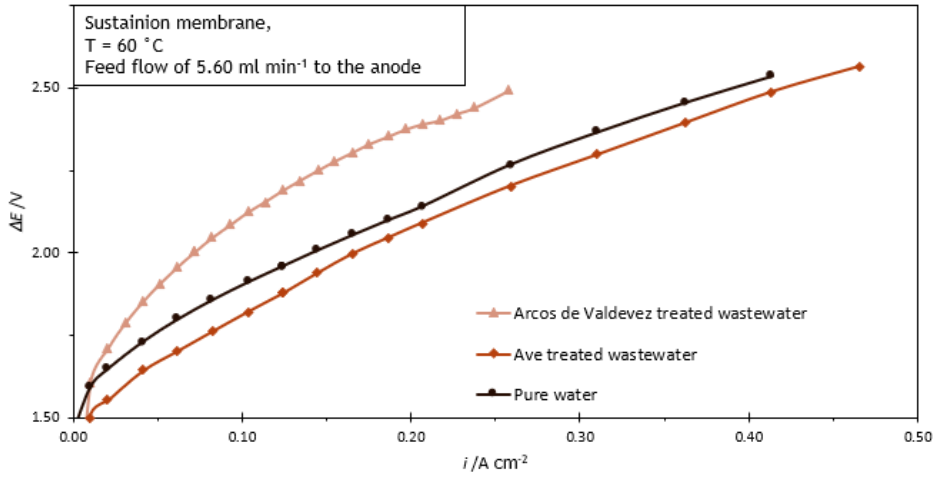

Figure L.1 – Polarization curve of a AEM water electrolysis cell, for ultrapure water, Arcos de Valdevez treated wastewater, and Ave treated wastewater feed flow rate of 5.60 ml min^{-1} to the anode of a cell with a Sustainion membrane, working at 60 °C.

However, during the first three hours of the AST, the performance of the electrolysis cell, for Arcos de Valdevez treated wastewater feeding, increases by 21 % at 2 V, while the cell's performance for Ave treated wastewater is kept constant in the first hours of operation; between the third and fourteenth hours of operation, the performance is kept constant and similar for both tests, at 2 V: 0.22 A cm^{-2} and 0.20 A cm^{-2} for Arcos de Valdevez treated wastewater feed and Ave treated wastewater feed, respectively – Figure L.2.

The improvement in performance for the electrolysis using Arcos de Valdevez treated wastewater could be attributed to the fact that, when the first polarization curve was performed, the membrane was not well adapted to the cell's environment and, over time, its ionic conductivity increased, resulting in an improvement in performance.

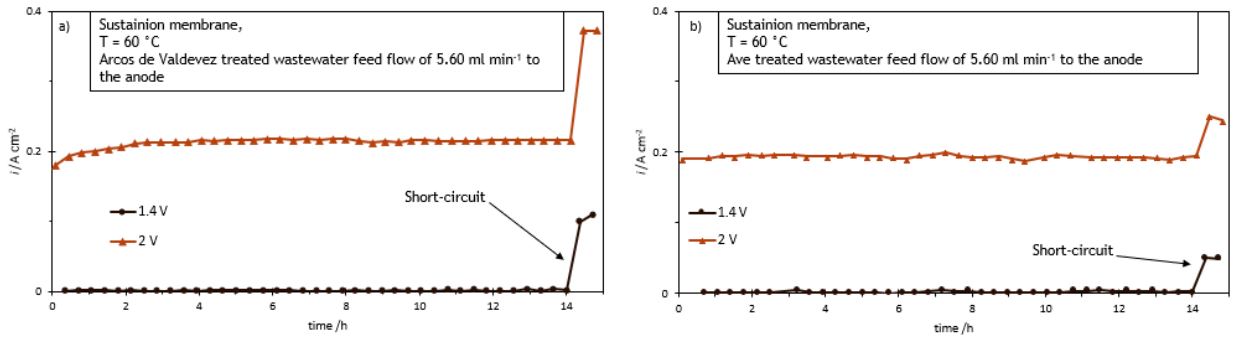

Figure L.2 – Evolution of the current density at 1.4 V and 2 V along the 15-hour AST, for a) Arcos de Valdevez treated wastewater and b) Ave treated wastewater, at a feed flow rate of 5.60 ml min^{-1} to the anode of an electrolysis cell with a Sustainion membrane and a working temperature of 60 °C.

Annex M - Solar and Wind Power Density in Portugal

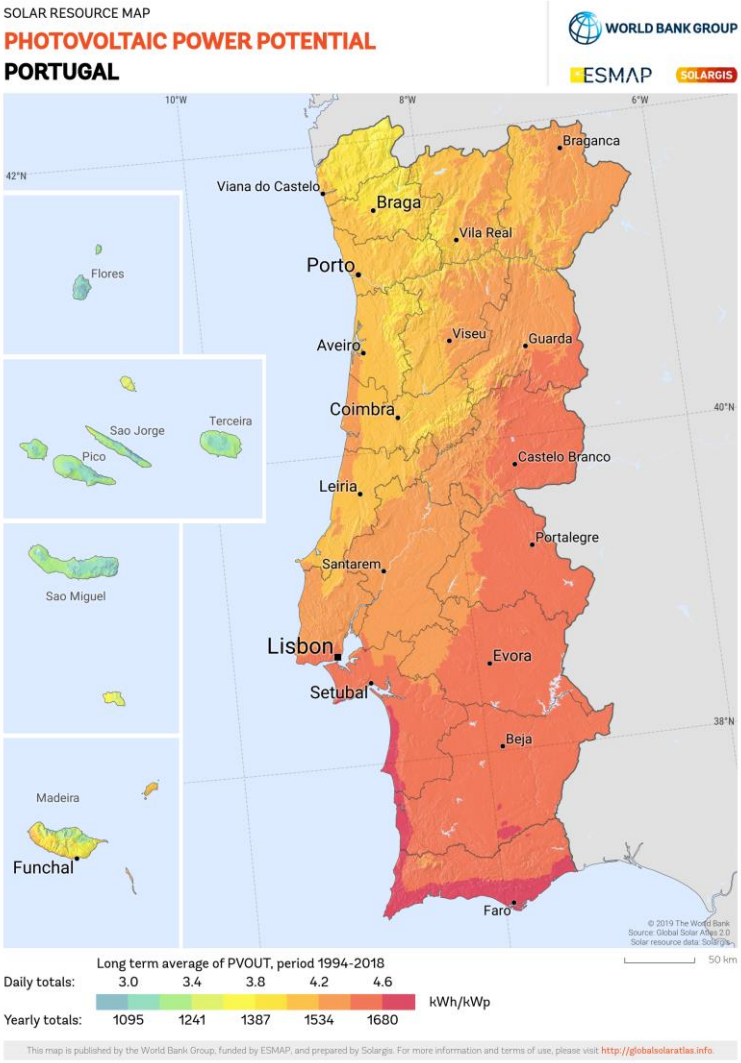

Figure M.1 - Photovoltaic power potential in Portugal [2].

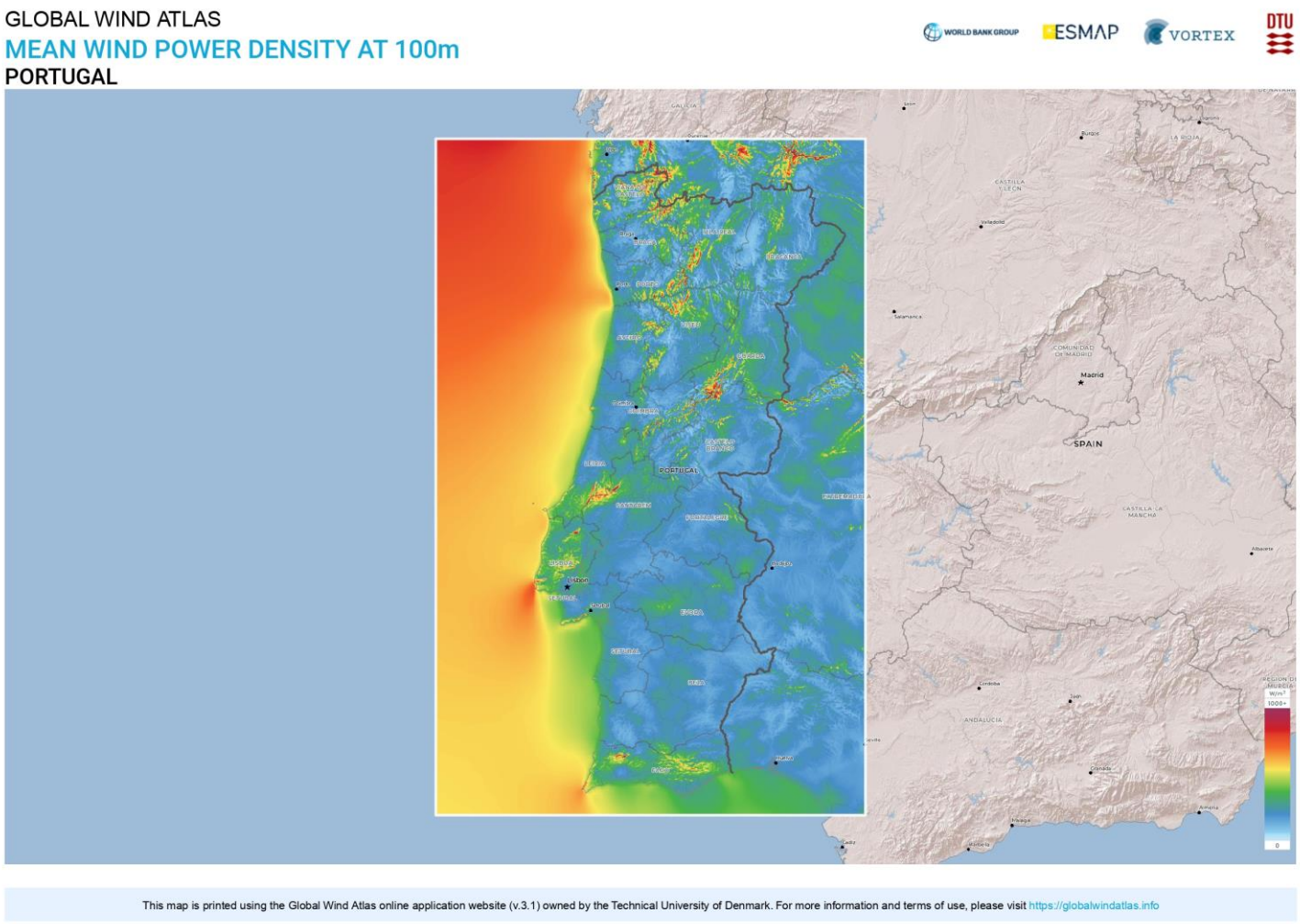

Figure M.2 - Wind power potential in Portugal [1].

Annex N – Composition of Tested Waters and Respective Oxidation Reactions

Table N.1 depicts the characterization of different wastewaters tested, as the parameters for exhausted water water from the cell, when working with Sustainion and Eurodia membranes.

Table N.1 – Parameters of the different wastewaters and waters exhausted from the cell.

Chemical Parameters	Sustainion exhausted water	Eurodia exhausted water	Arcos de Valdevez	Rio Ave	CIN
Condutivity /µS cm	51 200	137 200	2 140	924	2 700
Chemical oxygen demand /$mg_{O2}\,L^{-1}$	-	-	88.25	21.49	445.22
Biological oxygen demand /$mg_{O2}\,L^{-1}$	-	-	89	12	43
Total organic carbon /$mg\,L^{-1}$	378.4	671.5	17.21	12.16	102.3
Total nitrogen /$mg\,L^{-1}$	-	-	110.69	74.27	110.90
Nitrate /$mgN\,L^{-1}$	-	-	17.10	27.53	<0.50
Nitrite /$mg\,L^{-1}$	-	-	0.550	0.005	0.050
Sodium /$mg\,L^{-1}$	10.495	17.558	301.285	114.060	256.855
Potassium /$mg\,L^{-1}$	1407.28	4354.94	172.86	17.01	29.88
Iron /$mg\,L^{-1}$	0.0325	0.0414	0.157	0.424	0.0043
Nickel /$mg\,L^{-1}$	<0.005	<0.005	<0.005	<0.005	<0.005
Copper /$mg\,L^{-1}$	0.328	0.1187	0.0168	0.0164	0.0121
Magnesium /$mg\,L^{-1}$	0.169	0.364	1.856	8.200	17.208
Lead /$mg\,L^{-1}$	0.0207	0.0095	0.0030	0.0029	0.0029
Calcium /$mg\,L^{-1}$	1.39	2.13	155.605	32.27	207.88
Zinc /$mg\,L^{-1}$	0.1456	0.4746	0.3008	0.3489	0.0679

Sulfate /mg L^{-1}	-	-	452.04	55.04	86.90
Chlorine /mg L^{-1}	-	-	294.41	144.96	585.32

The preliminary tests for characterization of the AEM and PEM water electrolysis were performed using ultrapure water ($\rho = 201\ \mathrm{k\Omega\,cm}$ at 23 °C); nonetheless, this water may contain trace metal impurities which are harmless to the electrolyser operation at such low concentrations.

The concentration of the different impurities in the wastewaters was compared to those obtained from the analysis of the exhausted water from the cell, for operation with ultrapure water. The ultrapure water used contains several metal impurities, in low concentration. These impurities may already have been in the water supplied or could be dissolved during handling. Nonetheless, as these impurities were present in the ultrapure water fed to the cell, for the cases in which the content in the wastewaters was similar to the one in the ultrapure water and at low concentrations (< 0.5 mg L^{-1}), the influence of that contaminant was considered negligible. The exceptions to this are carbon, potassium, and copper, because these materials were present in the cell assembly and, therefore, could be leached into the ultrapure water during degradation. The contaminants considered negligible are, thus, nickel, copper, lead, and zinc.

Table N.2 shows the oxidation reactions associated with the ionic impurities in the wastewaters.

Table N.2 – Potential for the oxidation reactions characteristic of the different species present in the wastewaters [73].

Species	Oxidation Reaction	E^0 /V *vs* SHE
Cl^-	$2Cl^- \rightleftarrows Cl_2 + 2e^-$	1.358
	$Cl^- + 4H_2O \rightleftarrows ClO_4^- + 8H^+ + 8e^-$	1.389
	$Cl^- + H_2O \rightleftarrows HClO + H^+ + 2e^-$	1.482
SO_4^-	$S_2O_6^{2-} + H_2O \rightleftarrows 2SO_4^- + 4H^+ + 2e^-$	0.22
	$H_2SO_3 + H_2O \rightleftarrows SO_4^- + 4H^+ + 2e^-$	-0.172
	$2SO_4^{2-} \rightleftarrows S_2O_8^{2-} + 2e^-$	-2.010
Na^+	$Na \rightleftarrows Na^+ + e^-$	2.71
K^+	$K \rightleftarrows K^+ + e^-$	2.372
Fe	$Fe \rightleftarrows Fe^{2+} + 2e^-$	0.44
	$Fe \rightleftarrows Fe^{3+} + 3e^-$	0.037
Mg^{2+}	$Mg \rightleftarrows Mg^{2+} + 2e^-$	2.372
Ca^{2+}	$Ca \rightleftarrows Ca^{2+} + 2e^-$	2.868